COVARIANT DENSITY FUNCTIONAL THEORY FOR NUCLEAR MATTER

Inaugural-Dissertation
zur Erlangung des Doktorgrades der Naturwissenschaften
der Justus-Liebig-Universität Giessen im Fachbereich 07
(Mathematik und Informatik, Physik, Geographie)

vorgelegt von

Urnaa Badarch

aus Mandalgobi, Mongolei

Giessen, 2007

Dekan:	Prof. Dr. Bernd Baumann
I. Berichterstatter:	Prof. Dr. Horst Lenske
II. Berichterstatter:	Prof. Dr. Werner Scheid
Tag der mündlichen Prüfung:	14.06.2007

To my parents who are born to love me.

Contents

Chapter 1

Introduction

The nuclear matter equation of state (EOS) is a very important ingredient in the study of properties of nuclei, heavy-ion collisions as well as astrophysical objects like neutron stars and supernova. Recently, EOS studies for the asymmetric nuclear matter gained particular importance both due to astrophysical applications (neutron stars) [See95] and to the new radioactive beam facilities [KG] probing nuclei far from stability. A different regime of interest is the high density region, which will be soon studied by the Compressed Baryonic Matter (CBM) experiments at the new FAIR facility at GSI [GSI] at densities up to $\approx 8\rho_0$ [FW06]. However, so far the experimental information is available only for densities around normal nuclear density ρ_0 [FW06] and for symmetric nuclear matter, since the stable nuclei range is around $Z/A = 0.5$. Theoretical investigation, reliably predicting the EOS in the high ρ and high asymmetry regimes are necessary. The modern approach to theoretically investigate the nuclear structure is based on relativistic models of nuclear matter and finite nuclei as strongly interacting systems of baryons and mesons.

The prototype for such an approach is relativistic mean-field theory (RMF) [Wal74, SW86] where nuclear forces are obtained from the virtual exchange of mesons. In order to improve the results of this simple model, cubic and quartic self-interactions of the meson fields had to be introduced [BB77, Bod91]. In mean-field approximation the meson self-interactions correspond effectively to higher order density dependent contributions. Unfortunately, they lead to instabilities in the region above saturation density.

Therefore, one needs to use a more fundamental approach, *i.e.* to derive in-medium interactions microscopically. Dirac-Brueckner theory (DB) [Erk74, Hol74, HS87, HM87] has proven to be a successful method for this. By using realistic NN potentials, in-

medium interactions are derived as a resummation of all (two-body) ladder diagrams. DB calculation of the density dependence for the self-energies was originally performed in [FLW95] for the case of three meson fields (σ, ω, ρ) and extended to additionally include into consideration the δ-meson in [dJL98a, dJL98b]. A fully covariant and thermodynamically consistent field theory is obtained by treating the interaction vertices on the level of the Lagrangian as Lorentz scalar functionals of the field operators. This method is called Density-Dependent Relativistic Hadron field (DDRH) theory. Retaining a Lagrangian formulation we then introduce density dependent meson-nucleon coupling constants taken from DB self-energies. An important difference to the RMF treatment is that the DDRH approach accounts for quantal fluctuations of the baryon fields even in the ground state. These contributions significantly improve the reproduction of binding energies and radii of finite nuclei. In mean-field approximation DDRH theory reduces to a Hartree description with density dependent coupling constants similar (but not equal) to the initial proposal of Brockmann and Toki [BT92]. In contrast to the [BT92], the approach we advocate here (DDRH) is thermodynamically consistent as we will show in Chapter 6.

After the success of the microscopic DDRH approach, Typel and Wolter [TW99] developed the first phenomenological description of the density dependent meson-baryon vertices. In phenomenological approaches, the density dependent vertices are described by making an ansatz for the functional form with some parameters which are adjusted to reproduce the measured properties of symmetric and asymmetric nuclear matter, binding energies, charge radii and neutron radii of spherical nuclei. We choose to compare our results of the microscopical calculations to the results of the phenomenological approach utilizing the DD-ME1 parametrization from [NVFR02]. Since the latter is devised to fit the properties of the symmetric nuclear matter around the normal nuclear matter density, we make sure that our results agree with the phenomenological ones in this region.

The use of microscopically calculated vertices allows us to safely extrapolate our results to high densities. In contrast to previous applications of the DDRH approach with DB self-energies, we add momentum correction terms to the vertices and, also, account for the forces due to the exchange of δ-meson. By modifying the DDRH approach in this way, we achieve a more precise description of the binding energy and improve the reliability of our predictions for the properties of very asymmetric nuclear matter.

The present thesis is organized as follows. In Chapter 2 we study the Nucleon-

Nucleon (NN) interaction in DB approach. We start by considering the NN interaction in free-space in terms of the Bethe-Salpeter (BS) equation to the meson exchange potential model. Then we present the DB approach for nuclear matter by extending the BS equation for the in-medium NN interaction. From the solution of the three-dimensional in-medium BS equation, we derive the DB self-energies and total binding energy which are the main results of the DB approach, which we later incorporate in the field theoretical calculation of the nuclear equation of state.

In Chapter 3, we introduce the basic concepts of density functional theory in the context of Quantum Hadrodynamics (QHD-I) [Wal74]. The discussion starts with the proof of the existence theorem of Hohenberg and Kohn [HK64] for QHD-I. In Section. 3.2 we give a short review of QHD-I. This model is a simple example of a relativistic quantum approach to the investigation of nuclear matter and serves as an introduction to the following description of DDRH approach.

We reach the main point of this work in Chapter 4 where we introduce the DDRH approach. In the DDRH theory, the medium dependence of the meson-nucleon vertices is expressed as functionals of the baryon field operators. Because of the complexities of the operator-valued functionals we decide to use the mean-field approximation. The details of the mean-field reduction is reviewed in Section. 4.2.

In Chapter 5, we contrast microscopic and phenomenological approaches to extracting density dependent meson-baryon vertices. In Section 5.1 we present microscopic density dependent meson-baryon vertices deduced from nuclear matter DB self-energies. The momentum dependence of the DB self-energies and the meson-baryon vertices are discussed in Section 5.2. We present the parametrization of the momentum corrected meson-baryon vertices in Section 5.3. In Section 5.4, we introduce phenomenological density dependent meson-baryon vertices and compare them to the microscopically calculated ones.

Chapter 6 gives the results of our studies of the EOS of infinite nuclear matter in detail. Using formulas derived in Chapters 4 and 5 we calculate the following properties of symmetric and asymmetric nuclear matter and pure neutron matter:

- energy density,
- pressure,
- binding energy,
- symmetry energy,

- effective nucleon mass,
- compressibility and
- speed of sound in nuclear medium

as functions of the density and of the nuclear asymmetry parameter. The results compared to those of phenomenological DD-ME1 approach.

Finally, we summarize our results, draw conclusions and give an outlook to possible future work in Chapter 7.

Chapter 2

Ab initio Relativistic nuclear field theory

The strong interaction between two nucleons can be described using two completely different approaches. One is usually called the microscopic approach and the other is the phenomenological approach. In a phenomenological approach the input is a density-dependent effective nucleon-nucleon interaction with some parameters which are adjusted to reproduce various properties of nuclei and empirical saturation properties of nuclear matter [Sky59, VB72]. In the phenomenological approach one can obtain the Equation of state in a very simple way compared to the microscopic approach. However the phenomenological approach is less fundamental than the microscopic approach in which the input is the two body nucleon-nucleon (NN) interaction, described by the exchange of mesons. The most simplest meson exchange model is the One-Boson-Exchange potentials (OBEP), as e.g the Bonn potentials [MHE87, Mac89] which are usually based on the exchange of the six non-strange mesons: σ (scalar, iso-scalar), ω (vector, iso-scalar), δ (scalar, iso-vector), ρ (vector, iso-vector), π (pseudo-scalar, iso-vector), η (pseudoscalar, iso-scalar). In the OBE model one further assumes that no meson-meson interaction is present and each meson is exchanged in a different interval of the time from the others. One of the appropriate way to apply OBE models in nuclear matter calculations is the *ab initio* Dirac-Brueckner (DB) approach in which the full NN interaction is constructed from a particular summation of the OBE diagrams, so called the ladder summation.
In density dependent relativistic hadron field theory (DDRH), the in-medium interactions are described by density dependent vertices which can be derived from DB calculations. This allows that in DDRH approach, the calculations for infinite nuclear matter, neutron

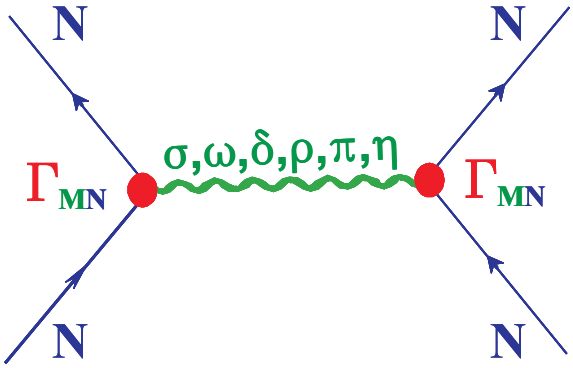

Figure 2.1: Diagrammatic structure of the Nucleon-Nucleon interaction via mesons

stars and ground state of the finite nuclei [Len04, HKL01b, HKL01a] and hypernuclei [KHL00, KL02] can be done by purely microscopic way i.e. without introducing any additional parameters. Therefore it is worthwhile to discuss the DB approach. Since DB approach has been discussed extensively in the literature [Erk74, Hol74, HS87, HM87] we shall be very brief here and aim to show the derivation of the DB self-energies.

2.1 The Nucleon-Nucleon interaction

In this section we discuss the free-space NN interaction, because the DB approach derives the in-medium interaction from free-space NN meson exchange potentials. Both the free-space and nuclear matter are translationally invariant. Therefore one can work in momentum space.

In momentum space the relativistic two-particle interaction is obtained by solving a covariant four-dimensional Bethe-Salpeter (BS) equation:

$$\langle q'|T|q\rangle = \langle q'|K|q\rangle + i\int \frac{d^4k}{(2\pi)^4}\langle q'|K|k\rangle G_0(k)G_0(-k)\langle k|T|q\rangle \ , \tag{2.1}$$

or schematically

$$T = K + i\int KG_0G_0T \ , \tag{2.2}$$

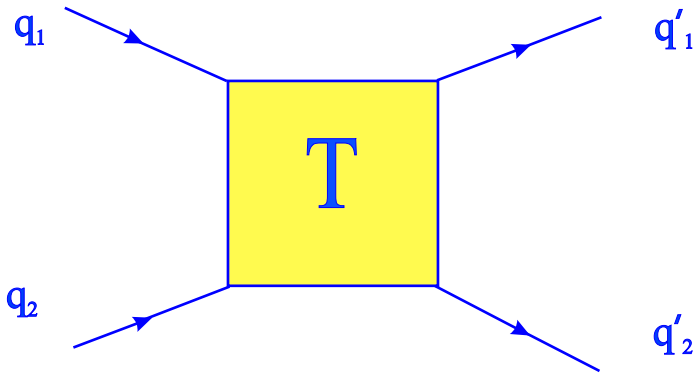

Figure 2.2: Graphical representation of the T-matrix.

where T is the scattering matrix for two nucleons in free space (see Fig. 2.2) and q, k and q' are the incoming, intermediate and outgoing relative four-momenta, respectively. For all four-momenta, our notation is $k = (k_0, \mathbf{k})$. K is the full two-nucleon kernel and it consists of infinite set of irreducible two-particle diagrams.
The one-nucleon propagator is given by

$$G_0(k) = \frac{1}{\not{k} - M + i\epsilon} \ , \tag{2.3}$$

where M denotes the nucleon mass and $\not{k} \equiv \gamma^\mu k_\mu$. Since this four-dimensional integral Eq. (2.1) is very difficult to solve, so called *three dimensional reduction schemes* have been proposed, in which four-dimensional BS problem is reduced to a model in three dimensions by finally the time-like energy component and considering explicitly only the space-like momentum components. The reduction schemes introduced by Thompson [Tho70] and the Blankenbecler-Sugar [BS66] are the most widely used [Mac89, LME93]. Following Thompson, by fixing the time-like component of all momenta, we obtain the three-dimensional reduction of the BS equation in center-of-mass (c.m.) frame,

$$\begin{aligned} \langle \mathbf{q}', -\mathbf{q}'|T(s)|\mathbf{q}, -\mathbf{q}\rangle &= \langle \mathbf{q}', -\mathbf{q}'|V(s)|\mathbf{q}, -\mathbf{q}\rangle \\ &+ \frac{1}{2}\int \frac{d^3k}{(2\pi)^3} \langle \mathbf{q}', -\mathbf{q}'|V(s)|\mathbf{k}, -\mathbf{k}\rangle g(\mathbf{k}, s) \langle \mathbf{k}, -\mathbf{k}|T(s)|\mathbf{q}, -\mathbf{q}\rangle \ , \end{aligned} \tag{2.4}$$

or schematically

$$T = V + VgT \tag{2.5}$$

where:

1. with q_1 and q_2 the individual four-momenta of particles 1 and 2, one can define the relative and the total four-momenta $q = \frac{1}{2}(q_1 - q_2)$ and $P = (q_1 + q_2)$, respectively. Accordingly in c.m. frame $P = (\sqrt{s}, \mathbf{0})$, with the total energy $\sqrt{s} = 2q^0$.

2. The K is approximated by first order contributions so-called ladder approximation[1], hence, replaced by the OBE interaction kernel V(s) in Eq. (2.4). $V(s)$ is defined as a sum of one-particle-exchange amplitudes of the six non-strange bosons with given masses (below 1 GeV/c^2) and couplings. (Details on the mathematical and numerical aspects of the OBEP with its computer code can be found in [LME93].)

3. The two-nucleon propagator $g(\mathbf{k}, s)$ is defined as

$$g(\mathbf{k}, s) = -i \int dk_0 G_0(k) G_0(-k) \ . \tag{2.6}$$

In the Thompson approximation, the negative energy contributions to $G_0(k)$ is neglected. Therefore the form of $g(\mathbf{k}, s)$ in the c.m. frame is given by

$$g(\mathbf{k}, s) = \Lambda^+(\mathbf{k}) \Lambda^+(-\mathbf{k}) \frac{M^2}{E_k^2} \frac{\pi}{\frac{1}{2}\sqrt{s} - E_k + i\epsilon} \tag{2.7}$$

with

$$\Lambda_i^+(\mathbf{k}) = \left(\frac{\gamma^0 E_k - \boldsymbol{\gamma} \cdot \mathbf{k} + M}{2M} \right)_i = \sum_{\lambda_i} |u(\mathbf{k}, \lambda_i)\rangle \langle \bar{u}(\mathbf{k}, \lambda_i)| \tag{2.8}$$

where Λ_i^+ is the on-shell positive energy projection operator for nucleon i and with $u(\mathbf{k})$ a positive energy Dirac spinor of momentum $\mathbf{k}$, $\bar{u} \equiv u^\dagger \gamma^0$ (see App. A.1). λ_i denotes either the helicity or the spin projection of the respective nucleon, and E_k its free energy $E_k = \sqrt{\mathbf{k}^2 + M^2}$. With the above expressions and Eq. (2.4) we obtain

$$\langle \mathbf{q}' | T | \mathbf{q} \rangle = \langle \mathbf{q}' | V | \mathbf{q} \rangle + \frac{1}{2} \int \frac{d^3k}{(2\pi)^3} \langle \mathbf{q}' | V | \mathbf{k} \rangle \frac{M^2}{E_k^2} \frac{1}{E_q - E_k + i\epsilon} \langle \mathbf{k} | T | \mathbf{q} \rangle \ . \tag{2.9}$$

[1] Here only the most simple 2 particle irreducible kernel is taken to account, namely the Born terms of the perturbation series.

2.2 Nucleon-Nucleon interaction in medium

A nucleon moving in the nuclear medium is affected by its interactions with the surrounding nucleons. As a result the nucleon gets "dressed". The interaction between *two-dressed nucleons* in-medium can be obtained analogous with *two-bare nucleon* interactions in free-space, discussed in previous section. Therefore the BS equation for the in-medium interaction of the nucleons can be written as

$$T^* = K^* + i \int K^* G G T^* \ , \tag{2.10}$$

which is similar to Eq. (2.2) but with dressed nucleon propagator G . The dressed nucleon interactions are denoted by asterisks.
The relation between the bare and dressed nucleon propagator is given by the Dyson equation

$$G = G_0 + G_0 \Sigma G \ , \tag{2.11}$$

where G_0 denotes the free nucleon propagator while the influence of the surrounding nucleons is expressed by the nucleon self-energy Σ, i.e. the "dressing " of nucleon is contained in Σ . In DB theory this self-energy Σ is determined by summing up the interaction with all the nucleons inside the Fermi level in Hartree-Fock approximation

$$\Sigma = -i \int_F \left(Tr \left[G T^* \right] - G T^* \right) \ , \tag{2.12}$$

where the first term is the direct, or Hartree contribution and the second term is exchange or Fock contribution within the Fermi sea F . The coupled set of equations (2.10-2.12) represents a self-consistency problem and to solve this problem is a main goal of the DB approach. The Eqs. (2.10-2.12) are represented diagrammatically in Fig. 2.3 .
After applying the Thompson three-dimensional reduction scheme, the Eq. (2.10) reduces to

$$T^* = V + i \int V Q G G T^* \ , \tag{2.13}$$

where V is the bare nucleon-nucleon interaction and iGG is the two-nucleon propagator in-medium which describes the intermediate off-shell nucleons. The Pauli operator Q accounts for the influence of the medium by the Pauli-principle and projects the intermediate nucleon states out of the Fermi level. In other word, two nucleons below the Fermi level can only scatter into states above the Fermi level because in nuclear matter

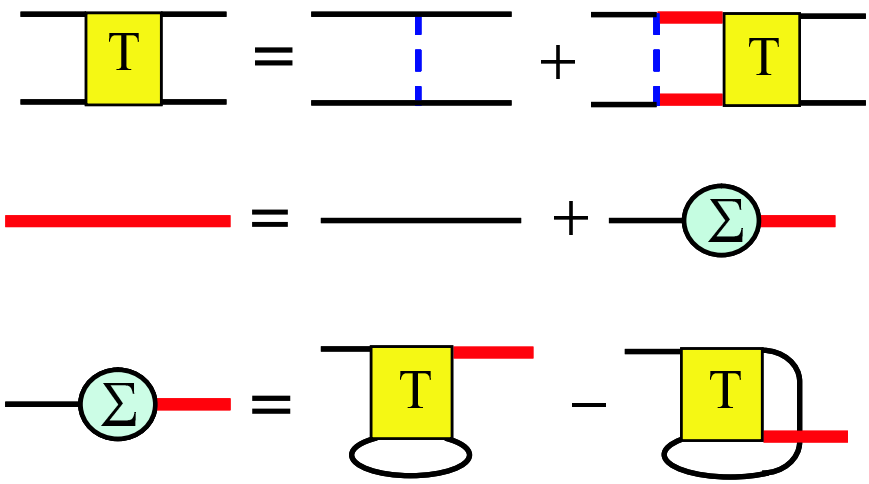

Figure 2.3: In Dirac-Brueckner approach, the in-medium interactions are described by the Bethe-Salpeter equations (Eq.(2.10), above) in which the in-medium single particle propagators appear, defined by the Dyson-Equation (Eq.(2.11), middle) in terms of the self-energies (Eq.(2.12), last line). The whole set of equations has to be solved simultaneously and self-consistently using medium-modified spinors for the baryonic Fermi-Dirac fields [Len04].

all states up to Fermi level are occupied and are thus excluded by the Pauli-principle. The bare-nucleon propagator $G_0(k)$ in Eq. (2.11) is given by

$$G_0(k) = (\not{k} + M)\left\{\frac{1}{k^2 - M^2 + i\epsilon} + \frac{i\pi}{E_k}\delta(k_0 - E_k)\Theta(k_F - |\mathbf{k}|)\right\} , \tag{2.14}$$

where k_F is the Fermi momentum.
The formal solution of the Dyson equation (2.11) is

$$G(k) = \frac{1}{\not{k} - M - \Sigma(k)} . \tag{2.15}$$

Due to the translational and rotational invariance, parity conservation and the time reversal invariance the self energy for infinite nuclear matter can be expressed by scalar

and vector components [IZ80, HM87]

$$\Sigma(k) = \Sigma^s(k) - \gamma^0\Sigma^0(k) + \gamma\cdot\mathbf{k}\Sigma^v(k) \ . \tag{2.16}$$

This structure suggests the following definitions for the effective mass and in-medium momentum

$$\begin{aligned} m^* &= M + \Sigma^s(k) \\ k_0^* &= k_0 + \Sigma^0(k) \\ \mathbf{k}^* &= \mathbf{k}(1+\Sigma^v(k)) \ , \end{aligned} \tag{2.17}$$

and one can rewrite Eq. (2.15) as $G(k) = (\not{k}^* - m^*)^{-1}$. The vector part of the self-energy Σ^v is very small. Therefore Eq. (2.17) can be simplified further as

$$\begin{aligned} m^* &\mapsto m^* = \frac{M+\Sigma^s(k)}{1+\Sigma^v} \\ \Sigma^{0*} &\mapsto \Sigma^{0*} = \frac{\Sigma^0(k)}{1+\Sigma^v} \\ k_0^* &\mapsto k_0^* = \frac{k_0+\Sigma^0(k)}{1+\Sigma^v} \end{aligned} \tag{2.18}$$

by dividing out the Σ^v term [HS87, HM87] . One thus obtains the solution of the Dirac equation for the one-particle motion in nuclear matter i.e. for the "dressed nucleon" (see Sec. 6.2)

$$u_\lambda^*(k) = \sqrt{\frac{E_k^*+m^*}{2m^*}} \begin{pmatrix} 1 \\ \frac{\sigma\mathbf{k}}{E_k^*+m^*} \end{pmatrix} \chi_\lambda \ . \tag{2.19}$$

The self-energy is found to depend weakly on the momentum inside the Fermi surface. Therefore in the practical calculation, one usually uses its fixed value at the Fermi momentum or uses an expansion up to order k^2 [HKL01a, HKL01b].

Using the above expressions for the two-nucleon propagator in-medium which is similar to Eq. (2.6) we obtain the integral form of the Thompson equation (2.13) in c.m. frame:

$$\langle\mathbf{q}'|T^*|\mathbf{q}\rangle = \langle\mathbf{q}'|V|\mathbf{q}\rangle + \frac{1}{2}\int\frac{d^3k}{(2\pi)^3}\langle\mathbf{q}'|V|\mathbf{k}\rangle\frac{m^{*2}}{E_k^{*2}}\frac{Q(k,s^*)}{E_q - E_k + i\epsilon}\langle\mathbf{k}|T^*|\mathbf{q}\rangle \ , \tag{2.20}$$

where $s^* = 4E_k^{*2}$ and $Q(k, s^*)$ is (the angle-averaged) Pauli-projector [HM87]. Comparing Eqs. (2.9) and (2.20), one can see the similarity between T and T^*. The T^* includes two additional effects i.e. the self-energy and the Pauli exclusion principle. Therefore, it is obvious that the in-medium interactions can be determined unambiguously by the Born terms which are fixed by identifying them with the NN meson exchange potentials.
In order to calculate the self-energy one must transform the G to the nuclear matter rest frame which requires projection techniques for the in-medium T-matrix as introduced by Horowitz and Serot in [HS84]. Doing so and plugging in the following expression

$$T^*(s^*) = \sum_{\alpha=1}^{5} T^\alpha f_1^\alpha f_2^\alpha \ , \qquad f_{1,2}^\alpha \in \left\{1, \gamma^\mu, \sigma^{\mu\nu}, \gamma^5\gamma^\mu, \frac{\gamma^5 \not{q}}{2m^*}\right\} \tag{2.21}$$

into Eq. (2.12) we obtain

$$\Sigma(k_F, k) = \sum_{\alpha=1}^{5} \int_0^{k_F} \frac{d^3k}{(2\pi)^3} \frac{1}{2E_q^*} f_1^\alpha \left\{ Tr\left[(\not{q} + m^*) f_2^\alpha\right] T_{dir}^\alpha - (\not{q} + m^*) f_2^\alpha T_{exc}^\alpha \right\} \ , \tag{2.22}$$

where antisymmetrized T-matrix (or G-matrix) is separated into direct and exchange contributions. The connection between these two terms can be expressed by the Fierz transformation the antisymmetrized amplitude T^α

$$T^\alpha = T_{dir}^\alpha - \sum_{k=1}^{5} F_{ki} T_{exc}^\alpha \ , \tag{2.23}$$

where F_{ki} is the Fierz matrix [Fie37]. Expressing the exchange parts in terms of direct parts can be used to simplify the Eq. (2.22) as for the direct parts. The self-consistent solution of T^* and Σ can be obtained by solving the Eqs. (2.21) and (2.22) iteratively (see [HM87] for details). Therefore the main result of the DB calculation is a self-consistent self-energy of the nucleon. Then one can calculate quantities like total binding energy and single particle energies.

Chapter 3

Density functional approach to quantum hadrodynamics

Density functional methods proved to be very successful for the discussion of the quantum many-body problem [DG90], quantum chemistry and condensed matter physics. For the nuclear case it has been demonstrated that these methods are useful for the description of average nuclear ground-state properties in the non-relativistic regime [BGH85, PnGB88, CPn$^+$90]. The success of the models on the basis of a non-relativistic formulation motivates the investigation of density functional methods in the context of relativistic theories of nuclei [SDE92, LRE04], such as Quantum hadrodynamics (QHD). This model provides a field dynamical description of hadrons where baryons interact by the exchange of mesons.

The simplest relativistic model for nuclear matter was outlined by Walecka [Wal74], in which the interaction between the two baryons is mediated by two mesons only, a scalar $\sigma-$meson which is responsible for the attractive force, and a vector $\omega-$meson responsible for the short range repulsion, necessary to reproduce saturation properties. This model is usually referred to as QHD-I.

In this chapter we review the basic concepts of the Density Functional Theory (DFT) in the context of QHD-I. The discussion starts with an extension of the existence theorem of Hohenberg-Kohn [HK64] for the case of a many fermion system interacting by the exchange of massive scalar (σ) and vector (ω) mesons.

3.1 Hohenberg-Kohn theorem for Quantum hadrodynamics

The Hohenberg-Kohn theorem [HK64] was first extended to relativistic systems by Rajagopal and Callaway [RC73, Raj78] and by MacDonald and Vosko [MV79] for the case of Quantum Electro Dynamic (QED). In contrast to the non-relativistic situation, in which the basic quantity of the theory is the ground state density, the covariant relativistic formulation, governed by an external four-potential, has to be based on the four-current density.

The Hohenberg-Kohn theorem for QED then states that the ground-state energy of a system of electrons interacting by the exchange of photons and with a classical external four-potential is a unique functional of the four-current density, $E = E[j^\mu]$. As a consequence of the additional scalar meson interaction, the scalar density has to be included in the context of QHD.

The Lagrangian density for the QHD-I model is given by Walecka [Wal74]

$$\begin{aligned}\hat{\mathcal{L}}_{QHD} = \; & \hat{\bar{\psi}}(i\gamma^\mu\partial_\mu - (M - g_s\hat{\phi}) - g_v\gamma^\mu\hat{V}_\mu)\hat{\psi} \\ & + \frac{1}{2}(\partial_\mu\hat{\phi}\partial^\mu\hat{\phi} - m_s^2\hat{\phi}^2) - \frac{1}{4}\hat{F}_{\mu\nu}\hat{F}^{\mu\nu} + \frac{1}{2}m_v^2\hat{V}_\mu\hat{V}^\mu \; . \end{aligned} \tag{3.1}$$

Here $\hat{\psi}$ denotes the baryon field operator, $\hat{\phi}$ and $\hat{V}_\mu$ the scalar and vector meson field operators, the field tensor $\hat{F}_{\mu\nu}$ is given by

$$\hat{F}_{\mu\nu} = \partial_\mu\hat{V}_\nu - \partial_\nu\hat{V}_\mu \; . \tag{3.2}$$

Furthermore, M is the nucleon mass and g_s, g_v and m_s, m_v are the scalar and vector coupling constants and masses, respectively.
The vector meson couples minimally to the conserved four-current

$$\hat{j}^\mu = \hat{\bar{\psi}}\gamma^\mu\hat{\psi} \; , \tag{3.3}$$

whereas the scalar meson couples to the scalar density

$$\hat{\rho}_s = \hat{\bar{\psi}}\hat{\psi} \; . \tag{3.4}$$

For the proof of the Hohenberg-Kohn theorem, we extend the QHD Hamiltonian derived from Eq. (3.1) by auxiliary, classical external potentials V^{μ}_{ext} and ϕ_{ext}, to give

$$\hat{H} = \hat{H}_{QHD} + \int d^3x \hat{j}^{\mu}(x) V^{ext}_{\mu}(\underline{x}) - \int d^3x \hat{\rho}_s(x) \phi^{ext}(\underline{x}) \ . \tag{3.5}$$

The potentials are assumed to be time independent and may be set equal to zero at the end of the argument. As for all field theoretical problems the Hamiltonian in Eq. (3.5) is not well-defined without further prescriptions concerning the elimination of ultraviolet divergencies and divergent vacuum expectation values. Only the inclusion of the appropriate counter term contributions (CTC) in the Lagrangian and subtraction of vacuum expectation values (VEV) (or alternatively use of normal ordering) renders the corresponding groundstate energy finite (see, e.g., [Chi77]). In the following proof we therefore use the modified Hamiltonian

$$\hat{H}_R = \hat{H} + CTC - VEV \ . \tag{3.6}$$

For a proof of the extension of the Hohenberg-Kohn theorem for QHD we shall work in a suitably defined Schrödinger picture in order and establish the connection to non-relativistic theory.
We start with the stationary relativistic wave equation for the groundstate $|g\rangle$,

$$\hat{H}_R |g\rangle = E|g\rangle \ , \tag{3.7}$$

which defines a map of the set of potentials ϕ_{ext} and V^{μ}_{ext} on the set of groundstates $|g\rangle$ (assumed to be nondegenerate) which is surjective by construction. As all four-potentials that differ only by a gauge transformation of the time-like vector potential V^0_{ext} , i.e. $V'^0_{ext}(\underline{x}) = V^0_{ext}(\underline{x}) + c$ ($c = const$), lead to the same groundstate the map should, more precisely, associate a class of potentials (differing only by these gauge transformation) with a class of groundstates (differing only by global phases).
A second map of all possible groundstates on the groundstate densities ρ_s and j^{μ} can be established by

$$\begin{aligned} \rho_{s,R} &= \langle g|\hat{\rho}_s|g\rangle + CTC \ , \\ j^{\mu}_R &= \langle g|\hat{j}^{\mu}|g\rangle + CTC \ , \end{aligned} \tag{3.8}$$

where renormalization of the densities is implied (of course, the CTC for the renormalization of j^μ are not identical with those of Eq. (3.6)). This map is surjective by construction. We will detail below that this map relates the class of all groundstates deriving from potentials which differ by general time-independent gauge transformations with the corresponding gauge invariant groundstate four-current.

The gist of the proof of the Hohenberg-Kohn theorem is the demonstration that both maps are injective and therefore, as a consequence of a general theorem from the theory of sets, bijective. The proof proceeds by reductio ad absurdum.

In order to demonstrate the injectivity of the first map, one assumes that either ϕ'_{ext} is not equal to ϕ_{ext} or that V'^{μ}_{ext} and V^{μ}_{ext} differ by more than a gauge transformation of the vector potential. If the groundstates of the eigenvalue problems with the primed and unprimed potentials,

$$\hat{H}|g\rangle = E|g\rangle \ ,$$
$$\hat{H}'|g'\rangle = E'|g'\rangle \ , \tag{3.9}$$

where identical, $|g'\rangle = e^{i\alpha}|g\rangle$ (up to global phases $e^{i\alpha}$) one finds upon subtraction of both eigenvalue equations

$$\int d^3x \left\{\hat{j}^\mu[V_{ext,\mu} - V'_{ext,\mu}] - \hat{\rho}_s[\phi_{ext} - \phi'_{ext}]\right\}|g\rangle = (E - E')|g\rangle \ . \tag{3.10}$$

Only for the case explicitly excluded, i.e., $\phi'_{ext}(\underline{x}) = \phi_{ext}(\underline{x})$ and at the same time $V'_{ext,0}(\underline{x}) = V_{ext,0}(\underline{x}) + c, \quad V'_{ext,k}(\underline{x}) = V_{ext,k}(\underline{x})$, would the left hand side of Eq. (3.10) reduce to

$$-c\int d^3x \hat{j}^0(\underline{x})|g\rangle = -cQ|g\rangle = (E - E')|g\rangle \ , \tag{3.11}$$

making use of the fact that the Hamiltonian commutes with the charge operator. Thus both potentials lead to the same groundstate with E' reflecting the energy shift introduced by this simple gauge transformation.

On the other hand one obtains for a general time-independent gauge transformation

$$V'_{ext,\mu}(\underline{x}) = V_{ext,\mu}(\underline{x}) + \partial_\mu \Lambda(\underline{x}, t) \ ,$$
$$\Lambda(\underline{x}, t) = ct + \lambda(\underline{x}) \tag{3.12}$$

the relation

$$-\int d^3x \left\{\hat{j}^i(\underline{x})\partial_i\lambda(\underline{x}) + c\hat{j}^0(\underline{x})\right\}|g\rangle = (E - E')|g\rangle \ . \tag{3.13}$$

As $|g\rangle$ is not an eigenstate of $\hat{j}^i(\underline{x})$ this equation leads to a contradiction, show that the eigenstate $|g'\rangle$ of the general gauge transformed system is not identical to $|g\rangle$.

One can also conclude, that $|g\rangle$ can not be an eigenstate of the operator on the left hand side of Eq. (3.10) if the potentials differ by more than a gauge transformation. Consequently the assumption $|g\rangle = |g'\rangle$ again leads to a contradiction. With the convention that potentials differing only by gauge transformations of the vector potential are equivalent, one may state that the map between the classes of equivalent potentials and corresponding groundstates $|g\rangle$ is injective.

The demonstration of injectivity of the second map also relies on reductio ad absurdum. If one supposes that two groundstates $|g\rangle$ and $|g'\rangle$ which belong to external potentials differing by more than a gauge transformation lead to the same densities $\rho_{s,R}$ and j^μ_R, then the Raleigh-Ritz principle states[1]

$$\begin{aligned} E &= \langle g|\hat{H}_R|g\rangle < \langle g'|\hat{H}_R|g'\rangle \\ &= \langle g'|\hat{H}'_R|g'\rangle + \langle g'|\hat{H}_R - \hat{H}'_R|g'\rangle \\ &= E' + \int d^3x \left\{ j^\mu_R(V_{ext,\mu} - V'_{ext,\mu}) - \rho_{s,R}(\phi_{ext} - \phi'_{ext}) \right\} . \end{aligned} \tag{3.14}$$

It should be noted, that the strict inequality, which is crucial for the following argument, does not hold if $|g\rangle$ and $|g'\rangle$ are eigenstates of potentials which are related by a general time-independent gauge transformation,as in Eq. (3.12). Although the proof of the injectivity of the first map demonstrated that the two states are not identical, this difference is not relevant if one considers physical observables i.e., expectation values. Expectation values exhibit only the gauge transformation properties of the operator under consideration, in our case the shift of the energy scale.

Interchanging the roles of primed and unprimed quantities one obtains the statement

$$E' < E - \int d^3x \left\{ j^\mu_R(V_{ext,\mu} - V'_{ext,\mu}) - \rho_{s,R}(\phi_{ext} - \phi'_{ext}) \right\} . \tag{3.15}$$

Addition of the two inequalities leads to the obvious contradiction

$$E + E' < E + E' . \tag{3.16}$$

[1] We assume that Raleigh-Ritz principle is valid for the renormalized Hamiltonian Eq. (3.6)

Thus the second map is also injective.

Combining the two maps one may state: The class of groundstates which is determined by all potentials differing by a general time-independent gauge transformation is uniquely related to the densities ρ_s and j^μ. Any member of this class can thus be considered to be a functional of the densities

$$|g\rangle = |g[\rho_s, j^\mu]\rangle \tag{3.17}$$

(dropping the index R for brevity). Of course, the explicit functional form will depend on the specific gauge chosen.

In nonrelativistic DFT the gauge dependence can be exploited by establishing a unique map between the gauge dependent states and the gauge dependent paramagnetic current [VR87, VR88]. In the relativistic theory, however, it should be preferable to work with the total current, as physical observables characterized by expectation values momentum

$$O[\rho_s, j^\mu] = \langle g[\rho_s, j^\mu]|\hat{O}|g[\rho_s, j^\mu]\rangle \ , \tag{3.18}$$

which are unique functionals of the groundstate densities must not depend on the specific gauge chosen.

In particular, insertion of the exact groundstate densities ρ_s and j^μ into

$$\langle g[\rho_s, j^\mu]|\hat{H}_R|g[\rho_s, j^\mu]\rangle \tag{3.19}$$

gives the exact groundstate energy E whereas the Raleigh-Ritz principle guarantees that all other ρ_s' , j'^μ lead to a higher energy,

$$\langle g[\rho_s', j'^\mu]|\hat{H}_R|g[\rho_s', j'^\mu]\rangle > E \ . \tag{3.20}$$

Ignoring the mathematical subtleties of the v-representability problem [SG95] one may use the unique groundstate energy functional

$$E[\rho_s, j^\mu] \equiv \langle g[\rho_s, j^\mu]|\hat{H}_R|g[\rho_s, j^\mu]\rangle \tag{3.21}$$

to obtain the groundstate densities by the variational equations

$$\frac{\delta}{\delta \rho_s} E[\rho_s, j^\mu] = 0 \ ,$$

$$\frac{\delta}{\delta j^\mu} E[\rho_s, j^\mu] = 0 \ , \tag{3.22}$$

to be solved under the condition of baryon number and current conservation which may be introduced by appropriate Lagragnge-multiplers.

Finally, the functional

$$F[\rho_s, j^\mu] \equiv E[\rho_s, j^\mu] - \int d^3x \left\{ j^\mu(\underline{x}) V_\mu^{ext}(\underline{x}) - \rho_s(\underline{x}) \phi^{ext}(\underline{x}) \right\} \tag{3.23}$$

is universal, i.e. it does not depend on the external potentials at all. Note that $F[\rho_s, j^\mu]$ is gauge invariant. It is the external potential energy term

$$- \int d^3x j^\mu(\underline{x}) V_\mu^{ext}(\underline{x}) \tag{3.24}$$

in Eq. (3.23) which produces exactly the required gauge transformation property of the total energy.

This completes the proof of the Hohenberg-Kohn theorem for QHD as we now can set the auxiliary external potentials equal to zero. The functional $F[\rho_s, j^\mu]$ is the energy functional of the QHD system without external potentials.

The proof of the existence of one-to-one mappings between groundstate observables and groundstates densities does not give any hint for the construction of explicit density functionals. However, the fact that the set of densities may be considered to be the basic variables of the theory makes it worthwhile to pursue this approach to the many body problem.

3.2 Quantum hadrodynamics (QHD)

The field equations for this model follow from the Euler-Lagrange equations using Eq. (3.1) and can be written as

$$(\partial_\mu \partial^\mu + m_s^2)\phi = g_s \bar{\psi}\psi \ , \tag{3.25}$$

$$\partial_\mu F^{\mu\nu} + m_v^2 V^\nu = g_v \bar{\psi}\gamma^\nu \psi \ , \tag{3.26}$$

$$[\gamma^\mu (i\partial_\mu - g_v V_\mu) - (M - g_s \phi)]\psi = 0 \ . \tag{3.27}$$

Equation (3.25) is a Klein-Gordon equation with a scalar source term. Equation (3.26) is the Proca equation for the vector ω field and it looks like massive QED with the

conserved baryon current

$$B^\mu = \bar{\psi}\gamma^\nu\psi, \ \partial_\mu B^\mu = 0 \ . \tag{3.28}$$

rather than the (conserved) electromagnetic current as source. Finally, Eq. (3.27) is the Dirac equation with scalar and vector fields entering in a minimal fashion.

The energy and momentum densities and currents associated with the fields are summarized in the form of the energy-momentum tensor $T_{\mu\nu}$, which is defined as

$$T_{\mu\nu} = -g_{\mu\nu}\mathcal{L} + \partial_\nu \frac{\partial \mathcal{L}}{\partial(\partial_\nu q_i)} \tag{3.29}$$

where the repeated index i stands for the sum over all the generalized coordinates (i.e. the fields). If $\mathcal{L}$ does not explicitly depend on space-time coordinates x^μ, these field equations imply that the canonical energy-momentum tensor $T_{\mu\nu}$ is conserved, i.e.

$$\frac{\partial}{\partial x_\mu} T_{\mu\nu} \equiv \partial^\mu T_{\mu\nu} = 0 \ , \tag{3.30}$$

indicating that $T_{\mu\nu}$ corresponds to the Noether current connected to the space-time translations. This implies that the four-momentum

$$P^\mu = (H, \mathbf{P}) = g^{\mu\nu} P_\nu$$

defined by

$$P_\nu = \int d^3x T_{0\nu} \tag{3.31}$$

is a constant of the motion. Inserting Eq. (3.1) into Eq. (3.29) and making use of the field equation Eq. (3.27) we get the following expression for the energy-momentum tensor:

$$\begin{aligned} T_{\mu\nu} = \ & \frac{1}{2}\left[-\partial_\lambda\phi\partial^\lambda\phi + m_s^2\phi^2 + \frac{1}{2}F_{\lambda\eta}F^{\lambda\eta} - m_v^2 V_\lambda V^\lambda\right] g_{\mu\nu} \\ & + i\bar{\psi}\gamma_\mu\partial_\nu\psi + \partial_\mu\phi\partial^\nu\phi + \partial_\nu V^\lambda F_{\lambda\mu} \ . \end{aligned} \tag{3.32}$$

For a uniform and isotropic system, the observed energy-momentum tensor must have the form [Wei72]

$$\langle T_{\mu\nu}\rangle = (\mathcal{E} + p)u_\mu u^\nu - p g_{\mu\nu} \ , \tag{3.33}$$

where p is the pressure, $\mathcal{E}$ is the energy density and u_μ is the four-velocity of the fluid. The four-velocity satisfies $u_\mu^2 = 1$ and, for a fluid at rest, $u^\mu = (1, \mathbf{0})$. This allows us to identify

$$P = \frac{1}{3}\langle T_{ii} \rangle \tag{3.34}$$

$$\mathcal{E} = \langle T_{00} \rangle. \tag{3.35}$$

Since Eqs. (3.25-3.27) are non-linear quantum field equations and they can not be solved exactly. But this model can be solved analytically for nuclear matter in the mean-field approximation (discussed in detail in [SW86]).
The feature of QHD-I is the fact that the nuclear saturation mechanism naturally arises from the relativistic description and in particular, from the appearance of two strong mean fields (σ and ω). The different Lorentz structure of these two strong mesonic fields leads to the correct minimum value ($E/A = -15,7$ MeV) for the binding energy per nucleon, and, on the other hand, to a strong spin-orbit splitting [HS84, HS87, HM87]. However, at the saturation density ($\rho_0 = -15.74$ fm^{-3}), the predicted value of the effective mass ($m^* = 0.55$M) is too small and the predicted value of the nuclear incompressibility ($K \simeq 540$) MeV is too high. These are the deficiencies of the QHD-I.

QHD-I represented first attempt to consistently describe equilibrium and dynamical properties of nuclear systems at the hadronic level and it has been extended in several ways. Scalar meson self interactions of order ϕ^3 and ϕ^3 have been introduced by Boguta and Bodmer [BB77, Bod91] where the strengths of these non-linear interactions are considered as additional, adjustable parameters to be determined by the saturation properties of the nuclear matter. Another extension of the original QHD was first considered by Serot [Ser79a, Ser79b], referred to as QHD-II where the Coulomb repulsion between the protons taken into account as well as an additional isovector particle, the ρ-meson, which accounts for the neutron excess in heavy nuclei.

Chapter 4

Density Dependent Relativistic Hadron Field theory (DDRH)

4.1 The DDRH Lagrangian

The starting point of relativistic models with baryonic and mesonic degrees of freedom is a Lagrangian density $\mathcal{L}$ with Dirac spinors describing the baryons interacting via the exchange of mesons and the photon which are Bose fields. The Lagrangian density $\mathcal{L}$ contains three terms:

$$\mathcal{L} = \mathcal{L}_B + \mathcal{L}_M + \mathcal{L}_{int} \ , \tag{4.1}$$

with

$$\mathcal{L}_B = \overline{\Psi}(i\gamma_\mu \partial^\mu - M)\Psi \ , \tag{4.2}$$

$$\begin{aligned} \mathcal{L}_M = & \frac{1}{2}\sum_{i=\sigma,\delta,\pi,\eta}\left(\partial_\mu \Phi_i \partial^\mu \Phi_i - m_i^2 \Phi_i^2\right) - \\ & \frac{1}{2}\sum_{k=\omega,\rho,\gamma}\left(\frac{1}{2}F_{\mu\nu}^{(k)}F^{(k)\mu\nu} - m_k^2 A_\mu^{(k)} A^{(k)\mu}\right) \ , \end{aligned} \tag{4.3}$$

and

$$\begin{aligned} \mathcal{L}_{int} = & \overline{\Psi}\hat{\Gamma}_\sigma(\hat{\rho})\Psi\Phi_\sigma - \overline{\Psi}\hat{\Gamma}_\omega(\hat{\rho})\gamma_\mu\Psi A^{(\omega)\mu} + \\ & \overline{\Psi}\hat{\Gamma}_\delta(\hat{\rho})\tilde{\tau}\Psi\mathbf{\Phi}_\delta - \overline{\Psi}\hat{\Gamma}_\rho(\hat{\rho})\gamma_\mu\tilde{\tau}\Psi\mathbf{A}^{(\rho)\mu} - \\ & \overline{\Psi}\hat{\Gamma}_\eta(\hat{\rho})\gamma_5\Psi\Phi_\eta - \bar{\Psi}\hat{\Gamma}_\pi(\hat{\rho})\gamma_5\gamma_\mu\tilde{\tau}\Psi\partial^\mu\mathbf{\Phi}_\pi - \\ & e\overline{\Psi}\hat{Q}\gamma_\mu\Psi A^{(\gamma)\mu} \ . \end{aligned} \tag{4.4}$$

Here $\mathcal{L}_B$ and $\mathcal{L}_M$ are the free baryonic and mesonic Lagrangians, respectively, and the meson-baryon interactions are described by $\mathcal{L}_{int}$ that includes the vertex functionals $\hat{\Gamma}_\alpha(\hat{\rho})$ $(\alpha = \sigma, \delta, \pi, \eta, \omega, \rho)$. In addition, here the bold-faced symbols indicate the vectors in isospin space and vectors in ordinary three-dimensional space.
The field strength tensor $F_{\mu\nu}^{(k)}$ of either the vector mesons $(k = \omega, \rho)$ or photon $(k = \gamma)$ is given by

$$F_{\mu\nu}^{(k)} = \partial_\mu A_\nu^{(k)} - \partial_\nu A_\mu^{(k)} \ . \tag{4.5}$$

The electric charge operator $\hat{Q}$ is given by

$$\hat{Q} = \frac{1}{2}(1 + \tau_3) \tag{4.6}$$

where $\tau_3 = \pm 1$ for protons and neutrons, respectively.

The different types of mesons are distinguished by their quantum numbers, such as spin, parity and isospin, which determine the Lorentz structure of these fields. For simplicity we use mesons with lowest quantum numbers to generate the effective fields in the nucleus and as few mesons as possible which are known from experiments in free space. Based on such consideration we can use in the simplest model only mesons with spin $J = 0$ and 1, i.e. scalar and vector mesons. For the nuclear structure calculations DDRH is used in Relativistic Mean Field (RMF) approximation. Parity (P) conservation of the mean field determines on the Hartree level the parity of the mesons, i.e. it excludes pseudo-scalars and pseudo-vectors. In a first approximation we also consider only mesons with isospin $I = 0$. In such a case the σ meson with quantum numbers $J^P = 0^+$, $I = 0$ and the ω meson with quantum numbers $J^P = 1^-$, $I = 0$ are included in the calculation. This is corresponds to the $\sigma - \omega$ model of Walecka as discussed in the Sec. 3.2, but with density dependent vertices.
In realistic nuclei the Coulomb field has to be considered, i.e. one has to take into account also the photon, and for medium-heavy and heavy nuclei the asymmetry energy requires an additional meson carrying isospin. This means we have to add also the ρ meson with quantum numbers $J^P = 1^-$, $I = 1$ and the $\delta/a_0(980)$ meson with quantum numbers $J^P = 0^+$, $I = 1$. We include therefore for the nuclear matter calculations the mean-field producing isoscalar mesons σ and ω, the isovector $\delta/a_0(980)$ and ρ mesons and the photon γ.

The important difference to standard QHD models [Wal74, SW86, GRT90] is that the meson-baryon vertices $\hat{\Gamma}_\alpha(\hat{\rho})$ are functionals of the baryon field operators Ψ. Lorentz

Meson i	$m_i\ [MeV]$	J spin/parity	I isospin	Type
σ	550	0^+	0	Scalar-IsoScalar
δ	983	0^+	1	Scalar-IsoVector
ω	783	1^-	0	Vector-IsoScalar
ρ	770	1^-	1	Vector-IsoVector

Table 4.1: Mesons

invariance requires that the vertices depend on Lorenz-scalar bilinear forms $\hat{\rho}(\overline{\Psi},\Psi)$ of the baryon field operators, where in principle the standard set of the five Dirac invariants $\{1,\gamma_5,\gamma_\mu,\gamma_5\gamma_\mu,\sigma_{\mu\nu}\}$ are allowed.
One can also use other choices, since the consistency of the theory is preserved for any Lorentz-invariant combination of baryon and meson field operators. However, there are some arguments, why to use the description of medium effects by functionals of baryon field operators only:

- This leaves the meson field unchanged and ascribes many body effects completely to the baryon self energies. Therefore, only the baryon sector of the model is affected. This choice is also consistent with the approach underlying (realistic) NN interactions.
- The vertices are dynamical entities even in the mean field limit, because the fermions are always treated as Dirac quantum fields.
- In this case, the uncertainties of parameters are kept on a controllable level and give more transparent relation to the QHD-type approaches.

The dynamics of the theory is obtained by deriving the field equations from the Lagrangian, Eq. (4.1), using the Euler-Lagrange equation of motion for a field,

$$\frac{\partial\mathcal{L}}{\partial\phi_i}-\partial_\mu\left(\frac{\partial\mathcal{L}}{\partial(\partial_\mu\phi_i)}\right)=0\ ,\quad \phi_i=\overline{\Psi},\Psi,\Phi_\sigma,\mathbf{\Phi}_\delta,A_\mu^{(\omega)},\mathbf{A}_\mu^{(\rho)},A_\mu^{(\gamma)}\ . \tag{4.7}$$

For the mesons, we obtained the Klein-Gordon and Proca equations being formally of the standard form but with a source term including the density dependent vertex functionals,

$$(\partial_\mu\partial^\mu+m_\sigma^2)\Phi_\sigma=\hat{\Gamma}_\sigma(\hat{\rho})\overline{\Psi}\Psi\ , \tag{4.8}$$

$$(\partial_\mu\partial^\mu+m_\delta^2)\mathbf{\Phi}_\delta=\hat{\Gamma}_\delta(\hat{\rho})\overline{\Psi}\tau\Psi\ , \tag{4.9}$$

$$(\partial_\mu F^{(\omega)\mu\nu} + m_\omega^2 A_\omega^\nu) = \hat{\Gamma}_\omega(\hat{\rho})\overline{\Psi}\gamma^\nu\Psi \ , \tag{4.10}$$

$$(\partial_\mu F^{(\rho)\mu\nu} + m_\rho^2 \mathbf{A}_\rho^\nu) = \hat{\Gamma}_\rho(\hat{\rho})\overline{\Psi}\tau\gamma^\nu\Psi \ , \tag{4.11}$$

$$\partial_\mu F^{(\gamma)\mu\nu} = e\overline{\Psi}\hat{Q}\gamma^\nu\Psi \ . \tag{4.12}$$

Since the Lagrangian contains parts, in Eq. (4.4), which depend intrinsically on the field operators, the Euler-Lagrange equations immediately lead to

$$\frac{\delta\mathcal{L}_{int}}{\delta\overline{\Psi}} = \frac{\partial\mathcal{L}_{int}}{\partial\overline{\Psi}} + \frac{\partial\mathcal{L}_{int}}{\partial\hat{\rho}}\frac{\delta\hat{\rho}}{\delta\overline{\Psi}} \tag{4.13}$$

which includes the variation of the vertex functionals. From the first term on the right hand side of this expression we get the normal scalar $\hat{\Sigma}^{s(0)}$ and vector $\hat{\Sigma}^{\mu(0)}$ self-energies as:

$$\hat{\Sigma}^{s(0)} = \hat{\Gamma}_\sigma(\hat{\rho})\Phi_\sigma + \hat{\Gamma}_\delta(\hat{\rho})\tilde{\tau}\mathbf{\Phi}_\delta \ , \tag{4.14}$$

$$\hat{\Sigma}^{\mu(0)} = \hat{\Gamma}_\omega(\hat{\rho})A^{(\omega)\mu} + \hat{\Gamma}_\rho(\hat{\rho})\tilde{\tau}\mathbf{A}^{(\rho)\mu} + e\hat{Q}A^{(\gamma)\mu} \ . \tag{4.15}$$

Before calculating the second term on the right hand side of the Eq. (4.13) the specific form of the $\hat{\rho}$ has to be defined in order to obtain the additional self-energies. In general, we may expand $\hat{\rho}$ into a superposition of the above considered Dirac-invariants, i.e.

$$\hat{\rho}(\overline{\Psi},\Psi) = A_s\overline{\Psi}\Psi + B(\overline{\Psi}\gamma_\mu\Psi)^2 + C_s(\overline{\Psi}\tilde{\tau}\Psi)^2 + D(\overline{\Psi}\gamma_\mu\tilde{\tau}\Psi)^2 + \ldots \tag{4.16}$$

where the unknown parameters A_s, B, C_s, D have to be determined independently.
In the Eq. (4.16) the first two terms are relevant for the scalar and vector densities and the last two terms are relevant for the isoscalar and isovector densities. Since all the terms appear quadratically the Lorentz-invariant is manifest Due to the aim of this work and for simplicity reasons determine only the scalar and vector densities. The reasons are following:

- The isovector density vanishes in the case of symmetric nuclear matter.

- The parametrization of DB density dependent vertices does not depend on the isovector density.

We choose therefore $C_s = D = 0$. The remaining two physically reasonable forms of $\hat{\rho}$ are the scalar and vector density dependences, SDD and VDD, given in the [FLW95],

$$\hat{\rho}_{SDD} \equiv \overline{\Psi}\Psi \ , \qquad \hat{\rho}_{VDD} \equiv \sqrt{(\overline{\Psi}\gamma_\mu\Psi)(\overline{\Psi}\gamma^\mu\Psi)} = \sqrt{j_\mu j^\mu} \ . \tag{4.17}$$

Here, j_μ is the baryon vector current and the variation of $\hat{\rho}$ with respect to the $\overline{\Psi}$ is

$$\frac{\partial\hat{\rho}_{SDD}}{\partial\overline{\Psi}} = \Psi \ , \qquad \frac{\partial\hat{\rho}_{VDD}}{\partial\overline{\Psi}} = \frac{\gamma_\mu j^\mu}{\sqrt{j_\mu j^\mu}}\Psi = \gamma_\mu \hat{u}^\mu \Psi \ . \tag{4.18}$$

Eq. (4.13) leads to the additional so called scalar $\hat{\Sigma}^{s(r)}$ and vector $\hat{\Sigma}^{\mu(r)}$ rearrangement self-energies [LF95] for the SDD and the VDD as:

$$\begin{aligned}\hat{\Sigma}^{s(r)} &= \left(\frac{\partial\hat{\Gamma}_\omega(\hat{\rho})}{\partial\hat{\rho}} A^{(\omega)\nu}\overline{\Psi}\gamma_\mu\Psi + \frac{\partial\hat{\Gamma}_\rho(\hat{\rho})}{\partial\hat{\rho}} \mathbf{A}^{(\rho)\nu}\overline{\Psi}\gamma_\mu\tilde{\tau}\Psi \right. \\ &\quad \left. - \frac{\partial\hat{\Gamma}_\sigma(\hat{\rho})}{\partial\hat{\rho}}\Phi_\sigma\overline{\Psi}\Psi - \frac{\partial\hat{\Gamma}_\delta(\hat{\rho})}{\partial\hat{\rho}}\mathbf{\Phi}_\delta\overline{\Psi}\tilde{\tau}\Psi \right) \ ,\end{aligned} \tag{4.19}$$

$$\begin{aligned}\hat{\Sigma}^{\mu(r)} &= \left(\frac{\partial\hat{\Gamma}_\omega(\hat{\rho})}{\partial\hat{\rho}} A^{(\omega)\nu}\overline{\Psi}\gamma_\mu\Psi + \frac{\partial\hat{\Gamma}_\rho(\hat{\rho})}{\partial\hat{\rho}} \mathbf{A}^{(\rho)\nu}\overline{\Psi}\gamma_\mu\tilde{\tau}\Psi \right. \\ &\quad \left. - \frac{\partial\hat{\Gamma}_\sigma(\hat{\rho})}{\partial\hat{\rho}}\Phi_\sigma\overline{\Psi}\Psi - \frac{\partial\hat{\Gamma}_\delta(\hat{\rho})}{\partial\hat{\rho}}\mathbf{\Phi}_\delta\overline{\Psi}\tilde{\tau}\Psi \right) \hat{u}^\mu \ .\end{aligned} \tag{4.20}$$

The four-velocity $\hat{u}^\mu$ is defined as $(1-v^2)^{-1/2}(1,v)$ and is related to the baryon vector current. In the rest frame of the nuclear matter $v = 0$, therefore $u_\mu = (1,\mathbf{0})$ and $\hat{u}^\mu\hat{u}_\mu = 1$. The rearrangement self-energies account physically for the static polarization effects in the nuclear medium, canceling certain classes of particle-hole diagrams [Neg82]. For non-relativistic many-body theory Negele was the first to point to the importance of the rearrangement self-energies in assuring that basic properties of the full theory are restored in the reduced model problem [Neg82]. These self-energies also assure the thermodynamical consistency and covariance which would not be given using a formulation based on densities only. The thermodynamical consistency means that:

- the thermodynamical and the mechanical pressure of the nuclear matter are an

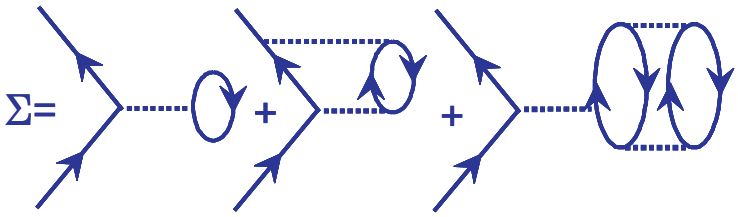

Figure 4.1: Diagrammatic representation of the total baryon self-energy, including the HF tadpole diagram and propagator and vertex renormalization due the rearrangement. The dashed lines indicate meson exchange, all vertices are to be calculated with the full DB-interaction.

equal at the zero temperature

$$P = \frac{1}{3}\sum_{i=1}^{3}\langle T^{ii}\rangle = \rho^2 \frac{\partial}{\partial \rho}\left(\frac{\epsilon}{\rho}\right) \tag{4.21}$$

- the Hugenholtz-van Hove theorem [HvH58]

$$\epsilon + P = \rho E(k_F) = \sum_{b=n,p} \rho_b E_b(k_F) \ , \tag{4.22}$$

is satisfied. Which states that at equilibrium density, the average energy per particle equals the single particle energy at the Fermi surface.

A rigorous proof of the thermodynamical consistency of the DDRH theory can be found in Chapter. 6 .

Defining the total baryon self-energies from Eqs. (4.14-4.15) and Eqs. (4.19-4.20)

$$\hat{\Sigma}^s = \hat{\Sigma}^{s(0)} + \hat{\Sigma}^{s(r)}, \qquad \hat{\Sigma}^\mu = \hat{\Sigma}^{\mu(0)} + \hat{\Sigma}^{\mu(r)} \tag{4.23}$$

which are graphically represented in Fig. 4.1 , The baryon field equations given by Dirac equations retain their standard form,

$$\left[\gamma_\mu(i\partial^\mu - \hat{\Sigma}^\mu) - (M - \hat{\Sigma}^s)\right]\Psi = 0 \ . \tag{4.24}$$

The dynamics of the Dirac equations are modified however by the rearrangement self-energies. From the Eqs. (4.23-4.24) we can easily conclude that the SDD description adds a correction to the scalar self energy, i.e., it modifies the nucleon effective mass

$$m^* = M - \hat{\Sigma}^s = M - \hat{\Sigma}^{s(0)} - \hat{\Sigma}^{s(r)} \ , \tag{4.25}$$

while the VDD description adds a correction to the vector self-energy. This shows that the dynamics of the fields are directly affected by the structure of $\hat{\rho}$. Obviously a clear definition is needed in order to avoid ambiguities in the choice of the density operator $\hat{\rho}$. For that issue VDD is a more natural choice for $\hat{\rho}$, because the baryon vector density is a conserved quantity, connected to the conserved baryon number. The scalar density is a dynamical quantity to be determined self-consistently by the equations of motion. In infinite nuclear matter this is scan very clearly because the expectation value $\rho_s = \langle \bar{\Psi}\Psi \rangle$ depends on the Fermi-momentum and, therefore, the density. Furthermore VDD gives a more direct relation between the self-energies of the DDRH and DB microscopic self-energies [HKL01b].
From a more parctical side, [FLW95] also show that compared to SDD, VDD leads to a better description of the bulk properties and low energy single particle excitations in spherical nuclei using DBHF interactions. Therefore in the following we assume the vector density dependence of the meson-nucleon couplings.

4.2 Relativistic Mean Field approximation

In the RMF approximation the complexities of the operator-valued functionals and their derivatives can be replaced by functions of ground state expectation values using Wick's theorem [Wic50, PS95]. According to Wick's theorem we can define

$$\hat{\rho} = \rho + C(\hat{\rho}) \tag{4.26}$$

where ρ denotes the c-valued, fully contracted product of the field operators contained in $\hat{\rho}$ and $C(\hat{\rho}) = \hat{\rho} - \rho$ the remaining higher correlations, which always contain at least one normal ordered product of field operators. Taking the expectation value of $\hat{\rho}$ with respect to a many-body ground state $|0\rangle$, only ρ will survive, since due to its normal ordered parts $\langle 0|C(\hat{\rho})|0\rangle = 0$ and $\langle \hat{\rho} \rangle = \rho$. Hence the vertex functionals are converted into

functions of the ground state density

$$\langle \hat{\Gamma}_\alpha(\hat{\rho}) \rangle = \Gamma_\alpha \left(\langle \hat{\rho} \rangle \right) = \Gamma_\alpha(\rho) \tag{4.27}$$

and accordingly

$$\left\langle \frac{\partial \hat{\Gamma}_\alpha(\hat{\rho})}{\partial \hat{\rho}} \right\rangle = \frac{\partial \Gamma_\alpha(\rho)}{\partial \rho} \ . \tag{4.28}$$

By taking ground state expectation values on both side of Eqs. (4.8-4.12) we can change the highly non-linear field equations into the tractable forms

$$(-\nabla^2 + m_\sigma^2)\Phi_\sigma = \Gamma_\sigma(\rho)\rho^s \ , \tag{4.29}$$

$$(-\nabla^2 + m_\omega^2)A_0^\omega = \Gamma_\omega(\rho)\rho \ , \tag{4.30}$$

$$(-\nabla^2 + m_\delta^2)\Phi_\delta = \Gamma_\delta(\rho)\rho_3^s \ , \tag{4.31}$$

$$(-\nabla^2 + m_\rho^2)A_0^\rho = \Gamma_\rho(\rho)\rho_3 \ , \tag{4.32}$$

$$-\nabla^2 A_0^\gamma = -e\rho_p \ , \tag{4.33}$$

with the corresponding source terms are given by

$$\rho^s = \langle \bar{\Psi}\Psi \rangle = \rho_n^s + \rho_p^s \ , \tag{4.34}$$

$$\rho = \langle \bar{\Psi}\gamma_0\Psi \rangle = \rho_n + \rho_p \ , \tag{4.35}$$

$$\rho_3^s = \langle \bar{\Psi}\tau_3\Psi \rangle = \rho_n^s - \rho_p^s \ , \tag{4.36}$$

$$\rho_3 = \langle \bar{\Psi}\gamma_0\tau_3\Psi \rangle = \rho_n - \rho_p \ , \tag{4.37}$$

where ρ^s and ρ are the scalar and the vector densities, ρ_3^s and ρ_3 are the isoscalar and isovector densities, respectively.

The meson fields are treated as a static classical fields. These fields describe in an average way the interaction produced by the exchange of the corresponding mesons. Time reversal symmetry is assumed, therefore only the zero component of the vector fields contributes.

The nucleons remain quantum fields and moving with relativistic dynamics under

the action of classical meson fields. The Dirac equation is

$$\left[\gamma_\mu(i\partial^\mu - \Sigma_b^\mu(\rho)) - (M - \Sigma_b^s(\rho))\right]\Psi_b = 0 \tag{4.38}$$

with the static self energies

$$\Sigma_b^{s(0)}(\rho) = \Gamma_\sigma(\rho)\Phi_\sigma + \tau_b\Gamma_\delta(\rho)\Phi_\delta \ , \tag{4.39}$$

$$\Sigma_b^{0(0)}(\rho) = \Gamma_\omega(\rho)A_0^{(\omega)} + \tau_b\Gamma_\rho(\rho)A_0^{(\rho)} + e\frac{1-\tau_b}{2}A_0^{(\gamma)} \ , \tag{4.40}$$

and the rearrangement self-energy

$$\begin{aligned}\Sigma^{0(r)}(\rho) = &\left(\frac{\partial\Gamma_\omega(\rho)}{\partial\rho}A_0^{(\omega)}\rho + \frac{\partial\Gamma_\rho(\rho)}{\partial\rho}A_0^{(\rho)}\rho_3\right.\\ &\left. - \frac{\partial\Gamma_\sigma(\rho)}{\partial\rho}\Phi_\sigma\rho_s - \frac{\partial\Gamma_\delta(\rho)}{\partial\rho}\Phi_\delta\rho_3^s\right) \ .\end{aligned} \tag{4.41}$$

The contribution of the rearrangement self-energy to the baryon field equations show that DDRH approach accounts for quantal fluctuations of the baryon fields even in the ground state.

In the RMF approximation DDRH theory reduces to the Hartree description with density dependent coupling constants similar to the initial proposal of Brockmann and Toki [BT92].

However, in DDRH theory the functional form of the vertices is determined theoretically from in-medium Dirac-Brueckner interactions, obtained from the realistic Bonn [Mac89, BM90] and Groningen free-space NN interactions [HM87, Mal88]. In infinite nuclear matter, density dependence of the vertices is obtained by mapping the self-consistent DBHF self-energies to the corresponding DDRH expressions.

Chapter 5

Density-dependent Meson-Baryon vertices

The density dependent meson-baryon vertices can be described by two different approaches, which one may call microscopic and phenomenological, respectively. The suitable and successful microscopic method is relativistic Dirac-Brueckner (DB) approach (see Chap. 2) where the density dependent meson-baryon vertices can be obtained from the calculations of the nucleon self-energies in symmetric and asymmetric nuclear matter [FLW95, dJL98a]. The phenomenological approach [TW99, NVFR02, LNVR05] determines the density dependence of the meson-baryon vertices empirically by making an ansatz for the functional form with some parameters which can be obtained from a fit to properties of nuclear matter and finite nuclei. In this chapter, we discuss these two approaches briefly.

5.1 Microscopic Meson-Baryon vertices in Infinite nuclear matter

In Chapter. 4 by using RMF approximation in DDRH we have shown that the density dependent vertex functionals are can be converted into functions of the ground state baryon density $\Gamma_i(\rho)$ in Eqs. (4.27-4.28). In addition, we have mentioned that this DDRH vertices $\Gamma_i(\rho)$ are deduced from microscopic Dirac-Brueckner (DB) calculations of symmetric and asymmetric nuclear matter. Therefore in this section we would like to discuss about that how the DB vertices $\Gamma_i^{DB}(\rho)$ of the isoscalar ($i = \sigma, \omega$) and isovector

($i = \delta, \rho$) mesons enter to the DDRH calculations.

One possible way to obtain such a relationship between $\Gamma_i^{DB}(\rho)$ and $\Gamma_i^{DDRH}(\rho)$ is to equalize the full DB energies to the mean field DDRH interaction energies.
The total ground state interaction energy for a spin-saturated system of quasi-particles at $T = 0$ is given by integrating the proton and neutron self-energies over the respective Fermi spheres K_F of occupied states [Len04] as

$$W_b^{DBHF}(k_F) = tr_s \int_{K_F} \frac{d^3k}{(2\pi)^3} \Sigma_b^{DBHF}(k, k_F) \tag{5.1}$$

where s is a spin ($s = 1/2$) and the index b distinguishes between neutrons and protons ($b = p, n$). Accordingly, the equality of the DB and DDRH total energies can be written

$$W_b^{DBHF}(k_F) = W_b^{DDRH}(k_F) = \rho_b(k_F)\Sigma_b^{DDRH}(k_F) \tag{5.2}$$

where $W_b^{DDRH}(k_F)$ is defined as in Eq. (5.1) but integrating the RMF self-energies $\Sigma_b^{DDRH}(k_F)$. Clearly, this approach is only applicable for the mean-field producing meson field.
The field Eqs. (4.29-4.33) simplify further by magic of translational and rotational invariance if we apply for infinite nuclear matter which is an isotropic and homogenous system. Doing so and neglecting the electromagnetic field, the meson field equations for infinite nuclear matter can be written

$$m_i^2 \Phi_i = \Gamma_i(\rho)\rho_i \ . \tag{5.3}$$

Plugging the mean-field self-energies $\Sigma^{MF} = \Gamma_i(\rho)\Phi_i$ into the meson field Eqs. (5.3) we find [HKL01b]

$$\frac{\Gamma_i^2(\rho)}{m_i^2}\rho_i = \Sigma^{DBHF} \ , \tag{5.4}$$

with ρ_i being the corresponding density to a meson field Φ_i as defined in Eqs. (4.34-4.37).
Results of the Dirac-Brueckner calculations are the binding energy and the DB self-energies Σ^{DB} and their expressions can be found in the literature, e.g. [HS87] for symmetric nuclear matter and [dJL98a, dJL98b] for asymmetric nuclear matter, respectively. From these scalar $\Sigma^{s(DB)}$ and vector $\Sigma^{0(DB)}$ self-energies of protons and neutrons, one can extract the intrinsic density dependence of isoscalar and isovector meson-baryon

vertices as in [dJL98a] for the asymmetric nuclear matter

$$\left(\frac{\Gamma_\sigma}{m_\sigma}\right)^2 = \frac{1}{2}\frac{\Sigma_n^{s(DB)}(k_{Fp},k_{Fn}) + \Sigma_p^{s(DB)}(k_{Fp},k_{Fn})}{\rho_n^s + \rho_p^s} \,, \tag{5.5}$$

$$\left(\frac{\Gamma_\omega}{m_\omega}\right)^2 = \frac{1}{2}\frac{\Sigma_n^{0(DB)}(k_{Fp},k_{Fn}) + \Sigma_p^{0(DB)}(k_{Fp},k_{Fn})}{\rho_n + \rho_p} \,, \tag{5.6}$$

$$\left(\frac{\Gamma_\delta}{m_\delta}\right)^2 = \frac{1}{2}\frac{\Sigma_n^{s(DB)}(k_{Fp},k_{Fn}) - \Sigma_p^{s(DB)}(k_{Fp},k_{Fn})}{\rho_n^s - \rho_p^s} \,, \tag{5.7}$$

$$\left(\frac{\Gamma_\rho}{m_\rho}\right)^2 = \frac{1}{2}\frac{\Sigma_n^{0(DB)}(k_{Fp},k_{Fn}) - \Sigma_p^{0(DB)}(k_{Fp},k_{Fn})}{\rho_n - \rho_p} \,. \tag{5.8}$$

From above expressions one can see that in general the vertices could depend on the proton and neutron scalar and vector densities independently. In practice though, this is usually done by neglecting the isovector density $\rho \equiv \rho_n - \rho_p$ dependence of the vertices due to its too weak influence and put the density dependence of the vertices only into the isoscalar vector density $\rho \equiv \rho_p + \rho_n$ or, equivalently, the mean Fermi momentum $k_F \sim \rho^{1/3}$.

5.2 Momentum dependence of the Self-energies

The ratios Γ_i/m_i play a crucial role to determine the properties of the equation of state (EOS) and it has been observed in [HKL01b] that description of the original DBHF nuclear matter EOS calculated by DDRH is considerably improved when accounting for the momentum dependence of the DB self-energies which is neglected in the original DB calculations. Expanding the full DB self-energies around the Fermi momentum into a Taylor series in k^2,

$$\begin{aligned}\Sigma^{DBHF}(k,k_F) &= \Sigma^{DBHF}(k_F,k_F) + (k^2-k_F^2)\frac{\partial\Sigma^{DBHF}(k,k_F)}{\partial k^2}|_{k=k_F} + \mathcal{O}(k^4) \\ &\equiv \Sigma^{DBHF}(k_F) + (k^2-k_F^2)\Sigma'^{DBHF}(k_F)\end{aligned} \tag{5.9}$$

where we identify the first term with the Hartree self-energy and we find

$$\begin{aligned}\rho(k_F)\Sigma^{DDRH}(k_F) &= \frac{4}{(2\pi)^3}\int_{|k|\leq k_F} d^3k\Sigma^{DBHF}(k,k_F) \\ &= \rho(k_F)\left[\Sigma^{DBHF}(k_F) - \Sigma'^{DBHF}(k_F)\frac{2}{5}k_F^5\right] \\ &= \rho(k_F)\Sigma^{DBHF}(k_F)\left[1-\frac{2}{5}k_F^2\frac{\Sigma'^{DBHF}(k_F)}{\Sigma^{DBHF}(k_F)}\right] . \end{aligned} \tag{5.10}$$

In Eq. (5.10), the term in brackets is the correction which assures the correct reproduction of the original DBHF equation of state in DDRH calculation. This correction term also modifies the vertices

$$\Gamma_i^2(k_F) \longrightarrow \tilde{\Gamma}_i^2(k_F) \equiv \Gamma_i^2(k_F)\left[1-\frac{2}{5}k_F^2\frac{\Sigma'^{DBHF}(k_F)}{\Sigma^{DBHF}(k_F)}\right] . \tag{5.11}$$

Assuming the ratio $\Sigma'^{DBHF}(k_F)/\Sigma^{DBHF}(k_F)$ to depend weakly on k_F and we introduce the momentum corrected meson-nucleon vertices as

$$\tilde{\Gamma}_i(k_F) = \Gamma_i(k_F)\sqrt{1+\zeta_i k_F^2} , \tag{5.12}$$

where ζ_i are constants determined by adjusting the DDRH binding energies to the DBHF equation of state. The rearrangement terms are modified as follows

$$\begin{aligned}\frac{\partial\tilde{\Gamma}_i(k_F)}{\partial\rho} &= \sqrt{1+\zeta_i k_F^2}\,\frac{\partial\Gamma_i(k_F)}{\partial\rho} \\ &+ \frac{k_F}{3\rho}\frac{k_F\zeta_i}{\sqrt{1+\zeta_i k_F^2}}\,\Gamma_i(k_F)\end{aligned} \tag{5.13}$$

On the other hand, one can make a more general ansatz that $\zeta_i(k_F)$ may depend on the Fermi momentum. In this case, the contributions from scalar mesons can be treated accordingly, however due to the consistency of these quantities $\Sigma^{s(0)}, m^*$ and ρ_s, it is not possible to make a closed form for the exact momentum correction. In other words, the scalar self-energy $\Sigma^{s(0)}$ is contained in the effective mass of the nucleon m^*, therefore any changes of the $\Sigma^{s(0)}$ would also affect the scalar density ρ_s and it couples back to the modified self-energies ($\Sigma^{s(0)} \longrightarrow m^* \longrightarrow \rho_s \longrightarrow \Sigma^{s(0)}$).

Meson i	$m_i\ [MeV]$	a_i	b_i	c_i	d_i	e_i	ζ_i
σ	550	13.1334	0.4258	0.6578	0.7914	0.7914	0.00804
ω	783	15.1640	0.3474	0.5152	0.5989	0.5989	0.00103
	$\rho_0 = 0.160\ [fm^{-3}]$						

Table 5.1: Parameters used in Eq. (5.14-5.15) for the calculation of the density dependent vertices for isoscalar mesons (σ, ω) in DDRH-MC.

5.3 Parametrization of DDRH vertices

Here we present the parametrization of the asymmetric nuclear matter results [dJL98a, dJL98b] derived from the Groningen nucleon-nucleon potential [HM87, Mal88] in DB calculations. It is obvious that such a parametrization enormously simplifies the very time consuming DB and DDRH calculations and the parameterized density dependent meson-nucleon vertices offer the opportunity to study the properties of infinite nuclear matter that we aim to do. It has shown in [HKL01b] that the asymmetry dependence of the vertices $\Gamma_i(k_F)$ defined from Eqs. (5.5-5.8), in the isoscalar channel was negligible; in the isovector channel it was extremely weak. For this reason, it is assumed that density dependent vertices $\Gamma_i(k_F)$ only depend on the total vector density $\rho(k_F)$ and parameterized as

$$\Gamma_i(\rho) = a_i \left[\frac{1 + b_i \left(\frac{\rho}{\rho_0} + d_i \right)^2}{1 + c_i \left(\frac{\rho}{\rho_0} + e_i \right)^2} \right] , \tag{5.14}$$

and this rational form defines the behavior at low and high densities very well and that is a contrast to the polynomial form as introduced in [HK93].

In the isoscalar channel, the momentum corrected vertices defined as

$$\tilde{\Gamma}_i(\rho) = \Gamma_i(\rho) \sqrt{1 + \zeta_i \left(\frac{3\pi^2}{2} \rho \right)^{2/3}} , \tag{5.15}$$

and the parameters are shown in Table. 5.1. Although the momentum correction constants $\zeta_\sigma = 0.00804$ fm^{-2} and $\zeta_\omega = 0.00103$ fm^{-2} are very small and adjusted only at the $\rho = \rho_0$, it reproduces the binding energies at low and as well as at high densities.

In the isovector channel, the momentum corrected vertices parameterized as

Meson j	$m_j\ [MeV]$	a_j	b_j	c_j	d_j	e_j
δ	983	19.1023	1.3653	2.3054	0.0693	0.5388
ρ	770	19.6270	1.7566	8.5541	0.7783	0.5746
	$\rho_0 = 0.160\ [fm^{-3}]$					

Table 5.2: Parameters used in Eq. (5.16) for the calculation of the density dependent vertices for isovector mesons (δ, ρ) in DDRH-MC.

$$\tilde{\Gamma}_j(\rho) = a_j \left[\frac{1 + b_j \left(\frac{\rho}{\rho_0} + d_j \right)^2}{1 + c_j \left(\frac{\rho}{\rho_0} + e_j \right)^2} \right] , \tag{5.16}$$

with parameters presented in Table. 5.2. In case of isoscalar channel, one obtanis the density dependent correction $\zeta_\rho(k_F)$ by keeping Γ_δ fixed and adjusting the ζ_ρ for each given DB binding energy to neutron matter. Therefore the correction is incorporated in the DB self-energies and the meson-nucleon vertex of the ρ meson is readjusted. This means that in Table. 5.2, the parameters for the ρ meson are readjusted and the parameters for δ meson are without momentum correction, i.e. $\tilde{\Gamma}_\delta(\rho) = \Gamma_\delta(\rho)$. In Fig. 5.1 we displayed the momentum dependent meson-nucleon vertex functions $\tilde{\Gamma}(\rho)$ for the scalar σ and δ and the vector ω and ρ mesons are as a functions of baryon density ρ. Here density region is relevant from nuclear structure to the neutron star studies. Note that in all cases the value of the vertices are an average, asymmetry independent. One can see in Fig. 5.1, vertices are continuously decreasing with increasing density except for the isovector-scalar δ meson case. In the isoscalar channel ω vertex is larger than σ vertex due to repulsive and attractive nucleon-nucleon potentials. The vertex of the ρ meson is smaller with a stronger variation with density. But the vertex of the δ meson is very special and it is increasing in the region of $\rho \geq \rho_0$ in contrast to other three mesons. In addition δ meson is a reason for the splitting of the neutron and proton effective masses that will be discussed in more detail in Section. 6.2.7. In the next section we will discuss about phenomenological version of the DDRH meson-nucleon vertices in where the δ meson is neglected.

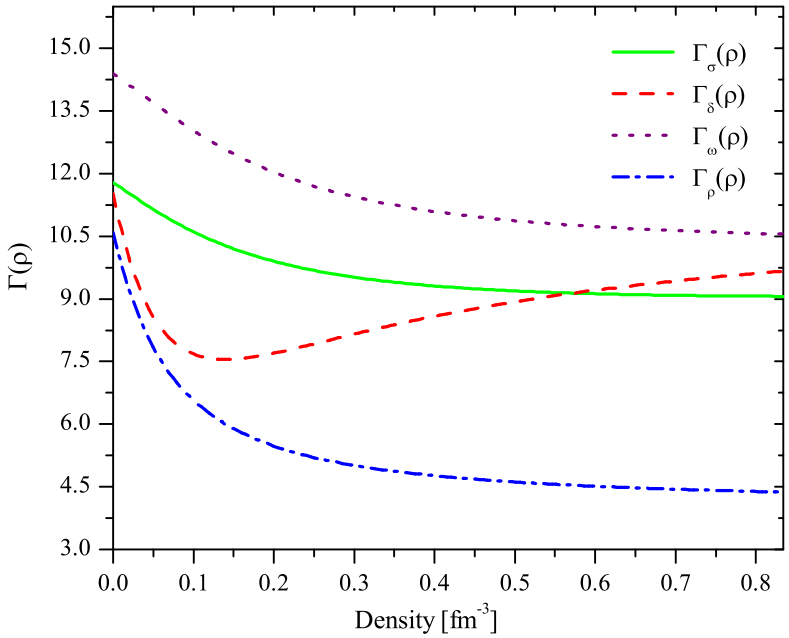

Figure 5.1: Density dependence of the meson-nucleon vertices for mesons: σ (solid line); δ (dashed line); ω (dotted line); ρ (dash-dotted line) in the DDRH-MC parametrization.

5.4 Phenomenological Meson-Baryon vertices

After the success of the microscopic DDRH approach Typel and Wolter [TW99] developed the first phenomenological description of the density dependent meson-baryon vertices for finite nuclei. It was shown that this approach was able to describe quantitatively properties of finite nuclei and nuclear matter using the vector density dependent vertices and the agreement with data were comparable to the non-linear models [LKP97].
Recently, a new empirical density dependent couplings introduced in [NVFR02] (DD-ME1) and it was improved by Lalazissis et al., in [LNVR05] (DD-ME2) which have been applied for the calculations of nuclear ground states and properties of excited states in Hartree-Bogoliubov (HB) [NVFR02, NDVR04] and the relativistic random-phase approximation (RRPA) [NVR02, PNVR04]. Furthermore it was also applied to the analysis of recent data on superheavy nuclei. In all these phenomenological approaches, the density dependent vertices are described by making an ansatz for the functional form with some parameters which are adjusted to reproduce the properties of symmetric and asymmetric

Meson i	m_i $[MeV]$	$g_i(\rho_{\rm sat})$	a_i	b_i	c_i	d_i
σ	549.5255	10.4434	1.3854	0.9781	1.5342	0.4661
ω	783.0000	12.8939	1.3879	0.8525	1.3566	0.4957
ρ	763.0000	3.8053	0.5008			
	$\rho_{\rm sat} = 0.152$ $[\mathrm{fm}^{-3}]$					

Table 5.3: Parameters used in Eqs. (5.17) and (5.19) for the calculation of the density dependent vertices for the mesons (σ, ω, ρ) in DD-ME1 [NVFR02].

nuclear matter, binding energies, charge radii and neutron radii of spherical nuclei.
The functional form of the density dependent couplings of the σ and the ω mesons are defined as

$$\Gamma_i(\rho) = g_i(\rho_{\rm sat}) f_i(y) \qquad i = \sigma, \omega \tag{5.17}$$

and the density-dependent effects are contained in

$$f_i(y) = a_i \left[\frac{1 + b_i(y + d_i)^2}{1 + c_i(y + d_i)^2} \right] \tag{5.18}$$

which is a function of $y = \rho/\rho_{\rm sat}$, and $\rho_{\rm sat}$ denotes the saturation density of symmetric nuclear matter. In Eq. (5.4), the parameters (a_i, b_i, c_i, d_i) are real and positive but not independent. It is clear that $f_i(1) = 1$. In order to reduce the number of independent parameters, one can additionally demand $f''_\sigma(1) = f''_\omega(1)$ and $f''_i(0) = 0$. Therefore these five restrictions reduced the number of independent parameters from eight to three. However there are another three parameters $g_\sigma(\rho_{\rm sat})$, $g_\omega(\rho_{\rm sat})$ and m_σ should be added in the isoscalar channel.
For the ρ meson coupling the functional form of the density dependence defined

$$\Gamma_\rho(\rho) = g_\rho(\rho_{\rm sat}) \exp[-a_\rho(y - 1)] \tag{5.19}$$

and with only one parameter a_ρ. This exponential dependence was suggested by DB calculation in [dJL98a] where it has been indicated that the ρ meson coupling has a very strong density dependence and it becomes very small at high densities.
The functional form of $f_i(y)$ is the same in the parameterizations DD-ME1 [NVFR02], DD-ME2 [LNVR05] and PKDD [LMGZ04] as introduced in [TW99]. In Table. 5.3, we displayed the parameters used in Eqs. (5.17) which are introduced in DD-ME1 [NVFR02] and values of the couplings are shown in Fig. 5.2. We chose only DD-ME1 parametriza-

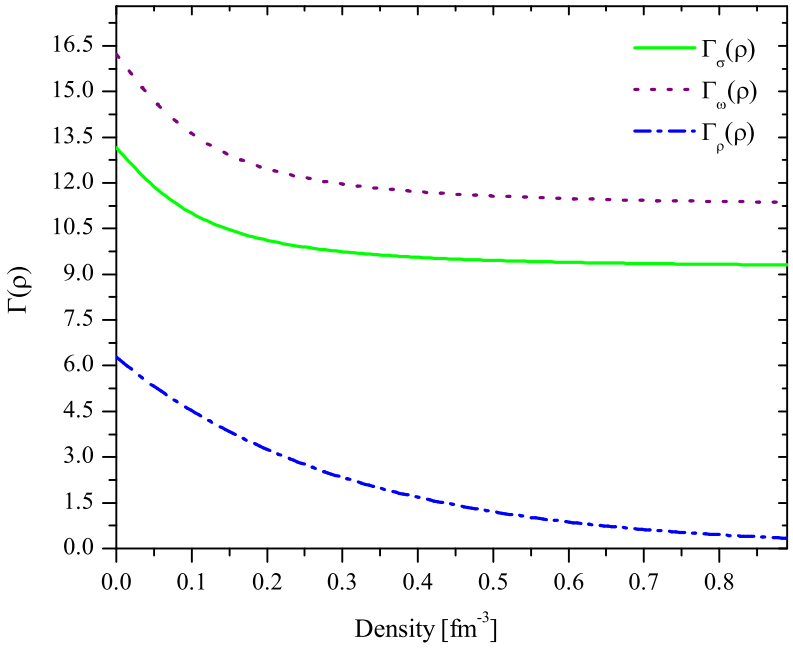

Figure 5.2: Density dependence of the couplings of the σ-meson (solid line), ω-meson (dotted line) and ρ-meson (dash-dotted line) in the DD-ME1 parametrization.

tion which is used in our analysis presented in the Chapter. 6. In Fig. 5.2, in all cases the value of the vertices continuously decreasing with increasing density which is similar to DDRH-MC vertices. But one can see clearly that the differences between the vertices defined from microscopic DDRH-MC (solid line) and phenomenological DD-ME1 (dashed line) approaches in Fig. 5.3.

The main difference is caused by the values of the parameters $(a_i, b_i, c_i, d_i, e_i)$ in Tables. 5.1 and 5.3 for $i = \sigma, \omega$ in the functional form of the density dependence (Eqs. (5.15) and (5.17)). For the both σ (panel a) and ω (panel b) mesons the DDRH-MC vertices are smaller than the DD-ME1 and the difference of the values at saturation density is about ± 5 %. For the ρ (panel d) meson the DDRH-MC vertex is much larger than the DD-ME1 and at the saturation density difference between these two approaches is about ∓ 34 %. Also ρ meson vertex in the DD-ME1 decreases faster than the DDRH-MC vertex with increasing baryon density. The reason for that behavior is at least partly that the δ meson is neglected in the DD-ME1. The δ meson vertex in DDRH-MC parametrization as shown in panel (c).

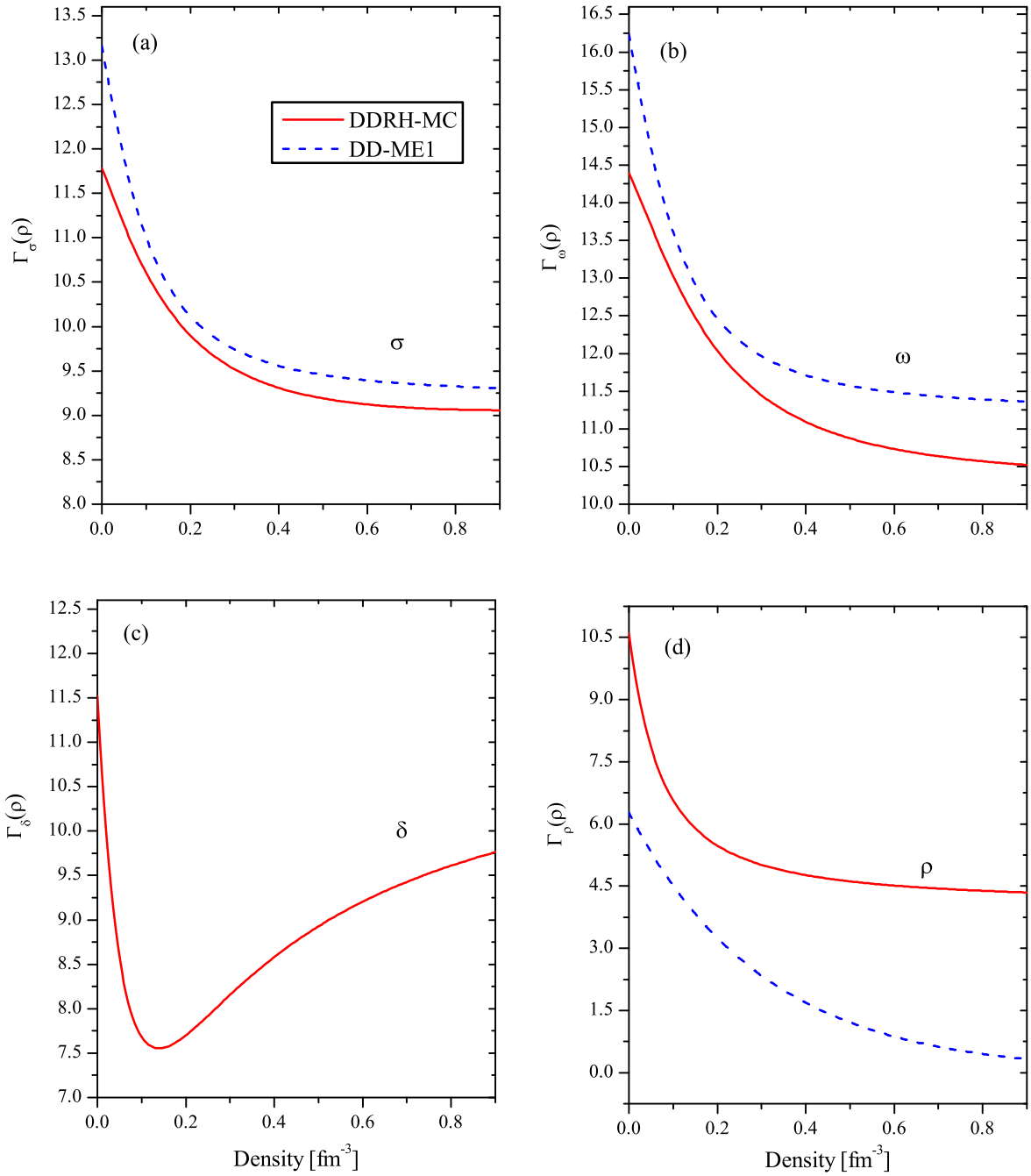

Figure 5.3: Density dependence of the momentum corrected meson-nucleon vertices in the DDRH-MC (solid line) parametrization compared to results of DD-ME1 (dashed line) parametrization for the : σ-meson (panel a), ω-meson (panel b), δ-meson (panel c) and ρ-meson (panel d).

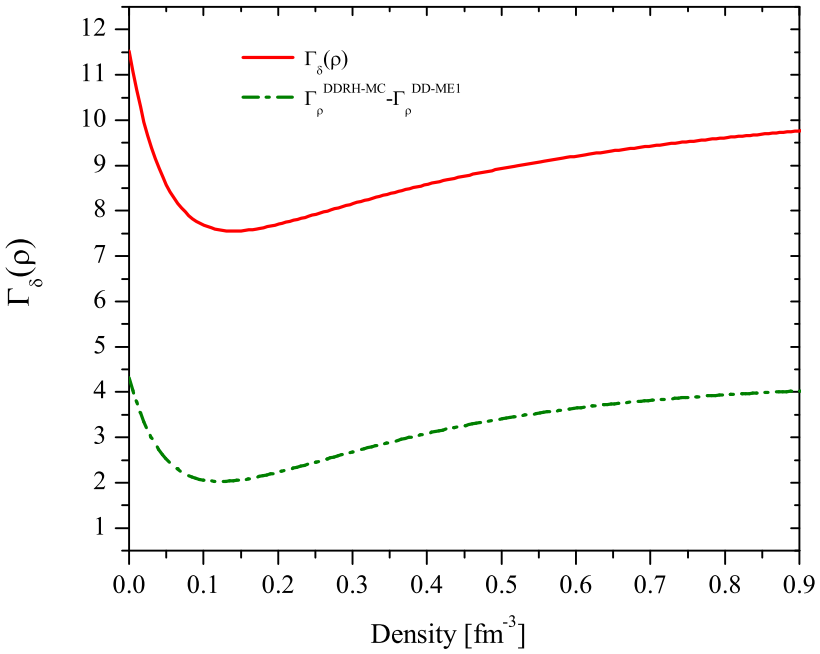

Figure 5.4: The dash-dotted line shows the difference of the ρ-meson vertices calculated in DDRH-MC and DD-ME1, and compared to the δ-meson vertex presented by solid line.

In fact, we displayed the difference of the ρ-meson vertices calculated in the DDRH-MC and DD-ME1 ($\tilde{\Gamma}_\rho^{DDRH-MC} - \Gamma_\rho^{DD-ME1}$) by dash-dotted line in Fig. 5.4 and the shape of this curve is very similar to the δ meson vertex in DDRH-MC parametrization as shown by solid line, but about 2.5-3.7 times smaller. Of course, this is not the only reason, the differences also may be caused by the fit. Due to the behavior of the vertices we expect to see the series of isospin effects in the properties of infinite nuclear matter, in particular, in the region of $\rho \geq \rho_0$.

Chapter 6

Results

In this chapter we are presenting the results of our calculation for the Equation of state of infinite nuclear matter. Our detailed investigation of the EOS of infinite nuclear matter is focused on the following features:

- the extremes of the low and high densities
- isospin effects in nuclear matter i.e. the role of the isovector scalar δ meson
- comparison to the phenomenological approach DD-ME1.

6.1 Nuclear matter

Nuclear matter is essentially, an idealization of a nucleus with a surface shifted to the infinity thus being free of boundary problems, i.e. an infinite uniform system with given ratio of neutrons to protons (N/Z) in which neutrons and protons interact with the nuclear forces in the absence of Coulomb interactions between the protons. From the nuclear chart, Fig. 6.1 as we know that the unbalanced neutron and proton numbers decrease the stability of a nucleus. Furthermore this gives an additional contribution to the energy density which is known as the symmetry energy (E_{sym}). This energy is repulsive which leads to a different occupation of the phase space for neutrons and protons in asymmetric nuclear matter. Therefore the equation of state of nuclear matter contains a symmetry energy term, i.e. the equation of state of nuclear matter depends on the baryon density and the asymmetry parameter, respectively. The asymmetry

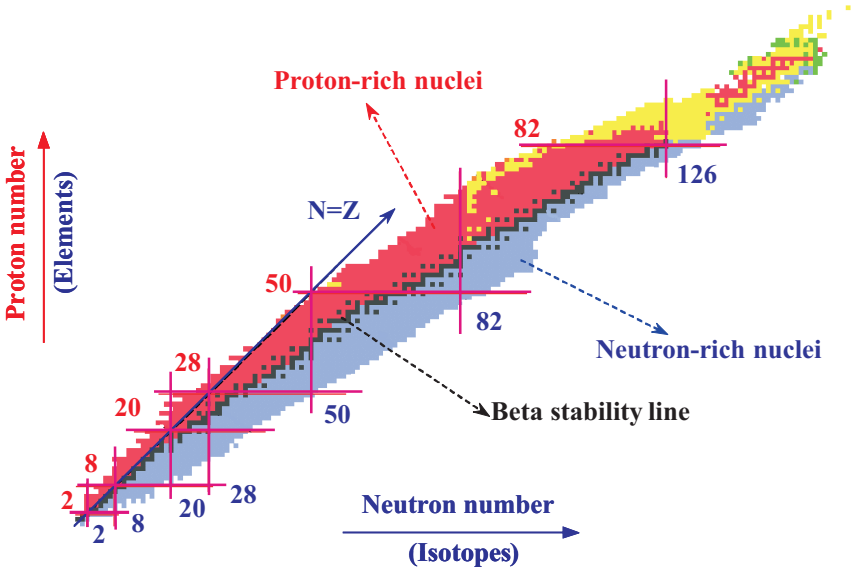

Figure 6.1: The nuclear chart [Fah98] .

parameter, x can be conveniently defined as

$$x = \frac{N-Z}{N+Z} = \frac{\rho_n - \rho_p}{\rho_n + \rho_p} \tag{6.1}$$

where ρ_n and ρ_p, N and Z are the neutron and proton densities and numbers, respectively. Using equations (4.35), (4.37) and proton fraction $\alpha = Z/N+Z$, the above equation can be rewritten as

$$x = \frac{\rho_3}{\rho} = (1-2\alpha) \tag{6.2}$$

so that

$$\rho_n = \frac{\rho(1+x)}{2} = \rho\ (1-\alpha)$$

and

$$\rho_p = \frac{\rho(1-x)}{2} = \rho\ \alpha\ . \tag{6.3}$$

The asymmetry parameter, x can have values between 0 to 1, $(0 \leq x \leq 1)$ while α have values between 0.5 to 0, $(0.5 \geq \alpha \geq 0)$, corresponding to symmetric nuclear matter and pure neutron matter, respectively. We will discuss in detail the properties of the neutron matter, symmetric matter and asymmetric nuclear matter in the following section.

6.2 Equation of state of Infinite nuclear matter

In the section 4.2 we described the field equations in RMF approximation. Using for the infinite nuclear matter the assumption that it is an isotropic and homogeneous system, derivatives of the fields vanish. Furthermore the electromagnetic interactions are neglected. As a result in the Hartree limit, the solution of the Dirac Eq. (4.38) is analogous with the solution of the free Dirac equation in the momentum-space

The modified Dirac equation is

$$\left[\gamma_\mu k_b^{*\mu} - m_b^*\right] u_b^*(k,s) = 0 \tag{6.4}$$

with solutions which are plane wave Dirac spinors obtained from the free Dirac spinors (see App. A.1) by replacing M by m^*

$$u_b^*(k,s) = \sqrt{\frac{E_b^* + m_b^*}{2m_b^*}} \begin{pmatrix} 1 \\ \frac{\sigma \mathbf{k}_b^*}{E_b^* + m_b^*} \end{pmatrix} \chi_s \ , \tag{6.5}$$

where $b = n,p$ and $s = \pm\frac{1}{2}$ for the neutron and the proton, respectively and χ_s denotes a two-component Pauli-spinor.
The kinetic and canonical four-momenta $k_b^{*\mu}$ and k_b^μ are related by

$$k_b^{*\mu} = k_b^\mu - (\Sigma_b^{(0)\mu} + \Sigma_b^{(r)\mu}) \tag{6.6}$$

and an additional shift is obtained from the rearrangement self energies. The effective mass m_b^*

$$m_b^* = M - (\Sigma_b^{(0)s} + \Sigma_b^{(r)s}) \tag{6.7}$$

is also modified and differs for neutrons and protons due to the inclusion of the δ meson in the scalar self-energy. We will discuss more about proton-neutron mass splitting in isospin asymmetric nuclear matter in Sec. 6.2.7.
The in-medium mass shell condition is $k_b^{*2} - m_b^{*2} = 0$ and the one particle energy is given by

$$E_b^* = k_b^{*0} = \sqrt{\mathbf{k}_b^{*2} + m_b^{*2}}. \tag{6.8}$$

The meson field equations in Eqs. (4.29-4.32) also changed to the simple algebraic equations

$$m_\sigma^2 \Phi_\sigma = \Gamma_\sigma(\rho)\rho^s \ , \tag{6.9}$$

$$m_\omega^2 A_0^\omega = \Gamma_\omega(\rho)\rho \ , \tag{6.10}$$

$$m_\delta^2 \Phi_\delta = \Gamma_\delta(\rho)\rho_3^s \ , \tag{6.11}$$

$$m_\rho^2 A_0^\rho = \Gamma_\rho(\rho)\rho_3 \ . \tag{6.12}$$

Integrating over all states $k \leq k_{F_b}$ inside the Fermi sphere and introducing the Fermi energy as

$$E_{F_b} = \sqrt{k_{F_b}^{*2} + m_b^{*2}} \ , \tag{6.13}$$

the scalar and vector densities in infinite nuclear matter are can be derived as following way.
The vector density ρ which is related to the Fermi momentum k_{F_b} obtained as

$$\begin{aligned} \rho = \langle \overline{\Psi}\gamma_0\Psi \rangle &= \sum_{b=p,n}\sum_{ss'}\int_{|k|\leq k_{F_b}} \frac{d^3k}{(2\pi)^3}\bar{u}_b^*(k,s')u_b^*(k,s) \\ &= \sum_{b=p,n}\frac{2}{(2\pi)^3}\int_{|k|\leq k_{F_b}} d^3k = \sum_{b=p,n}\frac{k_{F_b}^3}{3\pi^2} \ . \end{aligned} \tag{6.14}$$

The equation 6.14 becomes

- for symmetric nuclear matter (i.e.$\rho_n = \rho_p$ and $\alpha = 0$)

$$\rho = \frac{2k_F^3}{3\pi^2} \ , \tag{6.15}$$

- for pure neutron matter ($\rho_p = 0$ and $\alpha = 0.5$)

$$\rho = \frac{k_{F_n}^3}{3\pi^2} \ , \tag{6.16}$$

respectively.
The corresponding scalar density ρ^s determined by the self-consistency relation as

$$\begin{aligned} \rho^s = \langle \overline{\Psi}\Psi \rangle &= \sum_{b=p,n}\sum_{ss'}\int_{|k|\leq k_{F_b}} \frac{d^3k}{(2\pi)^3}\bar{u}_b^{*\dagger}(k,s')u_b^*(k,s) \\ &= \sum_{b=p,n}\frac{2}{(2\pi)^3}\int_{|k|\leq k_{F_b}} d^3k\frac{m_b^*}{E_b^*} \\ &= \sum_{b=p,n}\frac{m_b^*}{2\pi^2}\left[k_{F_b}E_{F_b} + m_b^{*2}\ln\left(\frac{k_{F_b}+E_{F_b}}{m_b^*}\right)\right] \ , \end{aligned} \tag{6.17}$$

and we find $\rho^s = \rho_p^s + \rho_n^s$.
The solution of the nuclear matter problem can be obtained with the following steps:

- With the given Fermi momentum k_{F_b} or the baryon density ρ_b, the nucleon effective masses can be calculated from the scalar density in Eq. (6.17).
- The meson fields can be calculated from Eqs. (6.9-6.12)

However the nucleon effective masses

$$m_b^* = M - \Gamma_\sigma(\rho)\Phi_\sigma - \tau_b\Gamma_\delta(\rho)\Phi_\delta \tag{6.18}$$

and because the meson fields $\Phi_{\sigma,\delta} = \Phi_{\sigma,\delta}(m_p^*, m_n^*)$ depend on the effective masses themselves, we account a highly non-linear system of coupled equations which can be solved only by a self-consistency procedures. This self consistency problem leads to a coupled set of equations for the effective masses m_b^* that we can solve with respect to the fields Φ_σ and Φ_δ using their field equations (6.9) and (6.11).
The solution techniques are following:

- One chooses a starting value for m^*, usually the free nucleon mass, which is inserted into the equation for ρ^s, Eq. (6.17).
- The value for ρ^s is then used to calculate the new m^*, Eq. (6.18) and this value is reinserted into the equation for ρ^s and this procedure is repeated until convergence is received.

In the Fig. 6.2 we plot our results for the scalar densities of the proton and the neutron versus the baryon density for the following three cases:

1. pure neutron matter where $\rho_p^s = 0$, ($x = 1$ and $\alpha = 0.00$); so that ρ^s becomes

$$\rho_n^s = \frac{m_n^*}{2\pi^2}\left[k_{F_n}E_{F_n} + m_n^{*2}\ln\left(\frac{k_{F_n} + E_{F_n}}{m_n^*}\right)\right] . \tag{6.19}$$

2. symmetric nuclear matter where $\rho_n^s = \rho_p^s$, ($x = 0$ and $\alpha = 0.50$);
3. asymmetric nuclear matter where $\rho_n^s > \rho_p^s$:
   - $x = 0.8$ and $\alpha = 0.10$,
   - $x = 0.5$ and $\alpha = 0.25$,

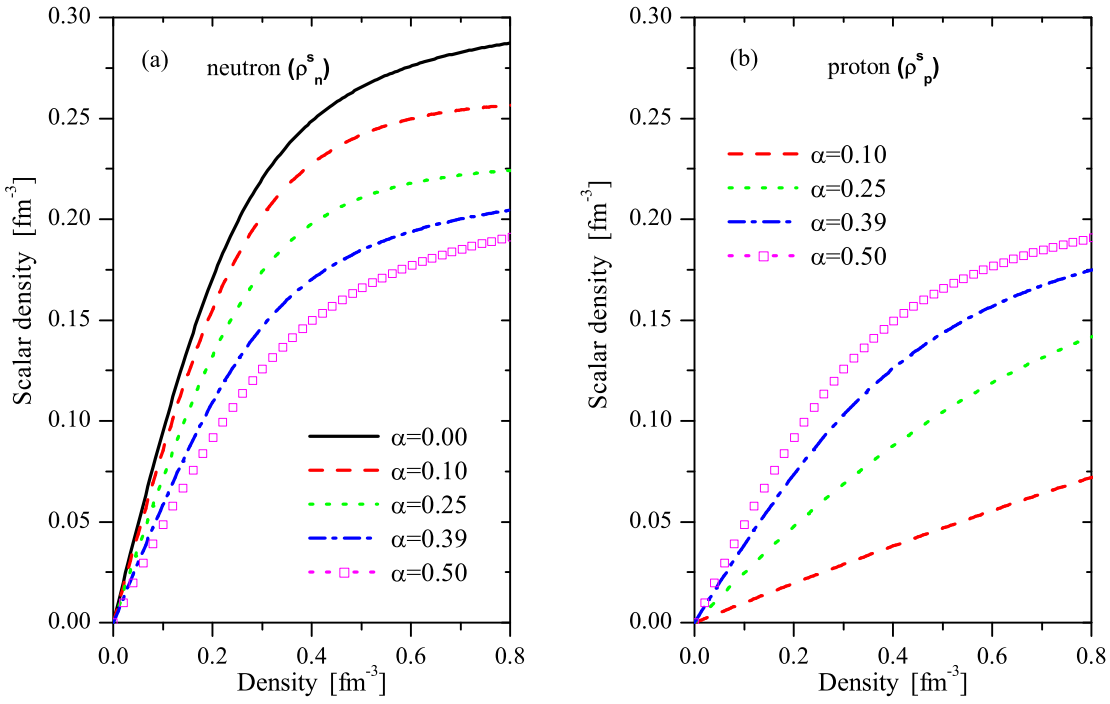

Figure 6.2: The scalar densities of the neutron (a) and the proton (b) are displayed as a function of the baryon density for pure neutron matter ($\alpha = 0.00$), symmetric nuclear matter ($\alpha = 0.50$) and asymmetric nuclear matter ($\alpha = 0.10, 0.25, 0.39$).

- $x = 0.22$ and $\alpha = 0.39$ (corresponding to the charge-to-mass relation of ^{208}Pb).

In infinite nuclear matter we always can write $\rho^s = \rho f(k_F, m^*)$. At low density, $k_{F_b} \to 0$, the scalar density ρ^s goes to the vector density, ρ as shown below

$$\rho^s = \underbrace{\frac{k_{F_b}^3}{3\pi^2}}_{\rho}\left(1 - \frac{3k_{F_b}^2}{10m^{*2}} + \frac{9k_{F_b}^4}{56m^{*4}} + O(k_{F_b}^6)\right) \quad . \tag{6.20}$$

For all three cases the scalar densities of the proton and the neutron increase linearly at low densities (below ρ_0) and at higher densities its increase slowly but difference due to the asymmetries gets more significant. Moreover the scalar density ρ^s is smaller than the baryon density due to Lorentz contraction factor M^*/E^* in Eq. (6.17) as depicted in Fig. 6.3.

In Fig. 6.3 also one can see clearly that the effect of the isovector channel ($\delta(a_0[983])$

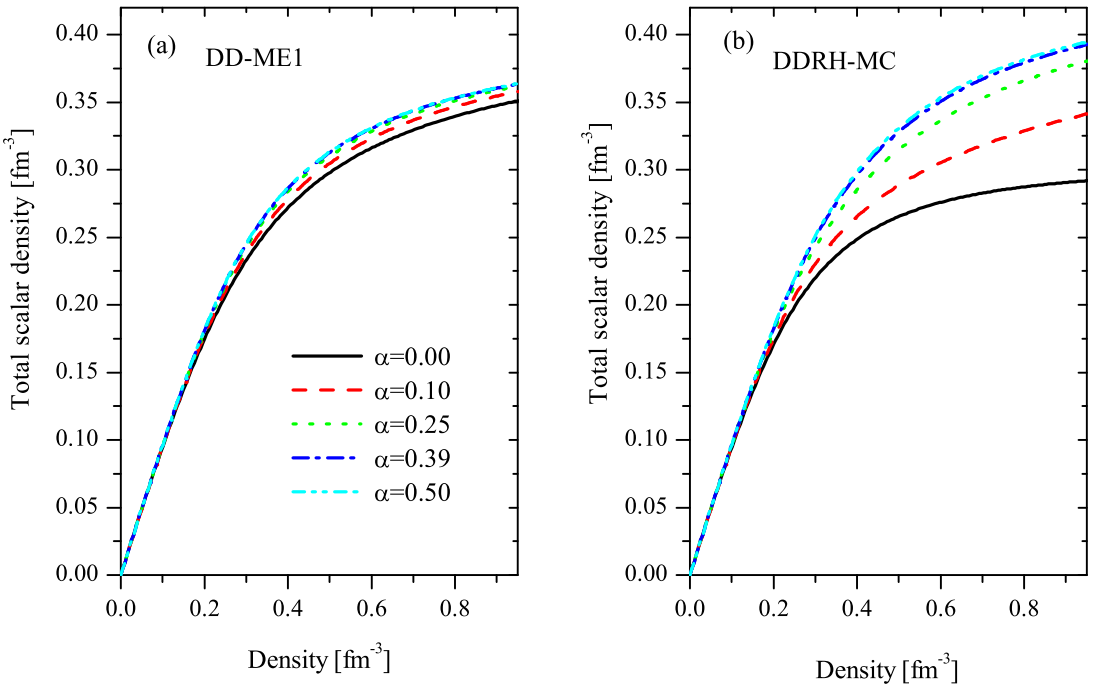

Figure 6.3: Total scalar densities are calculated in the DD-ME1 (a) and the DDRH-MC (b).

meson) in the asymmetric nuclear matter by comparing our result in DDRH-MC (b) to the results of DD-ME1 (a) in where δ is excluded. At low density ($\rho < 2$ fm^{-3}) both approaches lead to almost identical results but at higher densities there are differences. These differences (DDRH-MC results are smaller than DD-ME1) caused by δ meson in the asymmetric nuclear matter case ($\alpha = 0.00, 0.10, 0.25, 0.39$), but in the case of symmetric nuclear matter, DDRH-MC result is bigger than DD-ME1 as shown in Fig. 6.4.

The reason for this behavior is that the coupling of the σ in DDRH-MC is smaller than in DD-ME1 (see Fig. 5.3 a). From previous analysis also we expect the similar effects on the nucleon effective masses that will be discussed in Section. 6.2.7

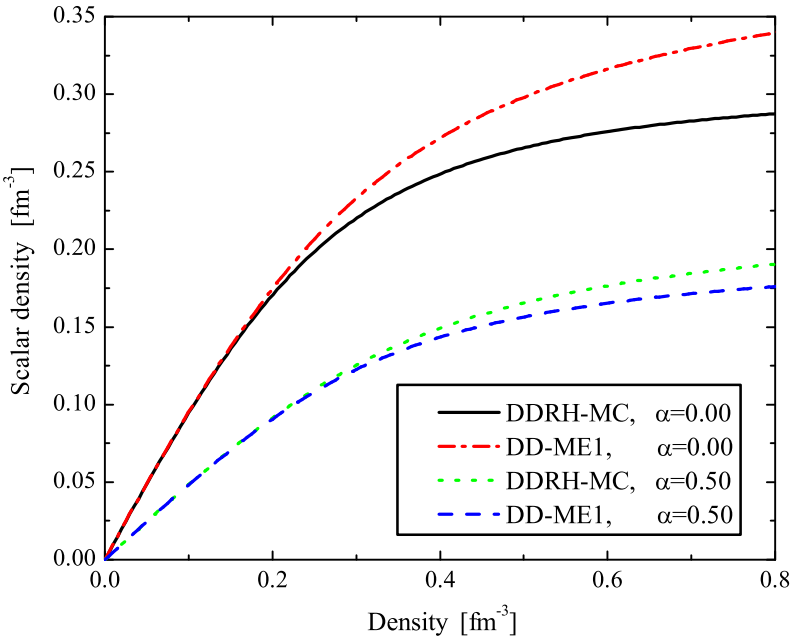

Figure 6.4: The scalar densities of the pure neutron matter ($\alpha = 0.00$) and symmetric nuclear matter ($\alpha = 0.50$) are calculated in the DDRH-MC and the DD-ME1.

6.2.1 Energy-Momentum-Tensor and Energy density

By definition, the Energy-Momentum-Tensor is given as

$$T^{\mu\nu} = \sum_i \frac{\partial \mathcal{L}}{\partial(\partial_\mu \phi_i)} \partial^\nu \phi_i - g^{\mu\nu}\mathcal{L}, \qquad \phi_i = \overline{\Psi}, \Psi, \Phi_\sigma, A_\mu^{(\omega)}, \mathbf{\Phi}_\delta, \mathbf{A}_\mu^{(\rho)}. \tag{6.21}$$

With the help of Eq. (4.1) and inserting the Dirac equation (4.24) we obtain the Energy-Momentum-Tensor for DDRH as

$$\begin{aligned} T^{\mu\nu} &= i\overline{\Psi}\gamma^\mu\partial^\nu\Psi - g^{\mu\nu}\overline{\Psi}\left[\gamma_\lambda \hat{\Sigma}^{\lambda(r)} - \hat{\Sigma}^{s(r)}\right]\Psi \\ &\quad + \sum_{i=\sigma,\delta}\left(\partial^\mu\Phi_i\partial^\nu\Phi_i - \frac{g^{\mu\nu}}{2}\left[\partial_\lambda\Phi_i\partial^\lambda\Phi_i - m_i^2\Phi_i^2\right]\right) \\ &\quad + \sum_{k=\omega,\rho}\left(\partial^\nu A_\lambda^{(k)} F^{(k)\lambda\mu} - \frac{g^{\mu\nu}}{2}\left[-\frac{1}{2}F_{\lambda\rho}^{(k)}F^{(k)\lambda\rho} + m_k^2 A_\lambda^{(k)}A^{(k)\lambda}\right]\right). \end{aligned} \tag{6.22}$$

An important property of $T^{\mu\nu}$ is energy-momentum conservation, i.e. for a field that is exchanging energy and momentum with a particle, the change rate of the particle energy and momentum must exactly match the change rate of the field energy and momentum. The energy-momentum conservation can be written as

$$\partial_\mu T^{\mu\nu} = 0. \tag{6.23}$$

To check the energy-momentum conservation above let us start with the divergence of the first term in Eq. (6.22)

$$\partial_\mu(i\overline{\Psi}\gamma^\mu\partial^\nu\Psi) = i\overline{\Psi}\gamma_\mu\overleftarrow{\partial^\mu}\partial^\nu\Psi + i\overline{\Psi}\gamma_\mu\overrightarrow{\partial^\mu}\partial^\nu\Psi \ . \tag{6.24}$$

This form enables us to use the Dirac equations for the baryon fields Ψ and $\overline{\Psi}$,

$$\left[\gamma_\mu(i\overrightarrow{\partial^\mu} - \hat{\Sigma}^{\mu(0)} - \hat{\Sigma}^{\mu(r)}) - (M - \hat{\Sigma}^{s(0)} - \hat{\Sigma}^{s(r)})\right]\Psi = 0 \ , \tag{6.25}$$

$$\overline{\Psi}\left[\gamma_\mu(i\overleftarrow{\partial^\mu} + \hat{\Sigma}^{\mu(0)} + \hat{\Sigma}^{\mu(r)}) + (M - \hat{\Sigma}^{s(0)} - \hat{\Sigma}^{s(r)}\right] = 0 \ , \tag{6.26}$$

so that Eq. (6.24) becomes

$$\partial_\mu(i\overline{\Psi}\gamma^\mu\partial^\nu\Psi) = \overline{\Psi}\left(\partial^\nu\left[\gamma_\mu(\hat{\Sigma}^{\mu(0)} + \hat{\Sigma}^{\mu(r)}) + (M - \hat{\Sigma}^{s(0)} - \hat{\Sigma}^{s(r)}\right]\right)\Psi \ . \tag{6.27}$$

Note that the divergence on the right hand side acts only on the term in brackets. The derivative of the second term in Eq. (6.22) consists of two parts

$$\begin{aligned} -\partial_\mu g^{\mu\nu}\overline{\Psi}\left[\gamma_\lambda\hat{\Sigma}^{\lambda(r)} - \hat{\Sigma}^{s(r)}\right]\Psi \ &= \ -\overline{\Psi}\left(\partial^\nu\left[\gamma_\lambda\hat{\Sigma}^{\lambda(r)} - \hat{\Sigma}^{s(r)}\right]\right)\Psi \\ &\quad -\left[(\partial^\nu\overline{\Psi}\gamma_\lambda\Psi)\hat{\Sigma}^{\lambda(r)} - (\partial^\nu\overline{\Psi}\Psi)\hat{\Sigma}^{s(r)}\right] \ . \end{aligned} \tag{6.28}$$

The sum of Eqs. (6.27) and (6.28) gives

$$\begin{aligned} \partial_\mu(i\overline{\Psi}\gamma^\mu\partial^\nu\Psi) - \partial_\mu g^{\mu\nu}\overline{\Psi}\left[\gamma_\lambda\hat{\Sigma}^{\lambda(r)} - \hat{\Sigma}^{s(r)}\right]\Psi \ &= \ \overline{\Psi}\gamma_\mu\Psi(\partial^\nu\hat{\Sigma}^{(0)\mu}) - \overline{\Psi}\Psi(\partial^\nu\hat{\Sigma}^{(0)s}) \\ &\quad -(\partial^\nu\overline{\Psi}\gamma_\lambda\Psi)\hat{\Sigma}^{\lambda(r)} - (\partial^\nu\overline{\Psi}\Psi)\hat{\Sigma}^{s(r)} \ . \end{aligned} \tag{6.29}$$

In the case of VDD, one finds the derivatives of the normal self energies from the first two terms on the right hand side of Eq. (6.29) as

$$\begin{aligned}\partial^\nu \hat{\Sigma}^{(0)\mu} &= \partial^\nu \left[\hat{\Gamma}_\omega(\hat{\rho})A^{(\omega)\mu} + \hat{\Gamma}_\rho(\hat{\rho})\tilde{\tau}\mathbf{A}^{(\rho)\mu} + e\hat{Q}A^{(\gamma)\mu}\right] \\ &= \hat{\Gamma}_\omega(\hat{\rho})\partial^\nu A^{(\omega)\mu} + \frac{\partial\hat{\Gamma}_\omega(\hat{\rho})}{\partial\hat{\rho}}A^{(\omega)\mu}\hat{u}_\lambda(\partial^\nu\overline{\Psi}\gamma^\lambda\Psi) \\ &\quad +\hat{\Gamma}_\rho(\hat{\rho})\partial^\nu\tilde{\tau}\mathbf{A}^{(\rho)\mu} + \frac{\partial\hat{\Gamma}_\rho(\hat{\rho})}{\partial\hat{\rho}}\mathbf{A}^{(\rho)\mu}\hat{u}_\lambda(\partial^\nu\overline{\Psi}\gamma^\lambda\tilde{\tau}\Psi)\ , \end{aligned} \tag{6.30}$$

$$\begin{aligned}\partial^\nu \hat{\Sigma}^{(0)s} &= \partial^\nu \left[\hat{\Gamma}_\sigma(\hat{\rho})\Phi_\sigma + \hat{\Gamma}_\delta(\hat{\rho})\tilde{\tau}\mathbf{\Phi}_\delta\right] \\ &= \hat{\Gamma}_\sigma(\hat{\rho})\partial^\nu\Phi_\sigma + \frac{\partial\hat{\Gamma}_\sigma(\hat{\rho})}{\partial\hat{\rho}}\Phi_\sigma(\partial^\nu\overline{\Psi}\Psi) \\ &\quad +\hat{\Gamma}_\delta(\hat{\rho})\partial^\nu\tilde{\tau}\mathbf{\Phi}_\delta + \frac{\partial\hat{\Gamma}_\delta(\hat{\rho})}{\partial\hat{\rho}}\mathbf{\Phi}_\delta(\partial^\nu\overline{\Psi}\tilde{\tau}\Psi)\ . \end{aligned} \tag{6.31}$$

In Eq. (6.29), the terms involving the derivatives of the vertices are therefore canceled and the last term with the rearrangement scalar self-energy $\hat{\Sigma}^{s(r)}$ vanishes due to the VDD. As a result the divergence of the first two terms of $T^{\mu\nu}$ becomes

$$\begin{aligned}\partial_\mu\left(i\overline{\Psi}\gamma^\mu\partial^\nu\Psi - g^{\mu\nu}\overline{\Psi}\left[\gamma_\lambda\hat{\Sigma}^{\lambda(r)} - \hat{\Sigma}^{s(r)}\right]\Psi\right) &= \hat{\Gamma}_\omega(\hat{\rho})\overline{\Psi}\gamma^\nu\Psi\partial^\nu A^{(\omega)\mu} + \hat{\Gamma}_\rho(\hat{\rho})\overline{\Psi}\gamma^\nu\tilde{\tau}\Psi\partial^\nu\mathbf{A}^{(\rho)\mu} \\ &\quad -\hat{\Gamma}_\sigma(\hat{\rho})\overline{\Psi}\Psi\partial^\nu\Phi_\sigma - \hat{\Gamma}_\delta(\hat{\rho})\overline{\Psi}\tilde{\tau}\Psi\partial^\nu\mathbf{\Phi}_\delta\ . \end{aligned} \tag{6.32}$$

The derivative of the remaining part of $T^{\mu\nu}$ with the help of the meson field equations Eqs. (4.8-4.11) one can easily show the following expressions:

$$\partial_\mu\sum_{i=\sigma,\delta}\left(\partial^\mu\Phi_i\partial^\nu\Phi_i - \frac{g^{\mu\nu}}{2}\left[\partial_\lambda\Phi_i\partial^\lambda\Phi_i - m_i^2\Phi_i^2\right]\right) = \hat{\Gamma}_\sigma(\hat{\rho})\overline{\Psi}\Psi\partial^\nu\Phi_\sigma + \hat{\Gamma}_\delta(\hat{\rho})\overline{\Psi}\tilde{\tau}\Psi\partial^\nu\mathbf{\Phi}_\delta \tag{6.33}$$

$$\begin{aligned}&\partial_\mu\sum_{k=\omega,\rho}\left(\partial^\nu A_\lambda^{(k)}F^{(k)\lambda\mu} - \frac{g^{\mu\nu}}{2}\left[-\frac{1}{2}F_{\lambda\rho}^{(k)}F^{(k)\lambda\rho} + m_k^2A_\lambda^{(k)}A^{(k)\lambda}\right]\right) \\ &\qquad = -\hat{\Gamma}_\omega(\hat{\rho})\overline{\Psi}\gamma^\nu\Psi\partial^\nu A^{(\omega)\mu} - \hat{\Gamma}_\rho(\hat{\rho})\overline{\Psi}\gamma^\nu\tilde{\tau}\Psi\partial^\nu\mathbf{A}^{(\rho)\mu}\ . \end{aligned} \tag{6.34}$$

The sum of the above two expressions gives the cancelation to the right hand side of Eq. (6.32). Therefore the energy momentum conservation is fulfilled without any doubts

but only when the rearrangement self-energy is taken into account in the baryon field equation.

In the case of application to the infinite nuclear matter, Energy-Momentum-Tensor of DDRH is simplified to

$$\begin{aligned} T^{\mu\nu} &= \sum_{b=p,n} \frac{2}{(2\pi)^3} \int_{|k|<k_{F_b}} \frac{d^3k}{E_b^*} \left[k_b^{*\mu} k_b^{*\nu} + k_b^{*\mu} \left(\Sigma_b^{\nu(0)} + \Sigma^{\nu(r)} \right) - k_{b\lambda}^* \Sigma^{\lambda(r)} g^{\mu\nu} \right] \\ &\quad + g^{\mu\nu} \left[\sum_{i=\sigma,\delta} m_i^2 \Phi_i^2 - \sum_{k=\omega,\rho} m_k^2 A_\lambda^{(k)} A^{(k)\lambda} \right], \end{aligned} \tag{6.35}$$

and the energy density ϵ is obtained as

$$\begin{aligned} \epsilon = \langle T^{00} \rangle &= \sum_{b=p,n} \left[\frac{2}{(2\pi)^3} \int_{|k|<k_{F_b}} d^3k \sqrt{\mathbf{k}^2 + m_b^{*2}} + \rho_b \Sigma_b^{0(0)} \right] \\ &\quad + \frac{1}{2} \left[m_\sigma^2 \Phi_\sigma^2 + m_\delta^2 \Phi_\delta^2 - m_\omega^2 A_0^{(\omega)^2} - m_\rho^2 A_0^{(\rho)^2} \right] \qquad (6.36) \\ &= \sum_{b=n,p} \frac{1}{4} \left[3E_{F_b} \rho_b + m_b^* \rho_b^s \right] + \sum_{b=n,p} \frac{1}{2} \left[\rho_b \Sigma_b^{0(0)} + \rho_b^s \Sigma_b^{s(0)} \right] . \qquad (6.37) \end{aligned}$$

The above expression shows that in the VDD case where $\Sigma_s^{(r)} = 0$, the rearrangement self-energy does not contribute to the energy density. This is an important result for the determination of the density dependent vertices from DB self-energies.

We plotted our results for the energy density as a function of baryon density in Figs. 6.5 and 6.6. In Fig. 6.5 we compared our results in DDRH-MC (solid line) to DD-ME1 model (dashed line) for symmetric nuclear matter and neutron matter.

One can see that in both DDRH-MC and DD-ME1 approaches, the energy density increases smoothly with increasing density. The differences due to asymmetries are very small and it appears only at high densities for asymmetric nuclear matter as shown in Fig. 6.6.

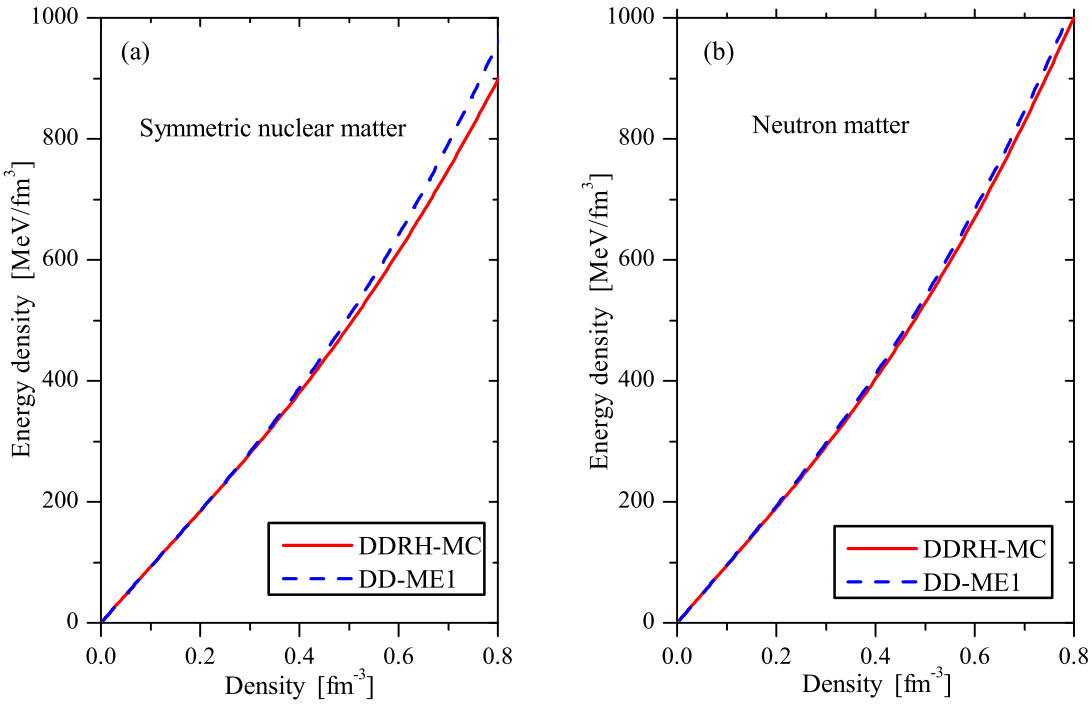

Figure 6.5: The energy density as a function of baryon density for neutron matter (a) and symmetric matter (b) in the DDRH-MC (solid) and DD-ME1 (dashed).

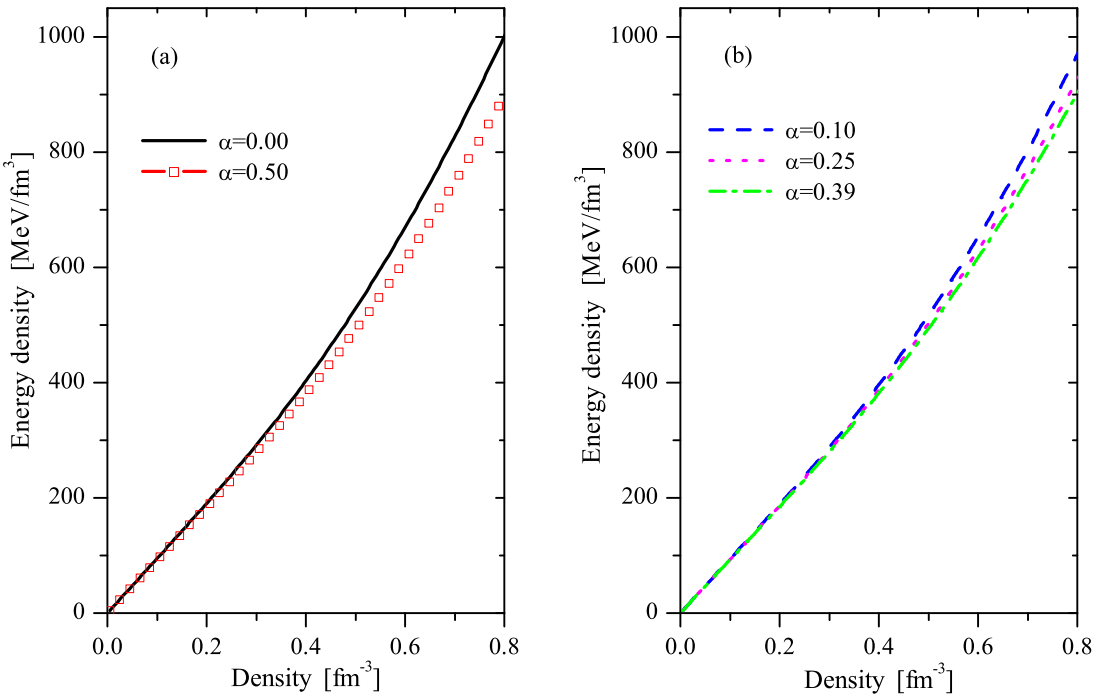

Figure 6.6: The energy density as a function of baryon density for neutron matter and symmetric matter (a) and for asymmetric nuclear matter (b) in the DDRH-MC approach.

6.2.2 Pressure and Thermodynamical consistency

Considering the pressure P is another way of presenting the nuclear matter EOS. The pressure is obtained from the energy-momentum tensor, Eq. (6.35), as

$$\begin{aligned} P = \frac{1}{3}\sum_{i=1}^{3}\langle T^{ii}\rangle &= \sum_{b=p,n}\left[\frac{2}{(2\pi)^3}\int_{|k|<k_{F_b}} d^3k \frac{\mathbf{k}^2}{\sqrt{\mathbf{k}^2+m_b^{*2}}} + \rho_b\Sigma^{0(r)}\right] \\ &\quad -\frac{1}{2}\left[m_\sigma^2\Phi_\sigma^2 + m_\delta^2\Phi_\delta^2 - m_\omega^2 A_0^{(\omega)^2} - m_\rho^2 A_0^{(\rho)^2}\right] \qquad (6.38) \\ &= \sum_{b=n,p}\frac{1}{4}\left[E_{F_b}\rho_b - m_b^*\rho_b^s\right] + \sum_{b=n,p}\frac{1}{2}\left[\rho_b\Sigma_b^{0(0)} - \rho_b^s\Sigma_b^{s(0)} + 2\rho_b\Sigma^{0(r)}\right] . \qquad (6.39) \end{aligned}$$

Contrary to the case of the energy density ϵ, the rearrangement self-energy contributes here directly to the expression of the pressure. In the Chapter. 4 we mentioned that the rearrangement self-energy assures the thermodynamical consistency yield the equality of the thermodynamical and mechanical pressures, which is an important property of the DDRH approach,

$$P = \rho^2\frac{\partial}{\partial\rho}\left(\frac{\epsilon}{\rho}\right) = \frac{1}{3}\sum_{i=1}^{3}\langle T^{ii}\rangle . \qquad (6.40)$$

In order to check the thermodynamical consistency in the equation above we calculate the thermodynamical pressure and compare it with the mechanical pressure expressed by Eq. (6.38),

$$\begin{aligned} P &= \rho^2\frac{\partial}{\partial\rho}\left(\frac{\epsilon}{\rho}\right) = \rho\frac{\partial}{\partial\rho}\epsilon - \epsilon \\ &= \rho\sum_{b=p,n}\left[\frac{\partial}{\partial\rho}\frac{2}{(2\pi)^3}\int_{|k|<k_{F_b}} d^3k\sqrt{\mathbf{k}^2+m_b^{*2}} + \frac{1}{2}\frac{\partial}{\partial\rho}\left(\rho_b\Sigma_b^{0(0)} + \rho_b^s\Sigma_b^{s(0)}\right)\right] \\ &\quad -\sum_{b=n,p}\left[\frac{3}{4}E_{F_b}\rho_b + \frac{1}{4}m_b^*\rho_b^s - \frac{1}{2}\left(\rho_b\Sigma_b^{0(0)} + \rho_b^s\Sigma_b^{s(0)}\right)\right] . \qquad (6.41) \end{aligned}$$

The derivative of the integral in Eq. (6.41) can be split into the following two terms:

- a derivative with respect to the upper boundary of the integral i.e., to k_F ,
- a derivative with respect to the implicit density dependence of the effective mass m^* which enters via Γ_σ and Γ_δ ,

and can be written as

$$\begin{aligned}
&\frac{\partial}{\partial\rho}\frac{2}{(2\pi)^3}\int_{|k|<k_{F_b}} d^3k\sqrt{\mathbf{k}^2+m_b^{*2}} \\
&= \frac{2}{(2\pi)^3}\frac{k_{F_b}}{3\rho}\frac{\partial}{\partial k_{F_b}}\int_{\Theta(k_{F_b})} d^3k\sqrt{\mathbf{k}^2+m_b^{*2}} + \frac{2}{(2\pi)^3}\frac{\partial m_b^*}{\partial\rho}\int_{\Theta(k_{F_b})} d^3k\frac{m_b^*}{\sqrt{\mathbf{k}^2+m_b^{*2}}} \\
&= \frac{\rho_b}{\rho}\sqrt{k_{F_b}^2+m_b^{*2}} + \rho_b^s\frac{\partial m_b^*}{\partial\rho} \ . \qquad (6.42)
\end{aligned}$$

Using the meson field equations and the definition of the self-energy, the derivative of the self-energy term in Eq. (6.41) can be expressed as:

$$\begin{aligned}
\frac{1}{2}\sum_{b=p,n}\frac{\partial}{\partial\rho}\left(\rho_b\Sigma_b^{0(0)}\right) &= \frac{1}{2}\frac{\partial}{\partial\rho}\left(\rho^2\frac{\Gamma_\omega^2}{m_\omega^2}+\rho_3^2\frac{\Gamma_\rho^2}{m_\rho^2}\right) \\
&= \sum_{b=p,n}\frac{\rho_b}{\rho}\left(\Gamma_\omega A_0^{(\omega)}+\tau_b\Gamma_\rho A_0^{(\rho)}\right)+\rho A_0^{(\omega)}\frac{\Gamma_\omega}{\partial\rho}+\rho_3 A_0^{(\rho)}\frac{\Gamma_\rho}{\partial\rho} \ . \qquad (6.43)
\end{aligned}$$

In the above equation, the first two terms can be identified as the vector self-energy and the two remaining terms can be identified as the contribution of the vector mesons to the rearrangement energy. One can describe now the derivative of the effective mass with the meson field equations as

$$\sum_{b=p,n}\rho_b^s\frac{m_b^*}{\partial\rho} = -\sum_{b=p,n}\rho_b^s\frac{\Sigma_b^s}{\partial\rho} = -\rho^s\frac{\partial}{\partial\rho}\left(\rho^s\frac{\Gamma_\sigma^2}{m_\sigma^2}\right)-\rho_3^s\frac{\partial}{\partial\rho}\left(\rho_3^s\frac{\Gamma_\delta^2}{m_\delta^2}\right) \ . \qquad (6.44)$$

Using the relation

$$\frac{1}{2}\frac{\partial}{\partial\rho}(f^2g^2)-f\frac{\partial}{\partial\rho}(fg^2) = -f^2\frac{\partial}{\partial\rho}(g^2) \ , \qquad (6.45)$$

the sum of the Eq. (6.44) and the scalar energy in Eq. (6.41) is simplified to

$$\sum_{b=p,n}\left[\rho_b^s\frac{m_b^*}{\partial\rho}+\frac{1}{2}\frac{\partial}{\partial\rho}\left(\rho_b^s\Sigma_b^{s(0)}\right)\right] = -\Phi_\sigma\rho^s\frac{\partial\Gamma_\sigma}{\partial\rho}-\Phi_\delta\rho_3^s\frac{\partial\Gamma_\delta}{\partial\rho} \ , \qquad (6.46)$$

obtaining a similar expression to Eq. (6.42). The term on the right hand side of the above equation corresponds exactly to the contribution of the scalar mesons to the rear-

rangement energy. Combining the results from Eqs. (6.42), (6.43) and (6.46) we obtain

$$\begin{aligned}\rho\frac{\partial}{\partial\rho}\epsilon-\epsilon &= \sum_{b=p,n}\left[E_{F_b}\rho_b+\rho_b\Sigma_b^{0(0)}+\rho_b\Sigma_b^{0(r)}\right]\\ &\quad-\sum_{b=n,p}\left[\frac{3}{4}E_{F_b}\rho_b+\frac{1}{4}m_b^*\rho_b^s-\frac{1}{2}\left(\rho_b\Sigma_b^{0(0)}+\rho_b^s\Sigma_b^{s(0)}\right)\right]\ , \end{aligned}\tag{6.47}$$

an expression which is equivalent to the mechanical pressure in Eq. (6.38) obtained from the energy-momentum tensor.

Using the Eqs. (6.39) and (6.37), we obtain at once the Hugenholtz-van Hove theorem,

$$\epsilon+P=\sum_{b=n,p}\left(E_b(k_F)\rho_b+\rho_b\Sigma_b^{0(0)}+\rho_b\Sigma_b^{0(r)}\right)=\sum_{b=n,p}\rho_bE_b(k_F)=\rho E(k_F)\ . \tag{6.48}$$

This verifies that for a system with zero pressure the Fermi energy is equal to the average energy per particle E/N of the system,

$$\frac{E}{N}=\frac{\epsilon}{\rho}=E(k_F)\ . \tag{6.49}$$

The results of our calculation (DDRH-MC) for the pressure using Eq. (6.39) is shown in Fig. 6.7 in the symmetric nuclear matter (panel a) and pure neutron matter (panel b) compared to results of the phenomenological DD-ME1 approach. For symmetric nuclear matter, both approaches agree very well at density below ≈ 0.10 fm^{-3} while at higher densities the differences increase. Most of this effect is a result of slightly different saturation densities, $\rho_0^{\mathrm{DDRH-MC}}\sim 0.18$ fm^{-3} $>\rho_0^{\mathrm{DD-ME1}}\sim 0.153$ fm^{-3} . Indeed a clear inspection shows that the pressure curve to a good approximation are shifted in density by about that amount.
For pure neutron matter differences of the two approaches appear for densities above ≈ 0.05 fm^{-3}. However the curves exhibit same shapes for both symmetric nuclear matter and pure neutron matter cases in two approaches. Moreover, the pressure in DDRH-MC increases slower than in DD-ME1 beyond the saturation density.

Since symmetric nuclear matter is a bound saturating system, it has a negative pressure ($P<0$) below the saturation density as shown in Fig. 6.8a . For the densities below ≈ 0.120 fm^{-3}, pressure decreases with increasing density, as a result, nuclear matter becomes unstable and heterogeneous. But in the region of $\rho\geq 0.120$ fm^{-3}, the pressure started increasing with increasing density and it becomes "*zero*" at the saturation

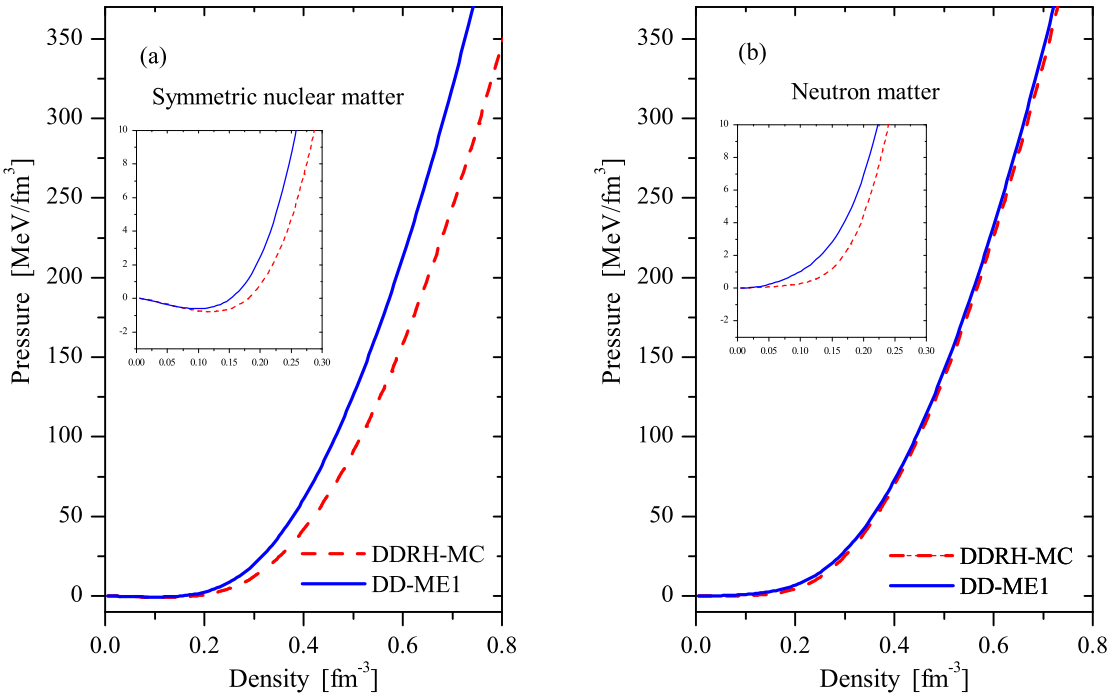

Figure 6.7: Pressure as a function of the baryon density at zero temperature for symmetric matter (a) and neutron matter (b) in DDRH-MC (dashed line) and DD-ME1 (solid line). Inserted panels show the behavior of the pressure at low density.

density, $P(\rho_{\text{sat}}) = 0$. This means that at the saturation density symmetric nuclear matter can be in mechanical equilibrium without external pressure. Therefore the point $\rho = 0.120$ fm^{-3} where the pressure has a minimum is a very important point which limits the instability region of nuclear matter. We note this density and minimum pressure by ρ_p and $P = P_{\text{min}}$, respectively. Also, it should be pointed out here that the instability region indicates a presence of a liquid-gas phase transition [BF99, ABMP04]. In Fig. 6.8b we plotted our results in asymmetric nuclear matter for three different asymmetries ($\alpha = 0.10, 0.25, 0.39$). Obviously, asymmetric nuclear matter also can have the same behavior as discussed above. However, the saturation densities of asymmetric nuclear matter depends on the asymmetry parameter x, Eq. (6.2) (or proton fraction α) and the saturation points shift to lower densities. As a result the region of negative pressure is different for the different asymmetric nuclear matters. The precise values of the P_{min} and corresponding densities ρ_{P} are presented in Table. 6.1. In addition instability of

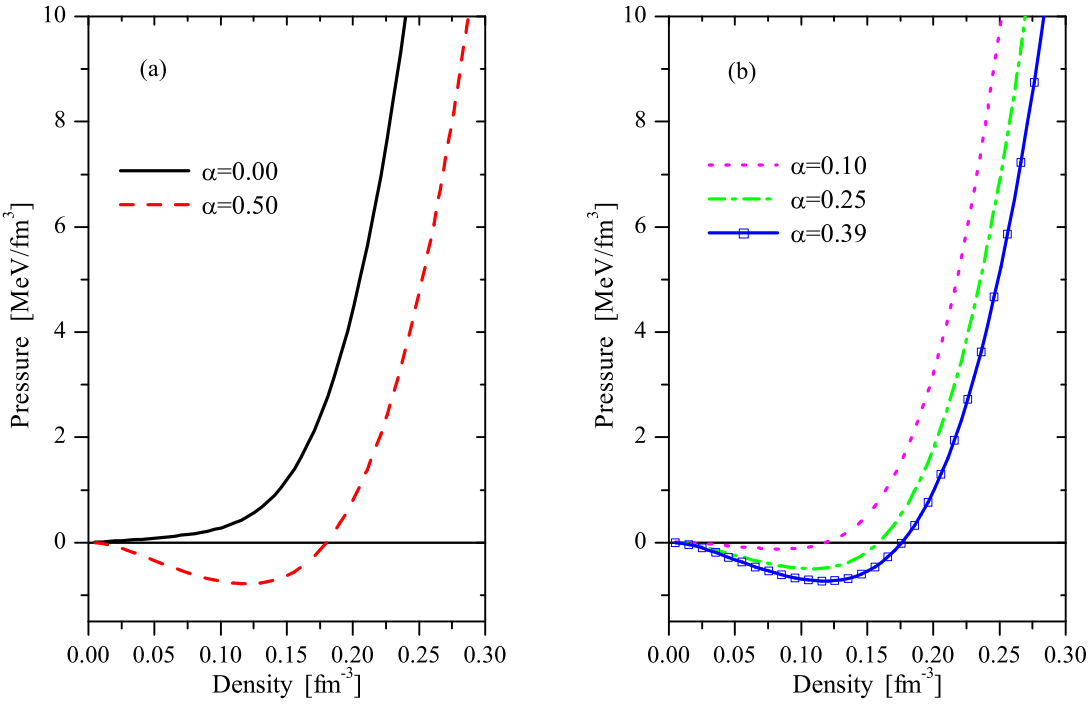

Figure 6.8: Pressure as a function of the baryon density at zero temperature for neutron and symmetric matter (a) and asymmetric matter (b) with various asymmetries in DDRH-MC.

nuclear matter decreases with increasing asymmetry parameters x (or decreasing proton fractions α). This tells that the liquid-gas phase transition disappears for some critical value of the asymmetry, for example, in our calculation $x > 0.8$. Therefore our model predicts stable neutron matter as well as DD-ME1.

In Fig. 6.10 we show a pressure versus energy density plot for pure neutron, symmetric and asymmetric nuclear matter in two different scales in order to see behavior at low and high densities. For all cases, as can be seen that the total energy density increases faster than the pressure, then $p/\epsilon < 1$ and $\partial p/\partial \epsilon < 1$. It is very important to examine these ratios. Because special relativity requires that the pressure must be less than the energy density of nuclear matter. Therefore our model becomes neither ultrabaric ($p > \epsilon$) nor superluminal $\partial p/\partial \epsilon > 1$ [BR68] and it will be discussed in detail in Section. 6.2.9.

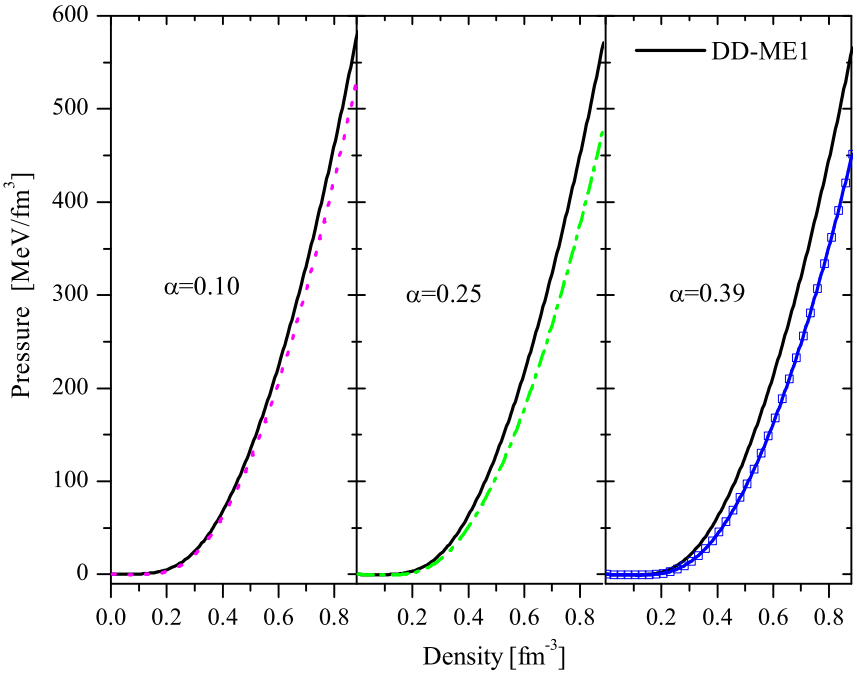

Figure 6.9: Same as Fig. 6.8b and compared to the results of DD-ME1.

x_i	ρ_P [fm^{-3}]	$P_{\min}$ [MeV/fm^{-3}]
0.00	0.12051	-0.78487
0.22	0.12051	-0.73339
0.5	0.11046	-0.50007
0.8	0.08536	-0.1214

Table 6.1: $P_{\min}$ and corresponding densities are calculated in DDRH-MC.

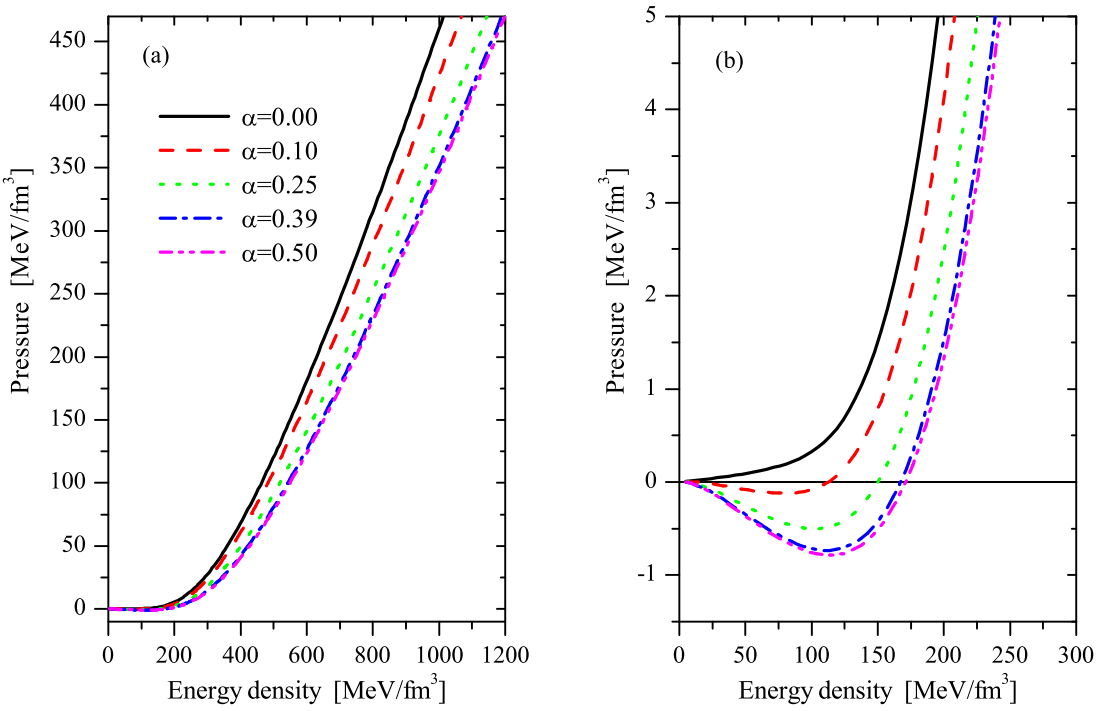

Figure 6.10: Pressure versus the energy density for various asymmetries in DDRH-MC. Note that panel (a) and panel (b) are same but in different scale.

6.2.3 The Chemical potential of the Cold nuclear matter

Since we verified the thermodynamical consistency of the DDRH theory, we have to consider the chemical potential μ which is an important quantity in thermodynamics. The chemical potential μ for a system with the fixed particle number N and with an energy density ϵ in a given volume V can be defined as

$$\delta = \left(\epsilon - \sum_{b=n,p} \mu_b (\rho_b - \frac{N_b}{V}) \right) \qquad \Longrightarrow \qquad \mu_b = \frac{\partial \epsilon}{\partial \rho} \tag{6.50}$$

Using Eqs. (6.36) and (6.42), the chemical potential for the asymmetric nuclear matter is

$$\mu_b = \frac{\partial \epsilon}{\partial \rho} = \frac{\partial}{\partial \rho}\sum_{b=n,p}\left[\frac{\partial}{\partial \rho}\frac{2}{(2\pi)^3}\int_{|k|<k_{F_b}} d^3k\sqrt{\mathbf{k}^2+m_b^{*2}} + \frac{1}{2}\left(\rho_b\Sigma_b^{0(0)} + \rho_b^s\Sigma_b^{s(0)}\right)\right]$$
$$= \sqrt{k_{F_b}^2+m_b^{*2}} + \left(\Sigma_b^{0(0)} + \Sigma_b^{s(0)}\right) = E_{F_b} + \Sigma_b^{(0)} = E(k_F)\ , \tag{6.51}$$

which states that in the infinite nuclear matter which is an isotropic and homogeneous system, the chemical potential is equivalent to the Fermi energy at zero temperature.

Equation (6.48) can be rewritten as

$$\epsilon + P = \sum_{b=n,p}\rho_b\mu_b\ . \tag{6.52}$$

6.2.4 Saturation curve

The energy per baryon E/N as a function of density is so called 'saturation curve', and it is often referred to as the equation of state (EOS) of the nuclear matter. The point where the saturation curve has a minimum is identified as the "saturation point" i.e. it marks the density (and corresponding energy) at which nuclear matter is able to self-sustain without any external pressure (positive or negative). In fact at such a point the pressure $P = 0$ as shown in Fig. 6.8 for symmetric and asymmetric nuclear matter. In our model the EOS defined as

$$E(\rho, x) = \frac{\epsilon(\rho, x)}{\rho} \tag{6.53}$$

here the energy density $\epsilon(\rho, x)$ is given by Eq. (6.37). Before going to discuss the EOS in detail, we have to define the following quantities:

$$K = 9\rho^2\frac{\partial^2}{\partial\rho^2}\left(\frac{\epsilon}{\rho}\right)_{|\rho=\rho_{sat}}\ , \tag{6.54}$$

and

$$a_4 = \frac{1}{2}\rho_0^2\frac{\partial^2}{\partial\rho_3^2}\frac{\epsilon}{\rho}(\rho, \rho_3)|_{\rho_3=0}\ . \tag{6.55}$$

Here K is the compressibility and a_4 is the bulk symmetry energy of nuclear matter, are very important quantities to describe the saturation properties of nuclear matter. (Detailed discussions for the density dependence of the K and the a_4 are presented in subsections. 6.2.5 and 6.2.8.)

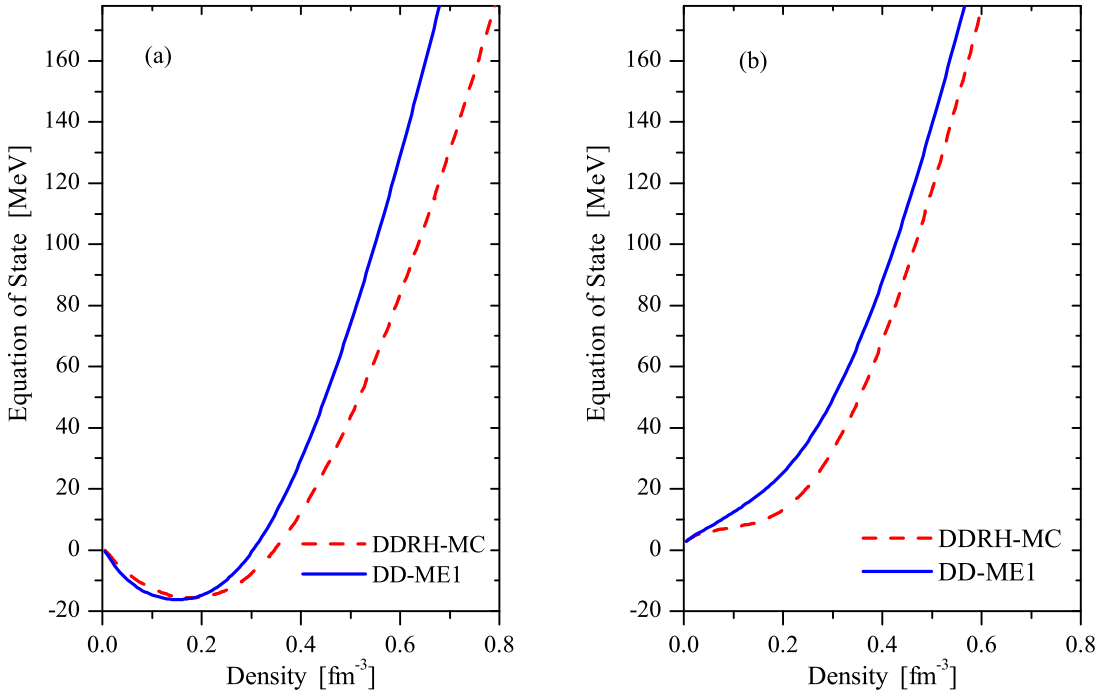

Figure 6.11: The equation of state of the symmetric (panel a) and neutron (panel b) matter in DDRH-MC (dashed) and DD-ME1 (solid) for comparison.

In Fig. 6.11, we plotted our results for the calculations of the EOS of the symmetric nuclear matter (panel a) and pure neutron matter (panel b) where dashed lines correspond to DDRH-MC and solid lines correspond to DD-ME1, respectively. For the symmetric nuclear matter, two curves are almost identical for densities below saturation density, but the saturation point of the DDRH-MC calculation is located at higher density with the small binding energy. From Table. 6.2 one can see that the difference between DDRH-MC and DD-ME1 binding energies is about ± 5 % which may caused by differences of the σ and ω meson vertices at the saturation density. (see Section. 5.4)
On the other hand, this is related to the roots of the density dependent vertices. In fact that DD-ME1 gives the empirical saturation point due to the fitting procedure and DDRH-MC also reproduces the DB saturation point. The saturation density in our model is $\rho_{sat} = 0.18$ fm^{-3} is somewhat higher than the accepted empirical value, $\rho_{sat} = 0.16$ fm^{-3}. The binding energy of $E(\rho_{\rm sat}) = \epsilon(\rho_{\rm sat})/\rho_{\rm sat} = 15.60$ MeV is in agreement with the value deduced from nuclear data.

	$\rho_0[fm^{-3}]$	$\epsilon/\rho\,[MeV]$	$K\,[MeV]$	$a_4\,[MeV]$	m^*/M
DDRH-MC	0.180	-15.60	282.4	26.1	0.553
DD-ME1	0.152	-16.20	244.5	33.1	0.578

Table 6.2: Bulk properties of the symmetric nuclear matter calculated with the density-dependent DDRH-MC and DD-ME1 vertices at saturation density.

The bulk properties of symmetric nuclear matter at saturation density, such as the density ρ_0, the binding energy per nucleon ϵ/ρ, the compressibility K, the effective mass m^*, and the symmetry energy a_4 are summarized in Table. 6.2 for the two parameter sets DDRH-MC and DD-ME1.
From Table. 6.2, one can see that the differences between DDRH-MC and DD-ME1 are for the incompressibility about 38 MeV and for the symmetry energy 7 MeV at saturation density, while they have 5 % difference for their effective masses. Moreover the DD-ME1 gives a steeper EOS than DDRH-MC and the difference between two approaches becomes larger as the density increases. In the case of the pure neutron matter, the EOS has no minimum and the difference between two approaches remains roughly constant with increasing density. The reason is that the inclusion of the δ meson whose contribution to the EOS of the neutron rich nuclear matter gets more significant that one can see from the EOS of the asymmetric nuclear matter as we displayed in Figs. 6.12-6.14. Results of the DDRH-MC calculation for EOS are shown in Figs. 6.12 where the solid square, circle and triangle curves are for the proton fraction α=0.10, 0.25 and 0.39, respectively (here, the big solid circle indicates the energy minimum). For increasing asymmetry, the saturation density shifts to lower values and is depicted in Fig. 6.13. Consequently, the properties of the asymmetric nuclear matter at saturation density are also changed that one can see explicitly from Table. 6.3 in where the values of the quantities: ρ_{sat}, ϵ/ρ , K, a_4 and m^* are given. In the both approach, by comparing these values, all quantities except effective baryon masses become smaller as the asymmetry parameter increases. Because, the effective baryon mass decreases with increasing baryon density in contrast to the symmetry energy and the compressibility, (see Subsections. 6.2.5, 6.2.7 and 6.2.8). However the difference between the two approaches becomes much larger for neutron rich nuclear matter. For example, the difference between the binding energies is about 4 % for the asymmetry parameter $x = 0.22$ but for the asymmetry parameter $x = 0.8$ the difference is about 10 %. In the case of the incompressibility which is extremely sensitive to changes in the saturation curve, the discrepancy between the compressibilities of the

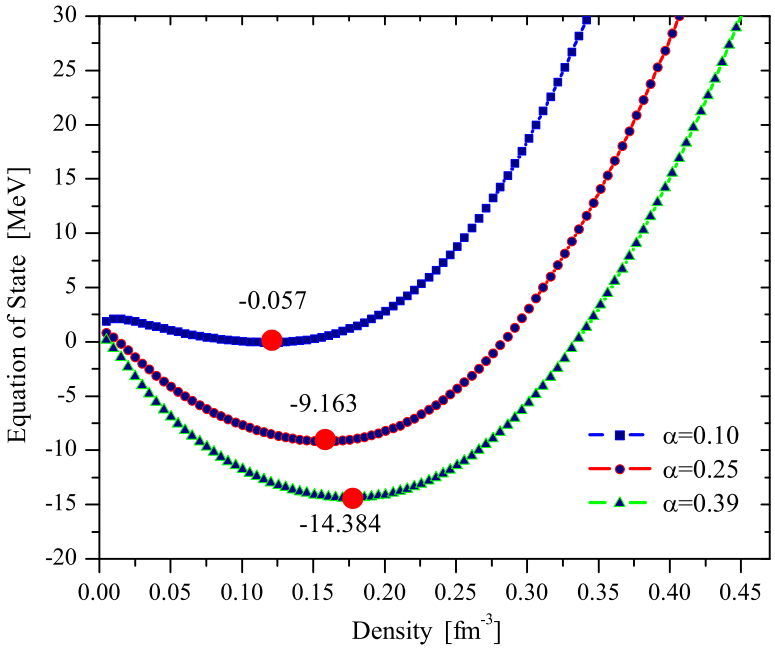

Figure 6.12: The equation of state of asymmetric nuclear matter with three different asymmetries ($\alpha = 0.10, 0.25, 0.39$) in DDRH-MC.

DDRH-MC and the DD-ME1 is about ranges between 48 MeV and 88 MeV.

In Fig. 6.14, we show the EOS of asymmetric nuclear matter for three different asymmetries calculated in DDRH-MC (dashed line) and DD-ME1 (solid line) and one sees that DD-ME1 gives larger energies than DDRH-MC above the saturation density. In addition, at higher density, two saturation curves are getting closer as the proton fraction decreases from α =0.39 to 0.00. This is due to the isovector scalar δ-meson in the DDRH-MC calculation. Because, in DDRH-MC approach the symmetry energy rises almost linearly with density. In contrast, in the DD-ME1 the symmetry energy flattens with density (see Fig. 6.15). Otherwise two saturation curves would have a constant changes caused by only α, because the meson-nucleon vertices are independent of the asymmetry.

Since, in this section we discussed mainly the properties of the symmetric and asymmetric nuclear matter only at the saturation point, the density dependence of these quantities will be discussed in detail in the following sections.

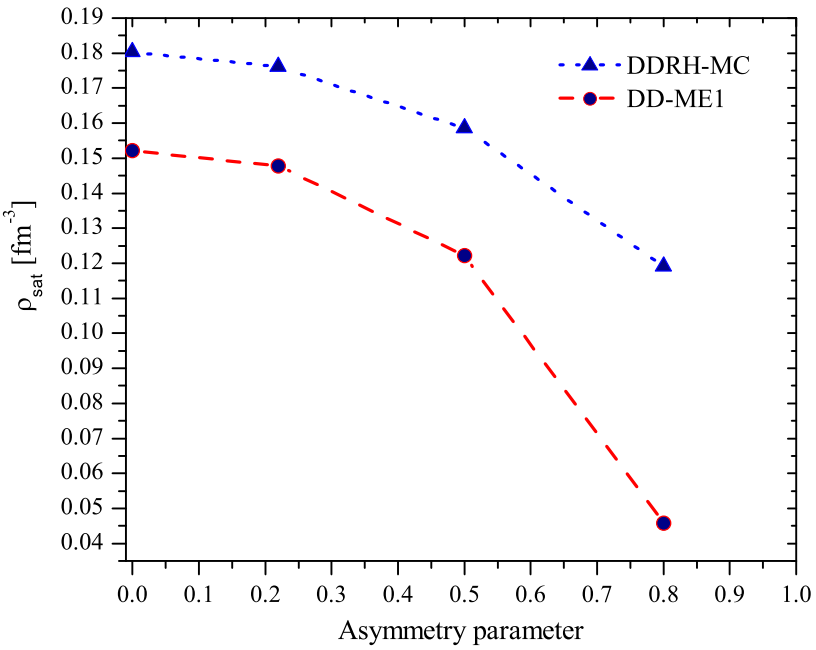

Figure 6.13: The saturation density versus asymmetry parameter in the DDRH-MC (dotted curve with triangles) and DD-ME1 (dashed curve with circles).

	x_i	ρ_{sat} [fm^{-3}]	ϵ/ρ [MeV]	K [MeV]	$a4$ [MeV]	m^*_{p}/M	m^*_{n}/M
DDRH-MC	0.22	0.176	-14.384	272.47	25.7	0.578	0.547
	0.5	0.158	-9.163	216.48	24.3	0.626	0.558
	0.8	0.119	-0.057	77.59	20.9	0.713	0.628
DD-ME1	0.22	0.148	-14.683	224.02	32.8	0.580	
	0.5	0.122	-8.178	128.32	28.9	0.640	$m^*_p = m^*_n$
	0.8	0.046	1.188	21.33	14.9	0.827	$(\delta = 0)$

Table 6.3: The properties of the asymmetric nuclear matter calculated in DDRH-MC and DD-ME1.

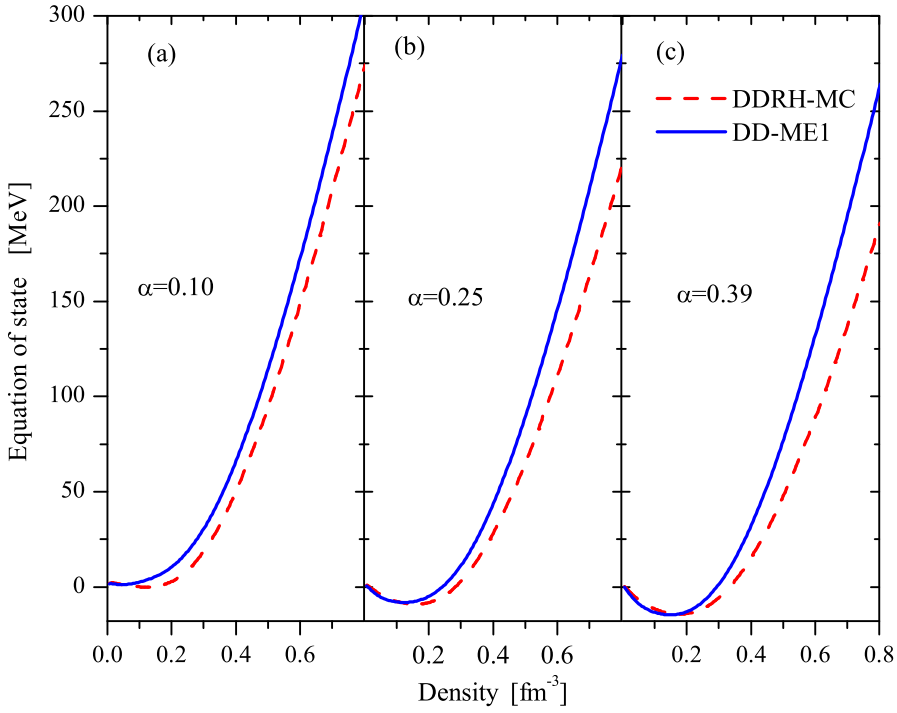

Figure 6.14: The equation of state of the asymmetric nuclear matter for three different asymmetries calculated in DDRH-MC (dashed line) and DD-ME1 (solid line).

6.2.5 Nuclear symmetry energy

Experimentally, the symmetry energy coefficient $E_{\rm sym}$ in nuclear matter at the saturation density ρ_0 can be extracted from a systematic study of the masses of atomic nuclei, based on, e.g., the liquid droplet model or the macroscopic-microscopic model. This, however, determines the symmetry energy only for a small asymmetry parameter and for around normal density.

In Section. 6.2.4 as we have shown in Fig. 6.12 that in asymmetric nuclear matter the saturation point shifts to lower densities and the difference of EOS becomes more noticeable at high density. In addition, the study of the nuclei with a large neutron excess which will be produced in future radioactive ion beam facilities, allows us to determine the symmetry energy for a large asymmetry parameter. Therefore, the experimental and theoretical study of the symmetry energy and its dependence on the density and the asymmetry is a very important topic.

The nuclear symmetry energy defined by

$$E_{\rm sym}(\rho) = \frac{1}{2}\rho^2 \frac{\partial^2}{\partial \rho_3^2}\frac{\epsilon}{\rho}(\rho,\rho_3) \ . \tag{6.56}$$

Based on the assumption of charge symmetry of the nuclear interaction, energy per particle $E(\rho,x) = \frac{\epsilon(\rho,x)}{\rho}$ of the asymmetric nuclear matter can be written

$$E(\rho,x) = E(\rho,0) + S_2(\rho)x^2 + S_4(\rho)x^4 + S_6(\rho)x^6 ... \ , \tag{6.57}$$

where x is the asymmetry parameter defined in (6.1). Calculations indicate that if the higher order terms $S_4, S_6, ...$, are negligible, for all densities. Thus to a good approximation the energy per particle of asymmetric nuclear matter can be written as

$$E(\rho,x) = E(\rho,0) + S_2(\rho)x^2 = E(\rho,0) + E_{\rm sym}(\rho)x^2 \ , \tag{6.58}$$

and the symmetry energy can be expressed in terms of the difference of the energy per particle between symmetric and asymmetric nuclear matter with corresponding asymmetry parameter:

$$E_{\rm sym}(\rho) \equiv S_2(\rho) = \frac{E(\rho,x) - E(\rho,0)}{x^2} \ . \tag{6.59}$$

In Fig. 6.15, we presented our results for the symmetry energy $E_{\rm sym}$ calculated according to its definition Eq. (6.56) compared to the results of DD-ME1 approach. In the DDRH-MC approach, the symmetry energy (dash-dotted line) increases almost linearly with density. The same behavior is found in the DBHF calculation [LKLB97]. In contrast, the DD-ME1 approach shows a considerable flattening at $\rho > 0.3$ fm^{-3}. The region $\rho < 0.3$ fm^{-3}, DDRH-MC approach predicts slightly lower $E_{\rm sym}$ than DD-ME1 approach but above the density DDRH-MC approach predicts much larger Esym than the DD-ME1 approach. Therefore in Tables. 6.2 and 6.3, the values of the $E_{\rm sym}$ calculated in DDRH-MC are smaller than the DD-ME1 values at saturation density. In the case of the symmetric nuclear matter, the $E_{\rm sym}$ at saturation density in the DDRH-MC is $E_{\rm sym}(\rho_{\rm sat}) = 26.1$ MeV which is in agreement with the empirical value of 30 ± 4 MeV [Hau88].

Although various different forms of the density dependence of the symmetry energy exist, in general, they can be divided into two different forms which are the stiff and soft dependence [SMK$^+$03]. The stiff dependence of the symmetry energy leads to a large

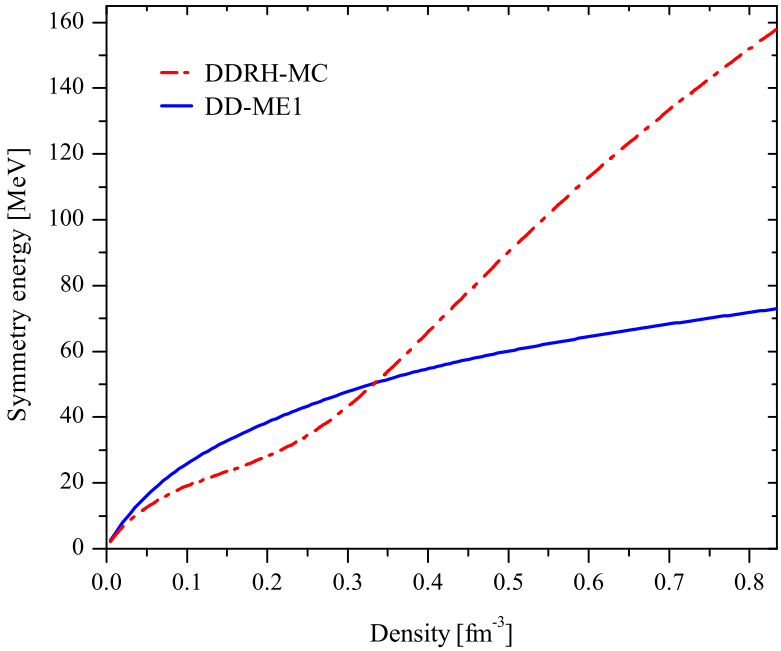

Figure 6.15: The symmetry energy $E_{\rm sym}$ in Eq. (6.56) as a function of the baryon density in DDRH-MC (dash-dotted) and the comparison with the DD-ME1 (solid).

neutron skin thickness and larger neutron radius compared to a soft density dependence [HP01, HP02].

Very recently, based on the experimental measurements (heavy ion collision) in [SYB$^+$04] carried out at the Cyclotron Institute, Texas A&M University, Shetty et al., have found that the density dependence of the symmetry energy in [SYS07] as

$$E_{sym}(\rho) \approx 31.6\ (\rho/\rho_0)^{\gamma}\ , \tag{6.60}$$

where $\gamma = 0.6 - 1.05$. This constrains the form of the density dependence of the symmetry energy at higher densities, exclude an extremely stiff and soft dependences. Moreover it is observed that the experimental data at low densities are consistent with the form of symmetry energy, $E_{\rm sym} \approx 31.6\ (\rho/\rho_0)^{0.69}$ which is in close agreement with the results of variational many-body calculation.

Therefore we also compared our results to this newly determined $E_{\rm sym}$ and is shown in Fig. 6.16. The results of the calculation for $E_{\rm sym}$ using Eq. (6.60) are plotted by

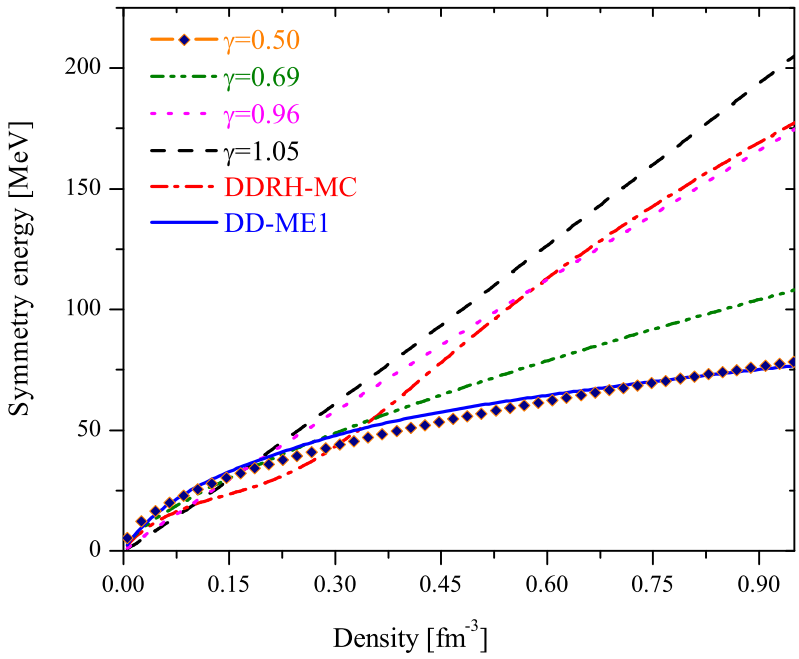

Figure 6.16: The same as in Fig. 6.15 for the DDRH-MC and DD-ME1, but the other lines correspond to the E_{sym} in Eq. (6.60) for $\gamma = 0.5$ (diamonds); $\gamma = 0.69$ (dash-dot dot); $\gamma = 0.96$ (dotted); $\gamma = 1.05$ (dashed).

the curves: diamonds ($\gamma = 0.5$), dash-dot dot ($\gamma = 0.69$), dotted ($\gamma = 0.96$) and dashed ($\gamma = 1.05$). One can see that our results (dash-dot) is in agreement with the curve for $\gamma = 0.96$ at high density but it has a significant difference at lower density. The results of the DD-ME1 calculation is very similar to curve of $\gamma = 0.5$ which is not in the region of $\gamma = 0.6 - 1.05$, suggested in [SYS07]. Although E_{sym} in the DD-ME1 calculation gives a too soft dependence at higher density, is in good agreement with all results of [SYS07] at low density.

6.2.6 Isospin dependence of Symmetry energy

Another investigation to be done is the calculation for S_2. In Fig. 6.17 we show the results for the $S_2(\rho)$ calculated using the four values $x = 1, 0.8, 0.5, 0.22$ in Eq. (6.59) with $E_{sym}(\rho)$ calculated from Eq. (6.56) in the approaches DDRH-MC and DD-ME1. In the all panels (a, b, c, d), the dash-dotted and dotted curves correspond to DDRH-MC

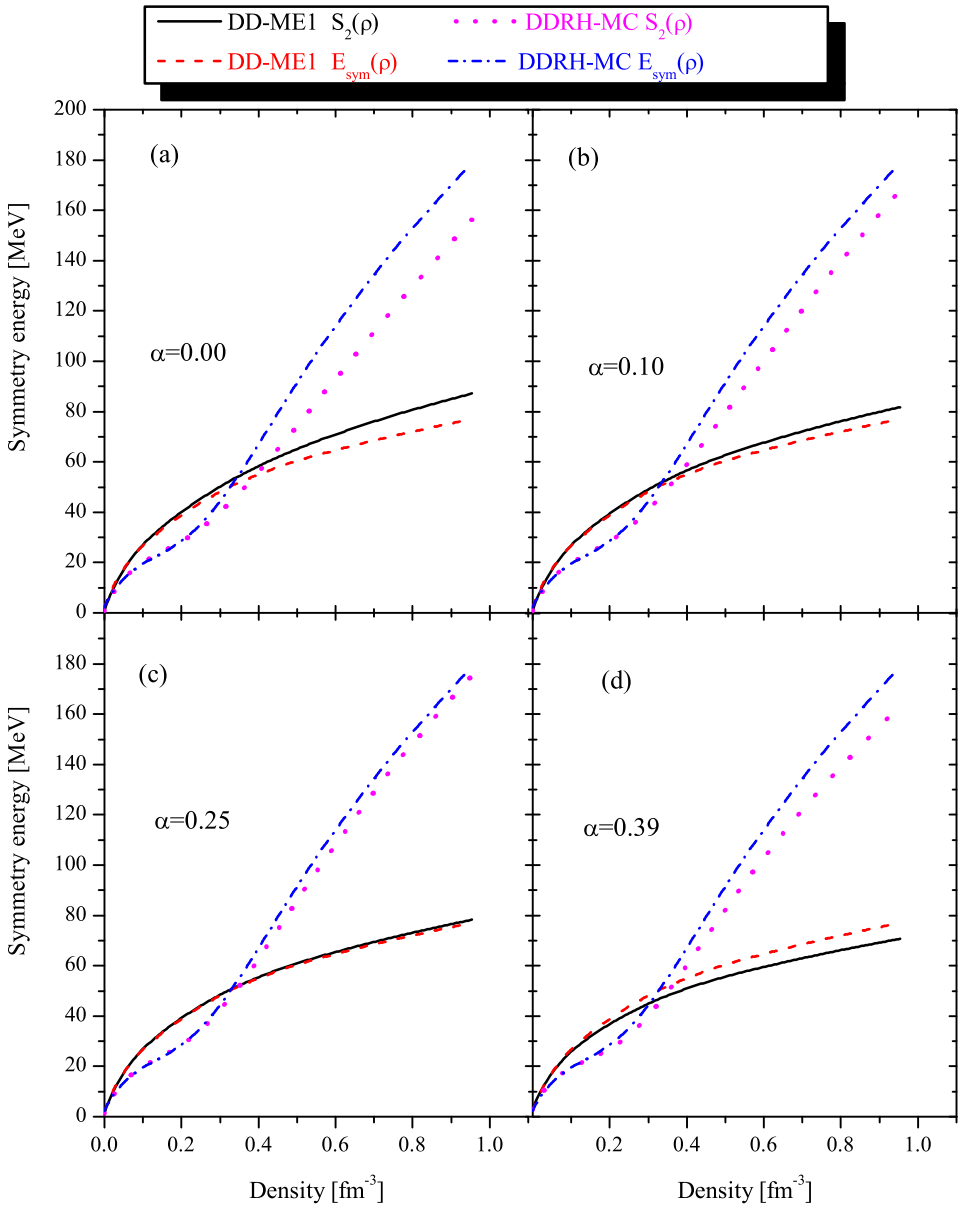

Figure 6.17: Comparision of the E_{sym} in Eq. (6.56) and S_2 in Eq. (6.59) for $x = 1$ (a); $x = 0.8$ (b); $x = 0.5$ (c); $x = 0.22$ (d) in DDRH-MC and DD-ME1 calculations.

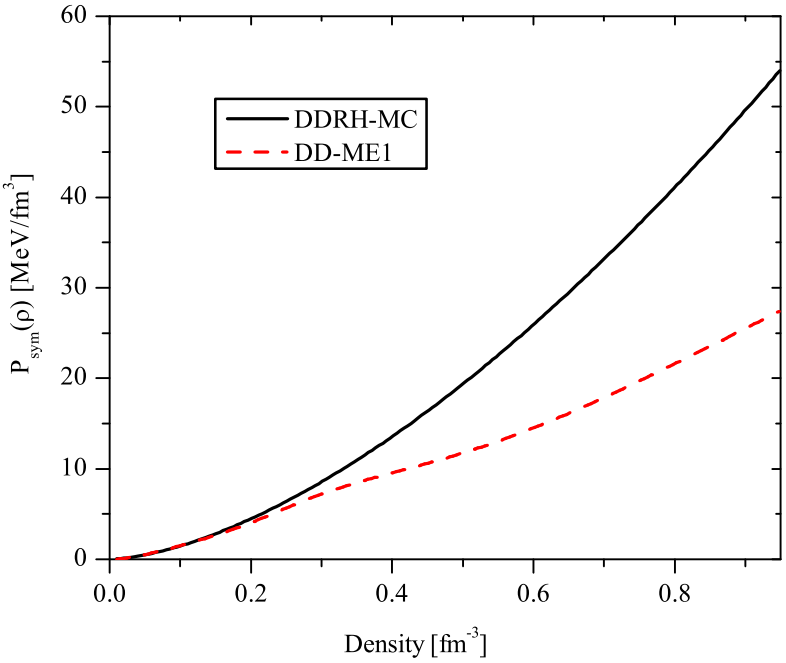

Figure 6.18: The symmetry pressure versus the baryon density in DDRH-MC and DD-ME1.

results for $E_{sym}(\rho)$ and $S_2(\rho)$, respectively. The solid and dashed curves correspond to DD-ME1 results for $E_{\rm sym}(\rho)$ and $S_2(\rho)$, respectively. One can see that the two approaches predict almost no difference between S_2 and $E_{\rm sym}$ for all values of α from 0 to 0.39 in the region of $\rho < 0.3$ fm^{-3}. But above the density, the difference between S_2 and $E_{\rm sym}$ is noticeable ($S_2 \leq E_{\rm sym}$ except in the case of $\alpha = 0.39$) for both DDRH-MC and DD-ME1 cases. In addition it increases with a large asymmetry parameter in the DDRH-MC approach more than in the DD-ME1 calculation. The reason for that is an inclusion of the δ-meson in DDRH-MC approach. Therefore one may take into account the higher order terms i.e. S_4 in Eq. (6.57) for the calculation of the $E(\rho, x)$ of the asymmetric nuclear matter at high density. On the other hand, it is clear that S_4 is very small and the same is found in [LKLB97]. Because the difference in Fig. 6.17 is a term $S_4(\rho)\, x^4$, not only $S_4(\rho)$. One of the nuclear structure properties connected to the symmetry energy is the symmetry pressure P_{sym} defined as

$$P_{\rm sym} = \rho^2 \frac{dE_{\rm sym}}{d\rho} \ . \tag{6.61}$$

	DDRH-MC	DD-ME1	TW-99
$\rho_0[\mathrm{fm}^{-3}]$	0.180	0.152	0.153
a_4 [MeV]	26.1	33.1	32.5
$P_{\mathrm{sym}}(\rho_0)[\mathrm{MeV/fm}^3]$	3.8	3.26	3.22
$K_{\mathrm{sym}}(\rho_0)[\mathrm{MeV}]$	-75.75	-128.5	-126.5

Table 6.4: The parameters a_4, $P_{\mathrm{sym}}(\rho_0)$ and $K_{\mathrm{sym}}(\rho_0)$ in Eqs. (6.62-6.64) calculated in the DDRH-MC, DD-ME1 and TW-99 [TW99].

This is an additional pressure source due to the different proton and neutron concentration and is also related to the neutron skin thickness of the neutron-rich nuclear matter. The density dependence of P_{sym} is depicted in Fig.6.18. Again, we see the stiff dependence from DDRH-MC calculation (dashed) and the very soft dependence from DD-ME1 result (solid) at high density which is similar to the behavior found for E_{sym}.
Another two parameters also connected to the symmetry energy, are the slope parameter L and the curvature parameter K_{sym} and its explicit expressions are obtained from the expansion of the symmetry energy around ρ_0 in [LGB$^+$02, LQMN$^+$88, Li01] as

$$E_{\mathrm{sym}} = a_4 + \frac{L}{3}\left(\frac{\rho-\rho_0}{\rho_0}\right) + \frac{K_{\mathrm{sym}}}{18}\left(\frac{\rho-\rho_0}{\rho_0}\right)^2 \tag{6.62}$$

with

$$L \equiv 3\rho_0\left(\frac{\partial E_{\mathrm{sym}}}{\partial\rho}\right)_{\rho=\rho_0} = \frac{3}{\rho_0}P_{\mathrm{sym}}(\rho_0) \tag{6.63}$$

and

$$K_{\mathrm{sym}} \equiv 9\rho_0^2\left(\frac{\partial^2 E_{\mathrm{sym}}}{\partial\rho^2}\right)_{\rho=\rho_0}, \tag{6.64}$$

the values are shown in Table. 6.4 and its density dependence are presented in Figs. 6.19 and 6.20. The empirical values of the parameters are [KBB$^+$94, SH94]: $a_4 \approx 30-34$ MeV, 2 MeV/fm^3 $< P_{\mathrm{sym}}(\rho_0) <$ 4 MeV/fm^3, and $-220\ MeV < K_{\mathrm{sym}}(\rho_0) < -50$ MeV. As we see the results of the DD-ME1 and TW-99 are agree very well the empirical values for all three parameters. Although our results of the $P_{\mathrm{sym}}(\rho_0)$ and $K_{\mathrm{sym}}(\rho_0)$ are in agreement with the empirical values, the value of a_4 is not in the interval.

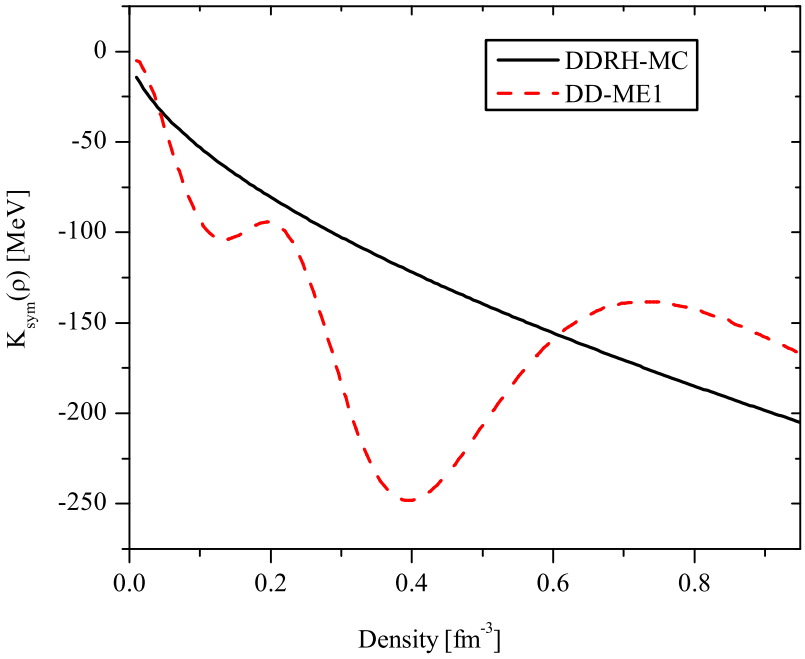

Figure 6.19: The curvature parameter K_{sym} versus the baryon density in DDRH-MC and DD-ME1.

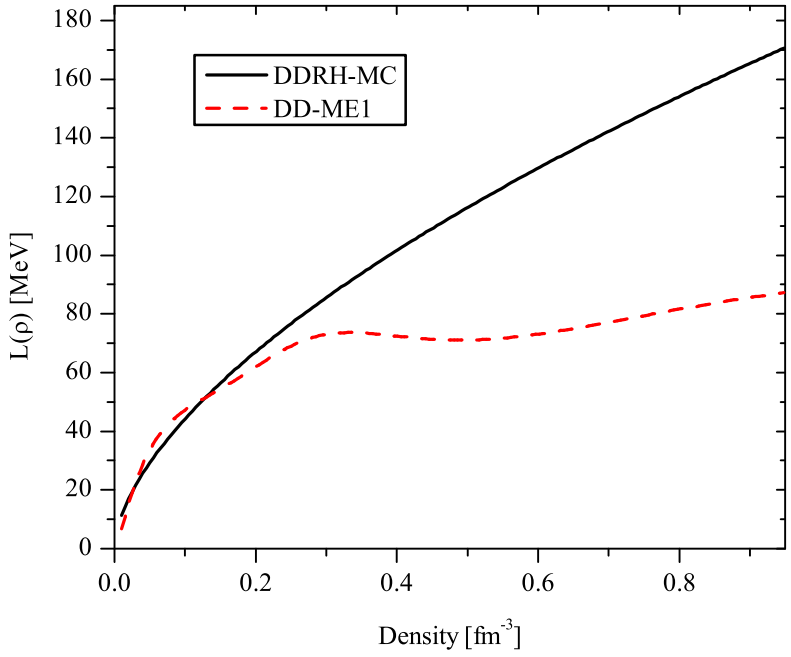

Figure 6.20: The slope parameter L versus the baryon density in DDRH-MC and DD-ME1.

6.2.7 Effective nucleon masses

In order to describe the properties of the nucleons inside an interacting nuclear medium, we investigate the effective mass of nucleons in symmetric and asymmetric nuclear matter.

The nucleon effective mass m^* can be determined from the analysis of the experimental data which is performed in the framework of the non-relativistic shell and optical models [BGH85, JHM87, JM89, Rei99]. The typical empirical value of the effective nucleon mass in nuclear matter is $m^*_{\rm emp}/M \approx (0.7-0.85)$. However, the relation to the relativistic Dirac-mass considered here is not well understood because of dispersion effects in $m^*_{\rm emp}$. Relativistically, the effective nucleon mass is defined through the scalar part of the nucleon self-energy in the Dirac field equation.

In our model, the neutron and proton effective masses defined as

$$m^*_p = M - \Gamma_\sigma(\rho)\Phi_\sigma - \Gamma_\delta(\rho)\Phi_\delta \tag{6.65}$$

$$m^*_n = M - \Gamma_\sigma(\rho)\Phi_\sigma + \Gamma_\delta(\rho)\Phi_\delta \tag{6.66}$$

where M and m^* are respectively the free-space and the effective nucleon mass (see the solution techniques in Section. 6.2). Therefore, inclusion of the scalar isovector δ-meson leads to $m^*_n \neq m^*_p$ in contrast to the DD-ME1 predicts equal masses $m^*_n = m^*_p$.

In Fig. 6.21 (panel a), the effective masses obtained in DDRH-MC calculation (dashed curve) is compared with DD-ME1 result (solid curve) in symmetric nuclear matter. The difference between two approaches which is quite small and almost constant is caused by the slightly different density dependence of the scalar-isoscalar σ-meson vertex. At saturation density, the DD-ME1 predicts $m^*/M = 0.578$ and DDRH-MC predicts $m^*/M = 0.553$ which is smaller, though $m^*_{\rm DDRH-MC} > m^*_{\rm DD-ME1}$ for whole range of the density. The reason for that is the saturation density in the DDRH-MC is shifted to the higher density and m^* becomes smaller for increasing density in both approaches. Neither the DDRH-MC nor the DD-ME1 agree the empirical values of m^* indicating the dispersion contributions mentioned above.

In Fig. 6.21 (panel b) we depicted the effective masses in neutron matter. The dashed, dash-dotted and dotted curves are the DDRH-MC results for m^*_p , m^*_n and the isoscalar part of m^* respectively. The solid curve is the result of the DD-ME1. Comparing the results for symmetric nuclear matter and pure neutron matter, we see the following features:

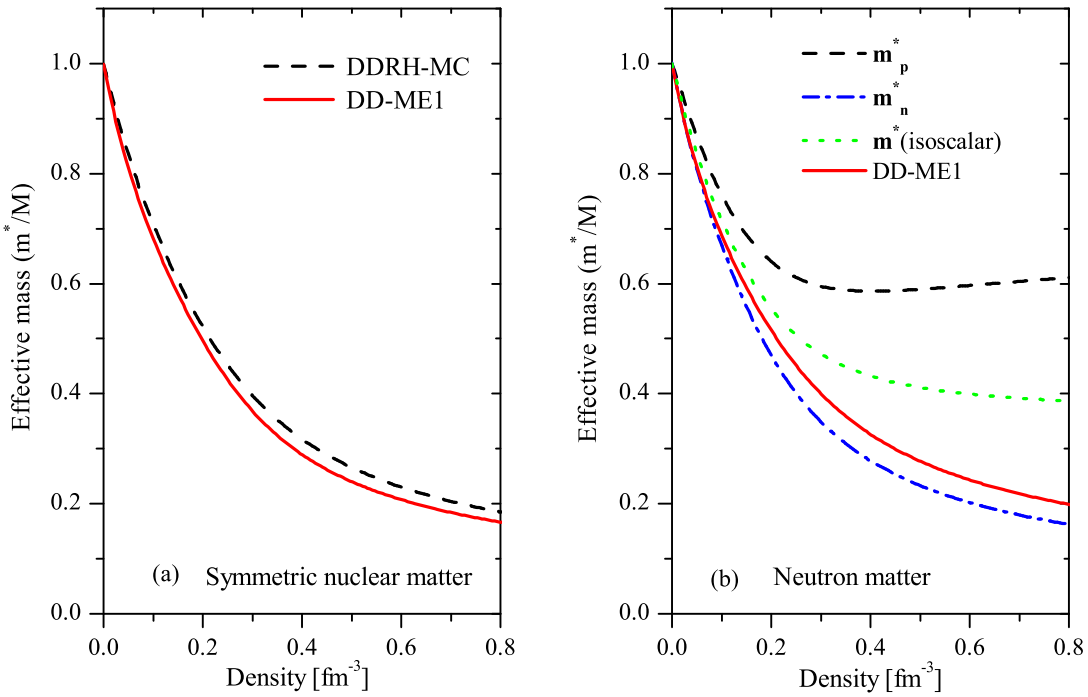

Figure 6.21: (a) Effective mass obtained in DDRH-MC calculation (dashed curve) is compared with DD-ME1 (solid curve) depicted as a function of the baryon density in symmetric nuclear matter. (b) Effective masses in neutron matter. The dashed, dash-dotted and dotted curves are the DDRH-MC results corresponding to proton, neutron and isoscalar effective masses, respectively. The solid curve represents result of DD-ME1 in neutron matter.

1. The m^* of the DD-ME1 for pure neutron matter is the almost same as for symmetric nuclear matter case because the scalar-isovector interaction is missing. Slight differences occur due to in pure neutron matter the selection between Fermi-momentum and density is changed, $\rho = \rho_{\rm n} = k_{F_{\rm n}}^3/3\pi^2$ and $\Phi_\sigma \sim \rho f_\sigma(k_{F_{\rm n}}/M)$.

2. In the case of DDRH-MC results, the m^* split into m_p^* and m_n^* in neutron matter according to Eqs. (6.65-6.66) and (4.34-4.36). In addition, $m_p^* > m_n^*$ for the whole range of the density because m_p^* is generated by the scalar density of the neutron ρ_n^s (see Fig. 6.25), though $\rho_p^s = 0$.

3. The DDRH-MC predicts much larger isoscalar m^* than the DD-ME1.

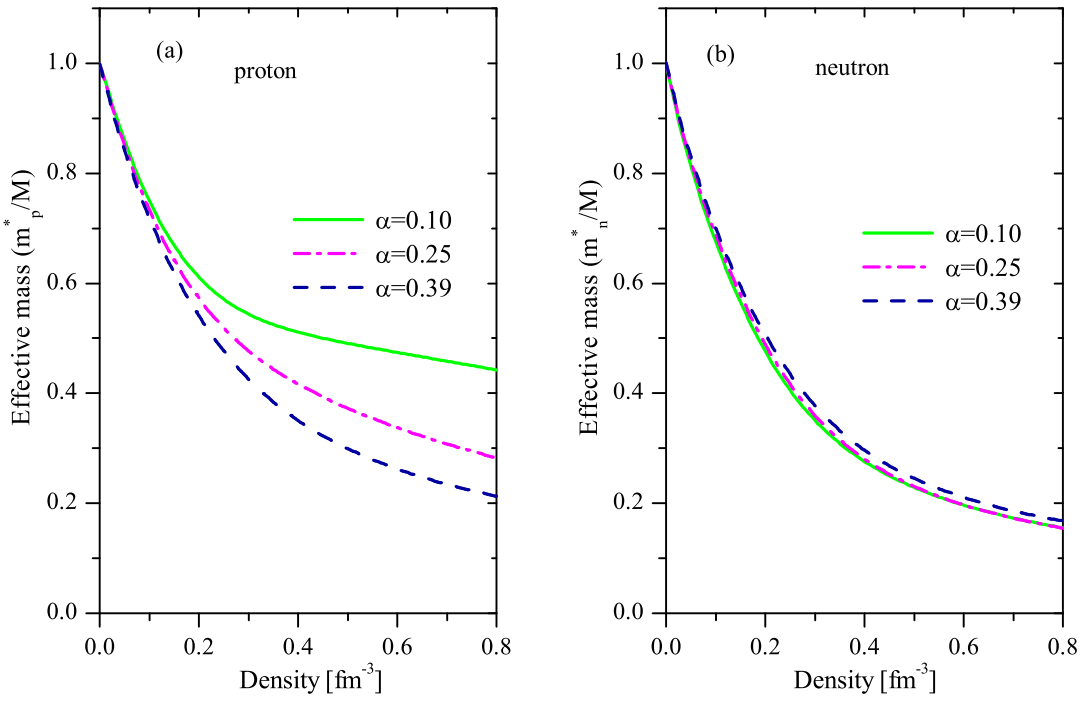

Figure 6.22: Proton (a) and neutron (b) effective masses versus the baryon density for asymmetric nuclear matter with different asymmetries in DDRH-MC.

We define the isoscalar (m_0^*) and isovector (m_1^*) part respectively, of the effective mass as follow

$$m_0^*(\rho) = M - \Gamma_\sigma(\rho)\Phi_\sigma = \frac{m_n^*(\rho) + m_p^*(\rho)}{2} , \tag{6.67}$$

$$m_1^*(\rho) = \frac{m_p^*(\rho) - m_n^*(\rho)}{2} . \tag{6.68}$$

In Fig. 6.22 we displayed the m_n^* (panel a) and m_p^* (panel b) in asymmetric nuclear matter for proton fraction α =0.10 (solid), 0.25 (dash-dotted) and 0.39 (dashed). m_p^* becomes larger for increasing asymmetry parameter in contrast to m_n^* gets smaller. Consequently, the difference between m_p^* and m_n^* becomes larger as the asymmetry increases. Also, a neutron effective mass is always smaller than the proton effective mass in neutron-rich matter as we expect. The values of the m_p^* and m_n^* at the saturation density are listed in Table. 6.3.

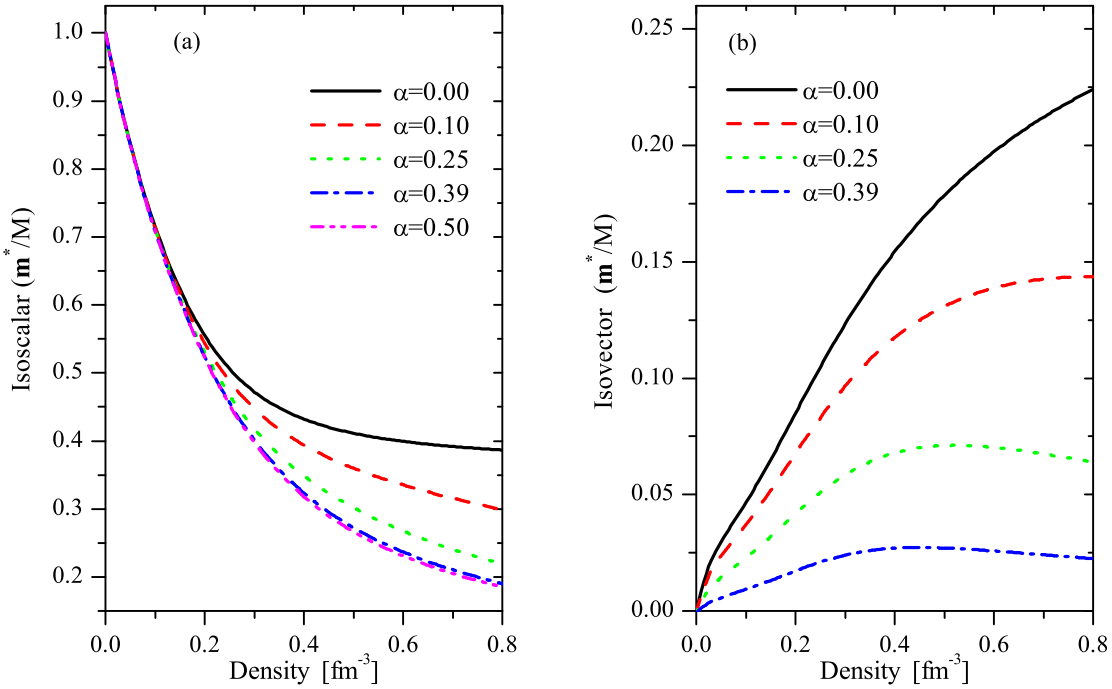

Figure 6.23: The isoscalar (a) and the isovector (b) components of the effective masses in nuclear matter for different asymmetries as a functions of the baryon density in DDRH-MC.

Fig. 6.23 shows the isoscalar (panel a) and the isovector (panel b) part of the effective masses as functions of the densities for several values of the asymmetry parameters using Eqs. (6.67-6.68). Although $m^*_{(1)}$ increasing with density and asymmetry parameter, it is very small compared to $m^*_{(0)}$. Also, we compared our results for $m^*_{(0)}$ to the effective masses calculated in DD-ME1 approach, is depicted in Fig. 6.24 and $m^*_{(0)}$ in DDRH-MC (solid) is larger than m^* in DD-ME1 (dash-dotted) for α =0.10 (panel a), 0.25 (panel b) and 0.39 (panel c) due to the scalar σ-meson.

We plotted the $m^*_{\rm n}$ (dashed) and $m^*_{\rm p}$ (solid) in neutron matter as a function of the neutron scalar density in Fig. 6.25.

In Fig. 6.26 we show the neutron and proton scalar density dependence of the $m^*_{\rm n}$ (panel a) and m^*_p (panel b) respectively for the proton fractions α from 0.10 to 0.50. The behavior of the $m^*_{\rm n}$ and $m^*_{\rm p}$ are similar to its vector density dependence. It is noted that $m^*_{\rm n} \sim \rho_s$ depends almost linearly on the scalar density. The reason is that the σ and

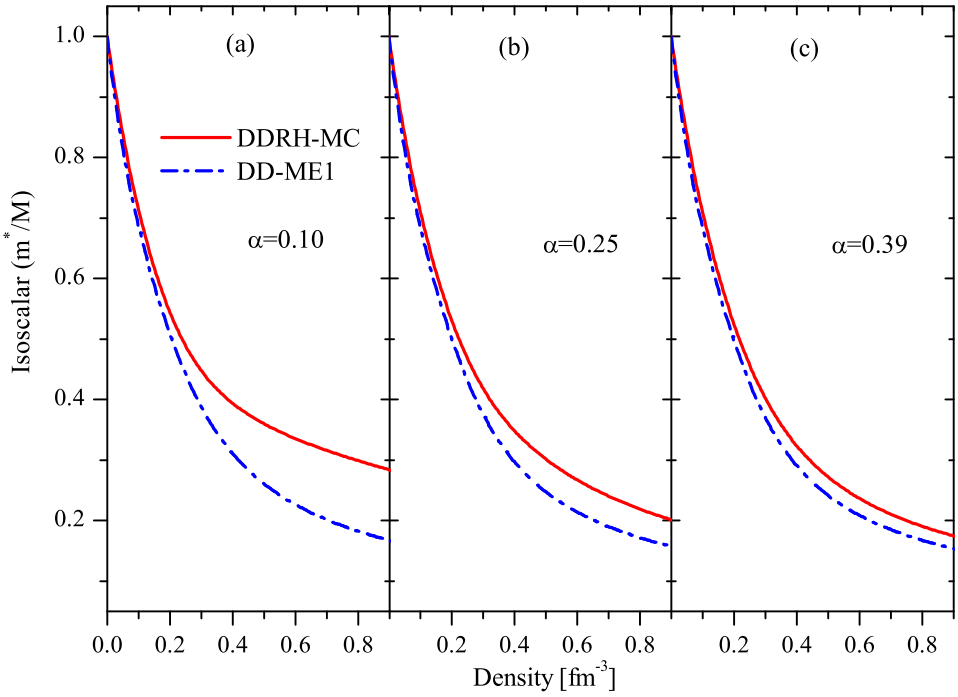

Figure 6.24: The isoscalar effective masses calculated in DDRH-MC (solid) and DD-ME1 (dashed) for three different asymmetries ($\alpha = 0.10, 0.25, 0.39$).

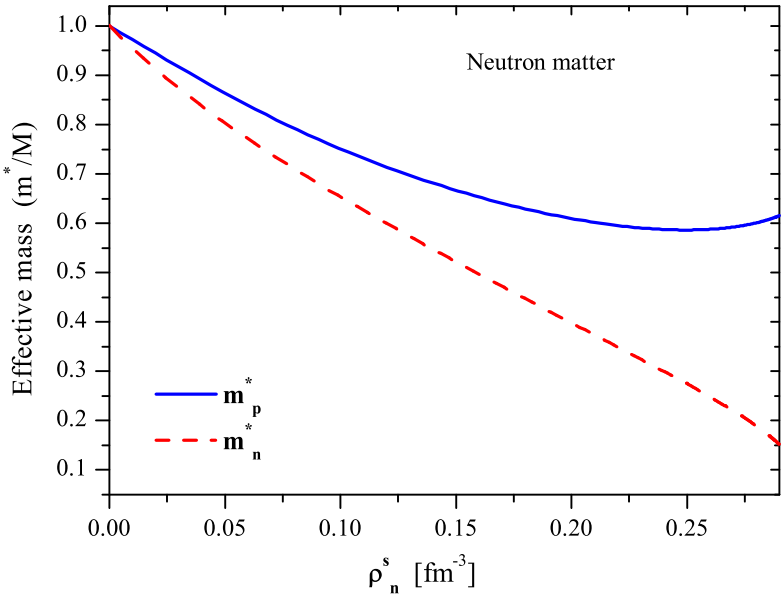

Figure 6.25: Proton (solid) and neutron (dashed) effective masses in neutron matter as a function of the neutron scalar density in DDRH-MC.

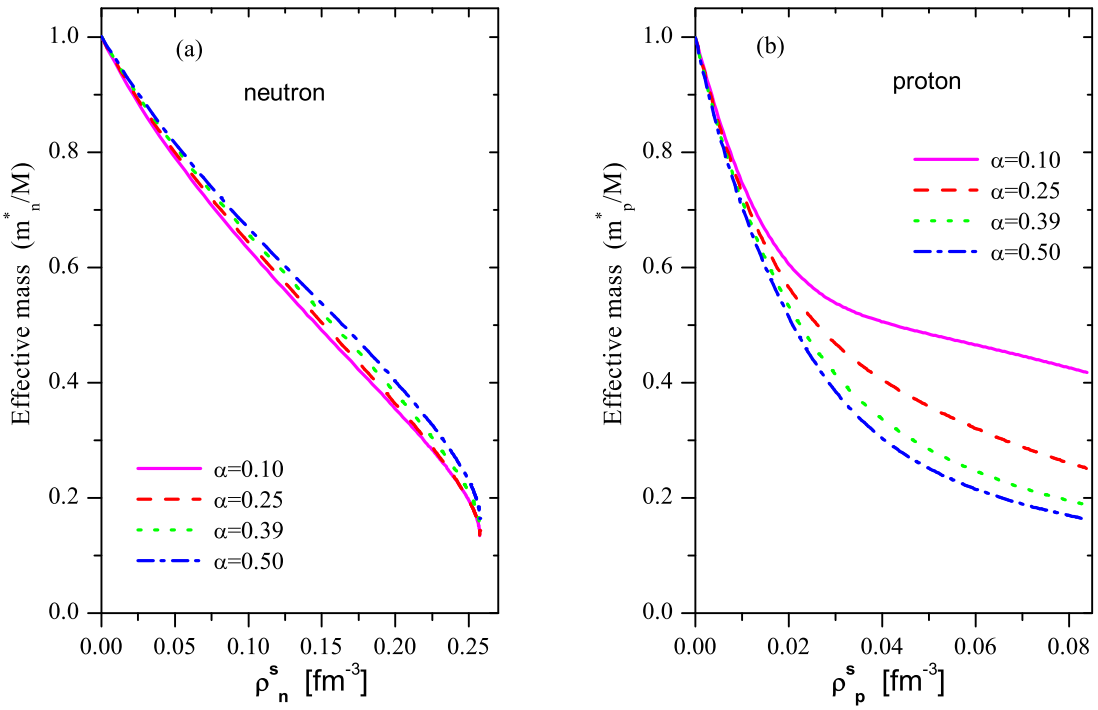

Figure 6.26: The scalar density dependence of the neutron (a) and the proton (b) effective masses for various asymmetries.

δ contribution both enter with the same sign into $m^*_{\rm n}$. In $m^*_{\rm p}$, however the two fields enter destructively and, thereby enhance considerably the non-linear pieces introduced by the coupled transcendental equations, Eqs. (6.65-6.66)

Proton-neutron mass splitting was explored in both non-relativistic and relativistic ways. However, based on their definition for the effective mass, i.e. in non-relativistic model, the effective mass reflects the momentum and energy dependence of the single particle energy while the relativistic effective mass is given by the scalar part of the static nucleon self-energy only. Its mentioned before we can not expect agreement. For example the relativistic Dirac-Brueckner and RMF calculations [HKL01b, LGB$^+$02] predict a proton-neutron mass splitting of $m^*_{\rm n} < m^*_{\rm p}$ which are consistent with our results. This stands in contrast to non-relativistic Brueckner-Hartree-Fock calculation [ZBL99]. Moreover the Skyrme-Lyon (SLya) force leads to $m^*_{\rm n} < m^*_{\rm p}$ in contrast to the other type of Skyrme forces [BCGT05].

	TW-99	DD-ME1	DDRH	DDRH-MC
$\rho_{sat}\ [fm^{-3}]$	0.153	0.152	0.161	0.180
$K\ [MeV]$	240.0	244.5	211.34	282.42

Table 6.5: The compressibility of the symmetric nuclear matter at saturation density calculated with the phenomenological TW-99 and DD-ME1, and the microscopic DDRH approaches.

6.2.8 Compressibility

The compressibility (or compression modulus) of the nuclear matter is an important characteristic of the nuclear matter equation of state and it enters in the discussion of a variety of phenomena such as supernovae explosions or heavy ion collisions. The compressibility of the nuclear matter, K is the quantity of energy required to compress the nuclear matter, usually defined as a slope of the pressure at saturation point:

$$K = 9\frac{\partial P}{\partial \rho}_{|\rho=\rho_{sat}} . \tag{6.69}$$

Although K is a static quantity, it can not be extracted from static properties, i.e. masses and charge distributions, alone [FPT97]. Moreover, the value of K can not be measured directly. However, it can be deduced from the experimental energies of isoscalar monopole vibrations of the excited nuclei, so called giant monopole resonances (GMR) where the nucleus performs density fluctuations around its ground state. A recent analysis of the giant monopole resonance in heavy nuclei [BBDG95] provides an experimental estimate for the compressibility, $K = 210 \pm 30$ MeV.
Calculations of the excitation energies of isoscalar GMR in spherical nuclei in the RMF framework [VLB$^+$97, VNR03] and in the relativistic randomphase approximation (RPA) [MGW$^+$01, NVR02] suggest that the nuclear matter compressibility should be in the range $K \approx 250 - 270$ MeV.
In order to calculate K in our model we applied

$$K = k_F^2 \frac{\partial^2}{\partial k_F^2}\left(\frac{E}{k_F}\right)_{|k_F=k_F^{sat}} = 9\rho^2 \frac{\partial^2}{\partial \rho^2}\left(\frac{\epsilon}{\rho}\right)_{|\rho=\rho_{sat}} , \tag{6.70}$$

following the convention used in nuclear physics for the compressibility. Results are presented in Figs. 6.27-6.29 and Tables. 6.5-6.7.

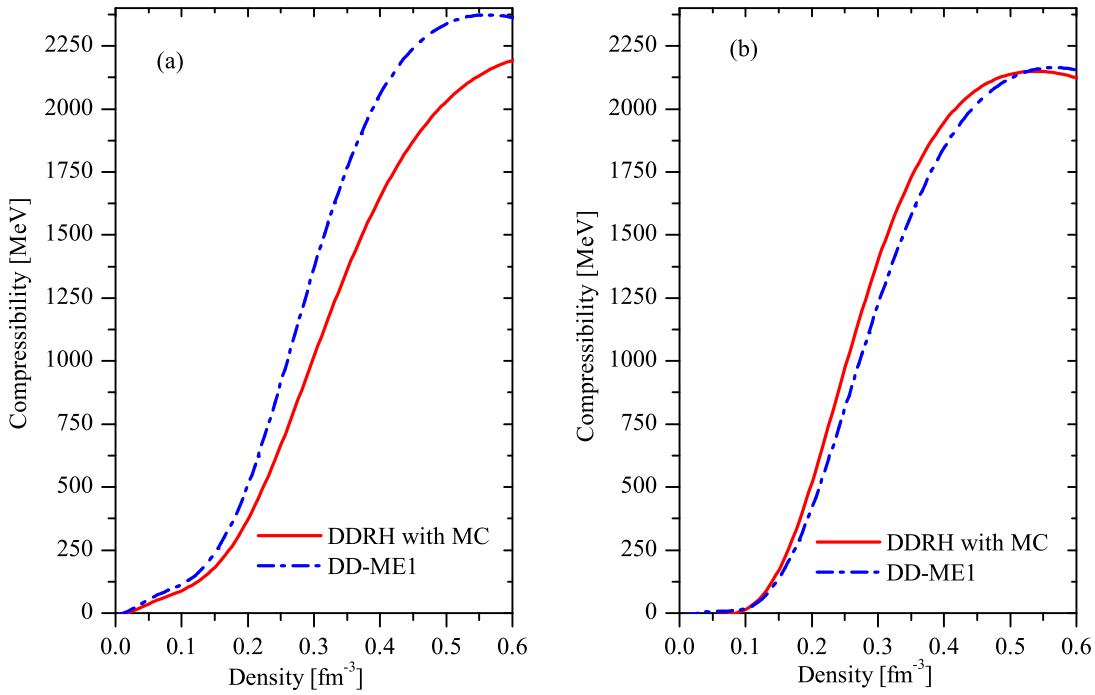

Figure 6.27: Density dependence of the compressibility for the symmetric nuclear matter (a) and pure neutron matter (b). The results of the DDRH-MC (solid) is shown in comparison with the DD-ME1 (dash-dotted).

In Fig. 6.27 we have plotted the compressibility for the symmetric nuclear matter (a) and pure neutron matter (b) as a function of baryon density and we compared DDRH-MC results with the DD-ME1. In these two approaches, the compressibility curves display a very similar dependence on density below the saturation point. However very noticeable differences show up at higher densities. We find that, at the saturation point, $\rho_{sat} = 0.180$ fm^{-3} using DDRH-MC, $K = 282.42$ MeV for symmetric nuclear matter. Due to the high saturation density, this value of K is larger than the value of K obtained using DD-ME1 where $K = 244.5$ MeV at saturation density, $\rho_{sat} = 0.152$ fm^{-3}. On the other hand, the difference may come from the difference of the nuclear matter EOS.
The values of K at the saturation density obtained for symmetric nuclear matter in the different approaches are shown in Table. 6.5.
In Figs. 6.29 and 6.30 we have shown the density dependence of the compressibility for asymmetries ranging from pure neutron matter ($\alpha = 0.00$) to the symmetric nuclear

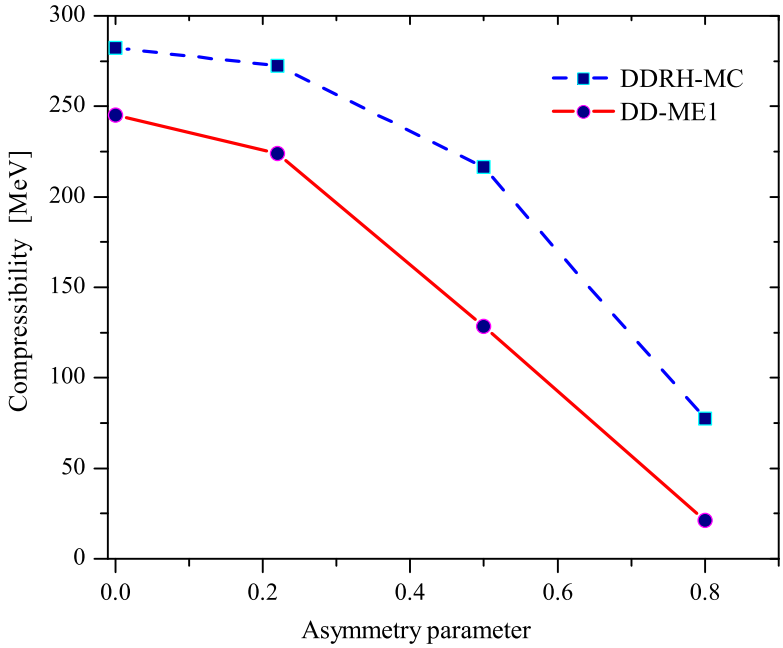

Figure 6.28: The compressibility at saturation density versus asymmetry parameter in the DDRH-MC (dashed curve with squares) and DD-ME1 (solid curve with cirles).

matter ($\alpha = 0.50$). In the both approaches, due to the different saturation points, the compressibilities are different and with increasing asymmetry they decrease as shown in Fig. 6.28 and in Table. 6.6. In DDRH-MC model, K of the symmetric nuclear matter is larger than the neutron rich nuclear matter at low density region in contrast to the behavior of the K at high density. It is interesting that for all asymmetries the curves pass through a common point at $\rho \sim 0.16$ fm^{-3} marked in Fig. 6.29 by a circle. This crossing point a hidden relationship to the empirical value of the K. We show the values of K for various proton fractions at empirical nuclear saturation density $\rho_{\rm sat}^{\rm emp} = 0.16$ fm^{-3} in Table. 6.7. In DD-ME1 model, the low density behaviour of the K is similar to the DDRH-MC and it does not change at high densities. Although we do not see any crossing point in this model, we showed the values of K at $\rho_{\rm sat}^{\rm emp}$ also in Table. 6.7.
As discussed in Sec. 6.2.2 that the instability regions occur in nuclear matter. In such region, the incompressibility K should be negative (see Fig. 6.10) which characterizes the spinodal region [BF99, LGB$^+$02, ABMP04] of the EOS. However, obviously, results of the calculation based on the nuclear physics definition for K can not describe the

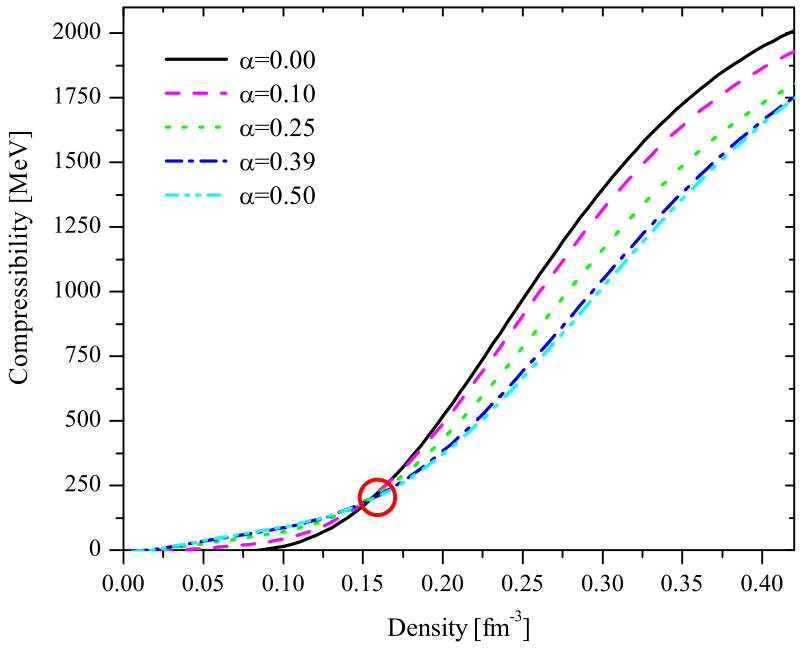

Figure 6.29: The compressibility (Eq. (6.70)) of the nuclear matter as a function of the baryon density, calculated in the DDRH-MC for different asymmetries. The circle describes the area in which the value of K at nuclear saturation density is empirically expected to occur.

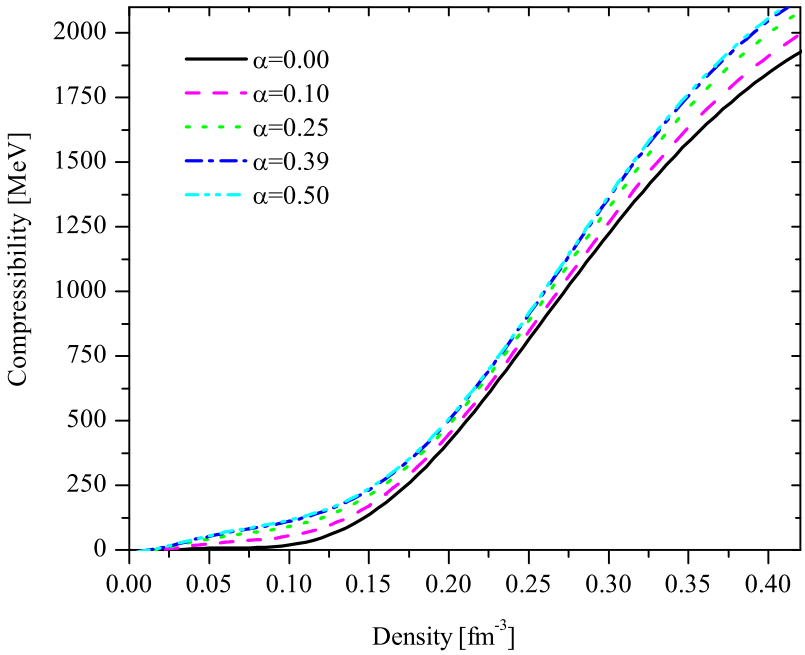

Figure 6.30: The compressibility (Eq. (6.70)) of the nuclear matter as a function of the baryon density, calculated in the DD-ME1 for different asymmetries.

	x_i	$\rho_{\text{sat}}[\text{fm}^{-3}]$	K [MeV]
DDRH-MC	0	0.180	282.42
	0.22	0.176	272.47
	0.5	0.158	216.48
	0.8	0.119	77.59
DD-ME1	0	0.152	245.29
	0.22	0.147	223.94
	0.5	0.122	128.28
	0.8	0.045	21.32

Table 6.6: The compressibility at saturation density for various asymmetry parameters (x_i) calculated in DDRH-MC and DD-ME1.

α_i	0.00	0.10	0.25	0.39	0.50
$K_{DDRH-MC}$ [MeV]	229.43	233.63	225.34	215.16	212.33
K_{DD-ME1} [MeV]	183.00	217.80	256.37	276.62	280.97

Table 6.7: The compressibility at empirical saturation density $\rho_{\text{sat}}^{\text{emp}} = 0.16\text{fm}^{-3}$ for various proton fractions α_i in DDRH-MC and DD-ME1.

spinodal region of EOS. Therefore our next test of the density dependence of the K is done using the more general expression of Eq. (6.69). Plugging the pressure, Eq. (6.40) into Eq. (6.69) we get

$$\tilde{K} = 9\rho^2 \frac{\partial^2}{\partial\rho^2}\left(\frac{\epsilon}{\rho}\right) + 18\rho \left.\frac{\partial}{\partial\rho}\left(\frac{\epsilon}{\rho}\right)\right|_{\rho=\rho_{sat}} . \tag{6.71}$$

Here the first term is a same as Eq. (6.70). The second term vanishes at $\rho = \rho_{\text{sat}}$, hence $\tilde{K}(\rho_{\text{sat}}) = K(\rho_{\text{sat}})$. In Figs. 6.31 and 6.32, one can see that $\tilde{K}$ is much larger than K at high density and at low density $\tilde{K} < 0$ except for neutron matter which as we expected (see Sec. 6.2.2) in both DDRH-MC (panel a) and DD-ME1 (panel b) approaches. In addition, for $\tilde{K}$, the both approaches give a same behavior i.e. there is no longer a crossing point as we discussed above for K. By definition $\tilde{K}$ and K predict the same values at saturation density, presented in Figs. 6.33 and 6.34. Therefore the second term of the Eq. (6.71) corresponding to the pressure, is responsible for low and high density behavior of the nuclear matter compressibility and the explicit density dependence of the compressibility is better described using Eq. (6.71) than Eq. (6.70).

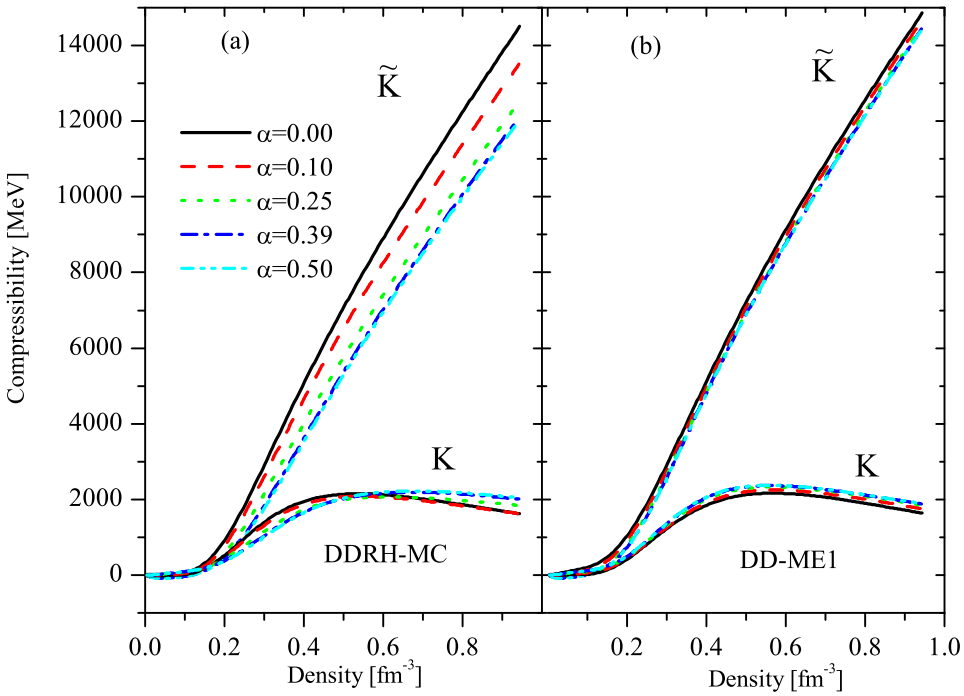

Figure 6.31: The compressibilities K (Eq. (6.70)) and $\tilde{K}$ (Eq. (6.71)) calculated in the DDRH-MC (panel a) and DD-ME1 (panel b) for different asymmetries.

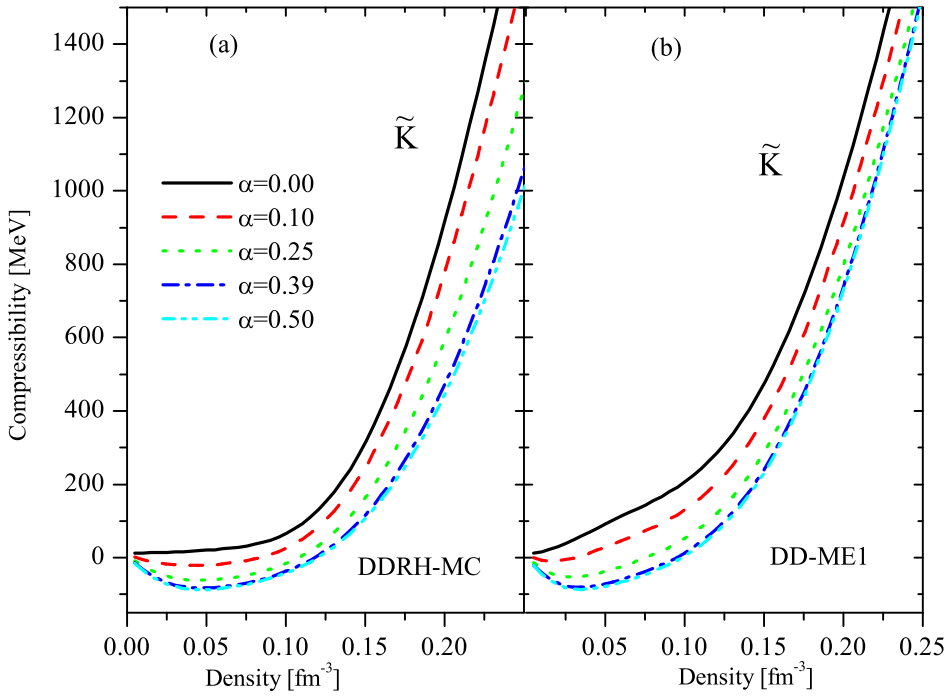

Figure 6.32: $\tilde{K}$, same as plotted in Fig. 6.31 but at low density.

Model	ρ_0 [fm^{-3}]	$\alpha = 0.32$	$\alpha = 0.33$	$\alpha = 0.39$	$\alpha = 0.50$
			$\rho_0(\alpha)$		
$DDRH-MC$	0.16	0.169	0.17	0.176	0.18
$DD-ME1$	0.16	0.138	0.146	0.147	0.152
Baron [BCK85]	0.16	0.144	0.146	0.154	0.16
	$K_0^{\rm sym}$ [MeV]	$\alpha = 0.32$	$\alpha = 0.33$	$\alpha = 0.39$	$\alpha = 0.50$
			$K_0(\alpha)$		
$DDRH-MC$	282.42	209.21	217.12	255.08	282.42
$DD-ME1$	245.29	181.71	188.58	221.54	254.29
Baron	218.00	161.49	167.60	196.90	218.00
Baron	180.00	133.34	138.38	162.57	180.00

Table 6.8: The saturation densities ($\rho_0(\alpha)$) calculated in DDRH-MC and DD-ME1 are compared to the results of Baron et al.,in [BCK85]. The compressibilities ($K_0(\alpha)$) are calculated using Eq. (6.72) with the compressibilities of the symmetric nuclear matter calculated in the DDRH-MC, DD-ME1 and [BCK85] approaches.

In [BCK85] the compressibility and saturation density are calculated using the expressions:

$$K_0(\alpha) = K_0^{\rm sym}[1-\alpha(1-2\alpha)^2] \tag{6.72}$$

$$\rho_0(\alpha) = 0.16[1-3(0.5-\alpha)^2] \tag{6.73}$$

in the range of the proton fraction $\alpha = 0.3$ to $\alpha = 0.5$. These expressions come from the calculations for asymmetric nuclear matter in [KPLT85] and where $K_0^{\rm sym}$ is compressibility of symmetric nuclear matter. We compared our results for the saturation density of the asymmetric nuclear matter to the saturation densities calculated using Eq. (6.73) for α from 0.32 to 0.50, are shown in Table. 6.8 (upper part). We see that our results for the saturation density are much higher and consequently our results for the compressibility are also much larger than results of Baron et al.

Also comparing Tables. 6.8 and 6.6, one can see that Eq. (6.72) produced smaller compressibilities than results of the DDRH-MC, but in the case of DD-ME1 approach, the compressibilities are quite similar. In [BCK85], it has been claimed that for typical supernova collapse K should be 162 MeV for $\alpha = 0.32$ which is much smaller than our results: $K_{\rm DDRH-MC} = 251.17$ MeV and $K_{\rm DD-ME1} = 183.05$ MeV. Therefore Eq. (6.72) is may not be a good tool to calculate the compressibility of the asymmetric nuclear matter, especially when the δ-meson is included.

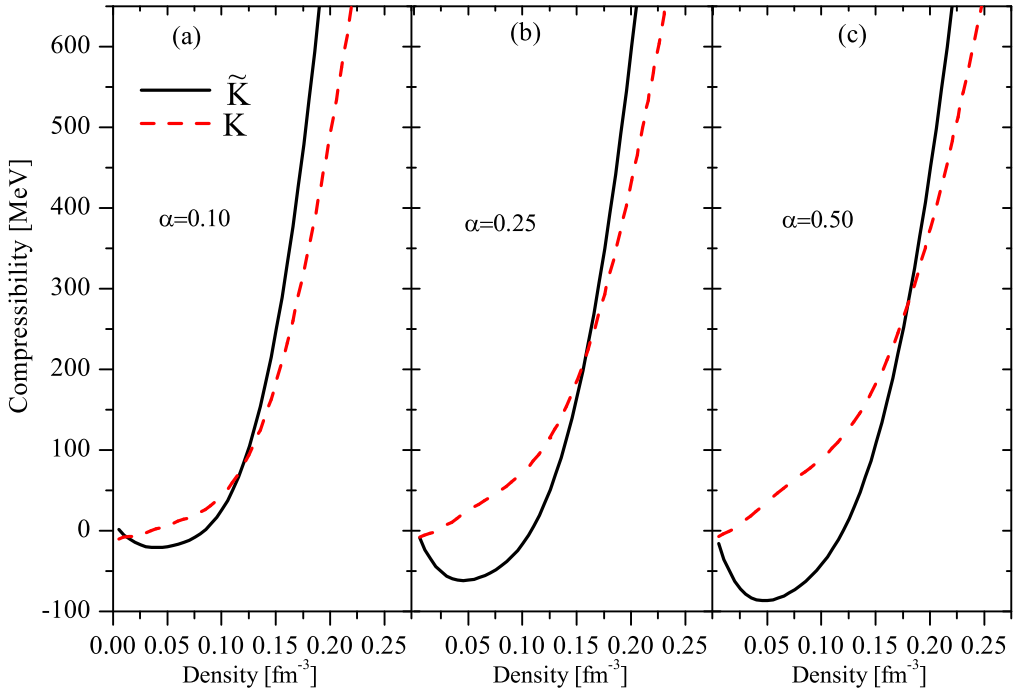

Figure 6.33: The comparison of the $\tilde{K}$ (solid) and K (dashed) at low density calculated in the DDRH-MC for three different asymmetries.

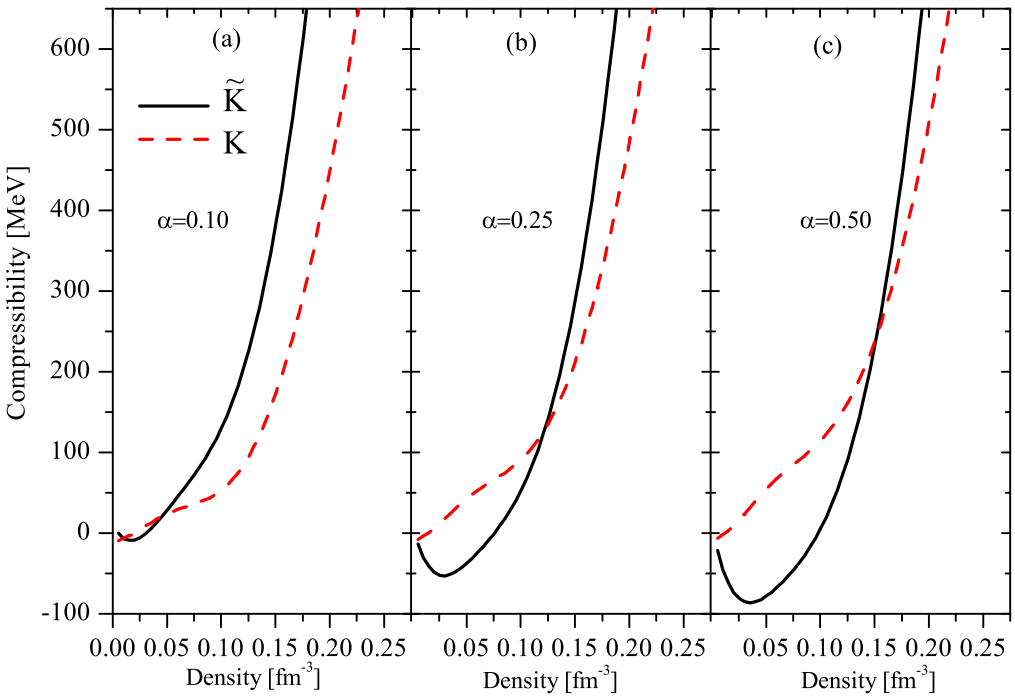

Figure 6.34: The comparison of the $\tilde{K}$ (solid) and K (dashed) at low density calculated in the DD-ME1 for three different asymmetries.

6.2.9 Speed of sound

Since we are investigating the EOS of nuclear matter for densities ranging up to 5 times ρ_0, we have to consider the speed of sound, V_s in nuclear matter. To satisfy relativistic causality which is one of the fundamental physical principles, we must require that the speed of sound does not exceed the speed of light in nuclear matter. That could happen when the baryon density becomes very large. Especially this anomalous behavior exists in non- relativistic nuclear models e.g. the Skyrme models, showing that causality is violated because the relativistic energy-momentum relations is not used. This causal violation, which is commonly known as superluminosity, has been investigated in detail by Osnes and Strottmann [OS86] and Su et al., [SYLK86, SYK87, SSK88] for the EOS of nuclear matter derived from Skyrme type interactions. In relativistic models this problem should not appear [TW99, LMB92, Gad05] but for density-dependent interactions we have to investigate the case explicitly.
The speed of sound in a nuclear medium, in units of the velocity of the light, (c) is defined [BR68] as

$$(V_s)^2 = \frac{dP}{d\epsilon} = \frac{dP/d\rho}{d\epsilon/d\rho} \ , \tag{6.74}$$

where P is the pressure and ϵ is the total energy density of the nuclear matter.
To study the relativistic causality in the present model, in Fig. 6.35 we plotted the ratio of the speed of sound to speed of light V_s/c for the symmetric nuclear matter (a) and the pure neutron matter (b) as functions of the baryon density. The solid line represents the results obtained in the DDRH-MC and dashed line represents the results of DD-ME1 model. While in both cases the speed of sound increases with density. The speed of sound calculated from DDRH-MC approach is smaller than the speed of sound calculated in DD-ME1 in symmetric nuclear matter. This is due to the fact that DDRH-MC yields a softer EOS than DD-ME1. However, the difference between DDRH-MC and DD-ME1 is negligible in the pure neutron matter.
The Fig. 6.36 presents the plots of the speed of sound in asymmetric nuclear matter with four different asymmetries ($\alpha = 0.00, 0.10, 0.25, 0.39$) as a function of baryon density for DDRH-MC calculations. In asymmetric nuclear matter, the differences of the speed of sound induced by asymmetries are very small because the total energy density has a very weak dependence on asymmetry. (see Fig. 6.6)
Evidently, even at very high values of the baryon density the speed of sound does not exceed the speed of the light.

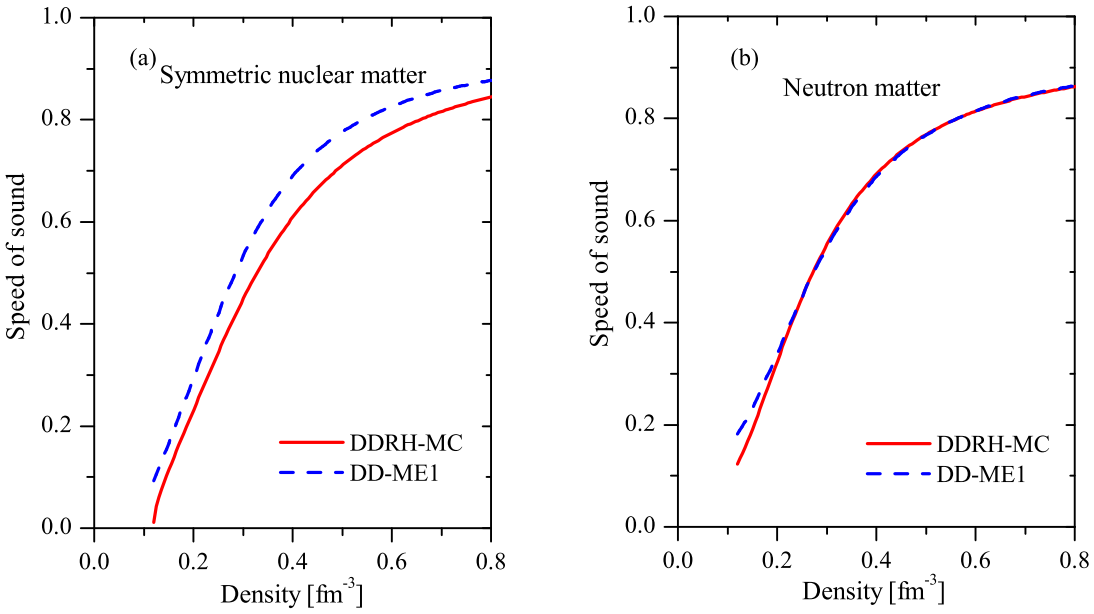

Figure 6.35: The density dependence of the Speed of sound (in units of c-speed of light) in symmetric nuclear matter (a) and pure neutron matter (b) are shown by the solid curves in the DDRH-MC and by the dashed curves in the DD-ME1 for comparison.

In the spinodal region of symmetric and asymmetric nuclear matter, the speed of sound becomes imaginary for $\rho < 0.12$ fm^{-3} (see Sec. 6.2.2 and Fig. 6.32) in both DDRH-MC and DD-ME1 approaches, indicating the onset of instabilities.

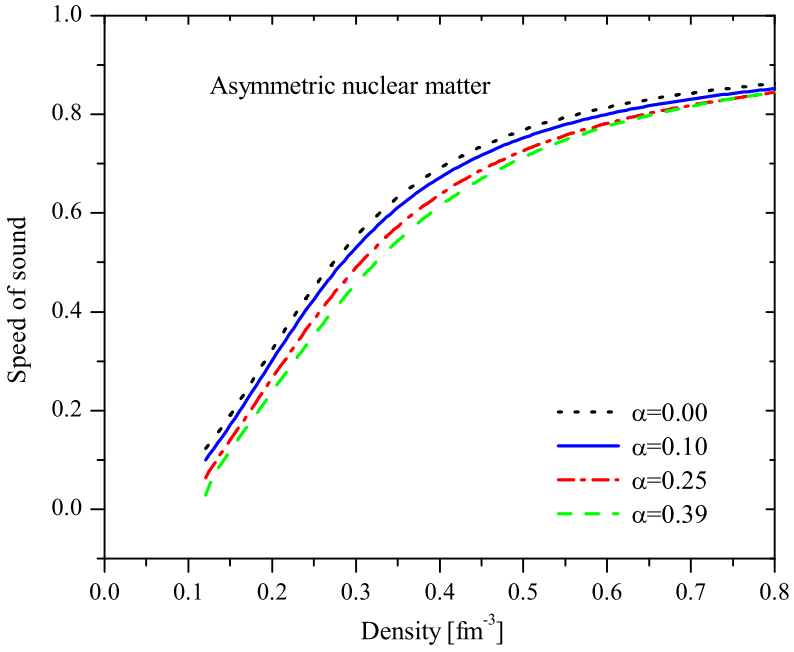

Figure 6.36: The density dependence of the Speed of sound (in units of c) in asymmetric nuclear matter for the different asymmetries in the DDRH-MC.

Chapter 7

Summary and Outlook

We studied the EOS of nuclear matter in the framework of relativistic density dependent hadron field theory (DDRH) and compared our results to the results of the phenomenological density dependent approach DD-ME1. Nuclear interactions were described by a covariant density functional theory using baryons and mesons. In our approach medium dependent modifications of the nuclear interactions were taken into account with density dependent meson-baryon vertices with momentum corrections. We showed that Lorentz invariance of the Lagrangian, the covariance of the field equations and thermodynamical consistency require a formulation in terms of vertex functionals depending themselves on the field operators. The relation of the DDRH vertex functionals to DB in-medium interactions was discussed. Solutions of the field equations were found in relativistic mean-field approximation.

We have calculated the following properties of symmetric and asymmetric nuclear matter and pure neutron matter: energy density, pressure, binding energy, symmetry energy, effective nucleon mass, compressibility and speed of sound in nuclear medium as functions of the density and of the nuclear asymmetry parameter.

Since the EOS at $\rho \gg \rho_0$ is very uncertain, it is important to impose model-independent bounds in order to analyze our results. The basic requirements are [Bom99]:

1. It must reproduce the empirical saturation point for symmetric nuclear matter $\rho_0 = 0.17 \pm 0.1$ fm^{-3} , $\epsilon(\rho_0)/\rho_0 = -16 \pm 1$ MeV;
2. it must give a symmetry energy at the saturation point $E_{sym}(\rho_0) \approx 30 \pm 2$ MeV,
3. for symmetric nuclear matter the compressibility at saturation density must be $K \approx 220 \pm 30$ MeV

4. EOS should respect Lorentz invariance and causality.

In general our model as well as DD-ME1 model satisfy above requirements. We found that in DD-ME1 model the bulk properties of symmetric nuclear matter is particularly in very good agreement with the empirical information. In our model the saturation density of symmetric nuclear matter is higher than in the DD-ME1. Therefore in our model the bulk properties of symmetric nuclear matter are slightly different than in DD-ME1. We also calculated the properties of asymmetric nuclear at saturation density for three different asymmetry parameters $x = 0.22, 0.5, 0.8$. We found that for increasing asymmetry, the saturation density shifts to lower values. Consequently, the properties of the asymmetric nuclear matter at saturation density are also changed. In the both approach, all quantities except effective baryon masses become smaller as the asymmetry parameter increases. Because, the effective baryon mass decreases with increasing baryon density.

The results of the calculation for the properties of the asymmetric nuclear matter show that at low density region these two models are in agreement. But in high density region, the difference between them is more significant and it increases with increasing asymmetry parameter. The main part of this difference can be understood as coming from the effects of the δ meson inclusion.

From study of the δ meson influence on the EOS we found following :

- The proton-neutron effective mass splitting is directly given by the δ coupling, and asymmetry. We find that in n-rich nuclear matter, a neutron effective mass is always smaller than the proton effective mass. The same is predicted from microscopic relativistic Dirac-Brueckner calculations.

- This proton-neutron effective mass splitting causes a negative contribution to the symmetry energy E_{sym}, since it reduces the gap between n-p Fermi energies, due to the different Fermi momenta in asymmetric nuclear matter. In fact, in n-rich matter, the neutron Fermi momentum increases while the neutron effective mass decreases contrast to the proton.

  We compared our result for the symmetry energy with the very recent experimental results [SYS07]. We found that both approaches are in good agreement at low density. However DD-ME1 calculation gives a too soft dependence at higher density contrast to our model.

- We have shown that the δ contributions are not negligible for the slope parameter, P_{sym} the symmetry pressure, and absolutely essential for the curvature parameter K_{sym} symmetry compressibility.

We found that the energy density of the nuclear matter is not very sensitive to asymmetry parameter for whole range of the density. Therefore our results of the calculation for the energy density are similar to the DD-ME1 results. In contrast the pressure of the nuclear matter becomes different at high density for different asymmetry parameter due to the inclusion of isovector scalar δ meson. The region of negative pressure occurs below the saturation density. This means that below the saturation density system becomes unstable and that indicates a presence of a liquid-gas phase transition [BF99, ABMP04] which disappears for some critical value of the asymmetry.

In instability region, the compressibility is negative which characterizes the spinodal region of the EOS. The both models agree this low density behavior.

The difference between our model and DD-ME1 model start at baryon densities roughly above $2\rho_0$ for asymmetric nuclear matter. This is the region where transitions to different forms of nuclear matter are expected, and so the result appears quite stimulating.

Since in the low density region field sources are (scalar and vector densities) too small to make a differences for different asymmetry parameters. Therefore, the effects due to the inclusion of the δ are more significant at high density and with large asymmetry parameter. This is the main reason for that why at low density region the microscopic DDRH and phenomenological DD-ME1 models are in agreement.

In [TW99] paper was claimed that there is no need to take into account the δ meson. But our results show that this is true for the low density regions, not for high density regions and it is not negligible the inclusion of the δ meson, especially for the study of the neutron rich nuclear matter.

We expect that future experiments with radio-active beams will be able to test these predictions.

In general, we think that the results of the DDRH approach are quite satisfactory and that the momentum correction provides a consistent scheme to reproduce DBHF calculations. (Improvements of the results could possibly be achieved by going beyond the ladder approximation and including, e.g., three-body interactions and ring diagrams.)

In future investigations we also plan to apply the density dependent interactions to neutron stars to gain additional insights in the properties of the isovector density

dependence.

It is possible to apply the density dependent vertices with momentum correction (parameterized) in relativistic transport models for heavy ion collisions. Then the high density behavior of our model can be examined more carefully.

List of Figures

List of Tables

Appendix A

A.1 The free Dirac equation

The Dirac equation for a particle of spin 1/2 in free-space is given by

$$[i\gamma_\mu \partial^\mu - M]\,\Psi(x) = 0 \tag{A.1}$$

with general plane wave solution [Cha90]

$$\Psi(x) = \sum_\lambda \int \frac{dk^3}{(2\pi)^{3/2}} \sqrt{\frac{M}{E_k}} \left[b(k,\lambda) u(k,\lambda) e^{-ik\cdot x} + d\dagger(k,\lambda) v(k,\lambda) e^{ik\cdot x} \right] \ , \tag{A.2}$$

where $u(k,\lambda)$ and $v(k,\lambda)$ are spinors and λ indices represent spin labels. In the momentum-space Eq. (A.1) for positive and negative energy fermions can be written

$$\begin{aligned} [\gamma_\mu k^\mu - M]\, u(k,\lambda) &= 0 \ , \\ [\gamma_\mu k^\mu + M]\, v(k,\lambda) &= 0 \ . \end{aligned} \tag{A.3}$$

Conjugated spinors are defined as

$$\begin{aligned} \bar{u} &= u^\dagger \gamma_0 \\ \bar{v} &= v^\dagger \gamma_0 \end{aligned} \tag{A.4}$$

with the covariant normalization

$$\begin{aligned} \bar{u}(k,\lambda') u(k,\lambda) &= \delta_{\lambda\lambda'} = -\bar{v}(k,\lambda') v(k,\lambda) \\ u^\dagger(k,\lambda') u(k,\lambda) &= \frac{E_k}{M} = v^\dagger(k,\lambda') v(k,\lambda) \ . \end{aligned} \tag{A.5}$$

The explicit form of the solution is

$$u(k,\lambda) = \sqrt{\frac{E_k + M}{2M}} \begin{pmatrix} 1 \\ \frac{\sigma \mathbf{k}}{E_k + M} \end{pmatrix} \chi_\lambda \ , \tag{A.6}$$

with $E_k = \sqrt{\mathbf{k}^2 + M^2}$ and the Pauli spinors

$$\chi_{\lambda=1/2} = \begin{pmatrix} 1 \\ 0 \end{pmatrix} \ , \qquad \chi_{\lambda=-1/2} = \begin{pmatrix} 0 \\ 1 \end{pmatrix} \ . \tag{A.7}$$

Bibliography

[ABMP04] S. S. Avancini, L. Brito, D. P. Menezes, and C. Providência. Instabilities in asymmetric nuclear matter. *Phys. Rev.*, C70:015203, (2004).

[BB77] J. Boguta and A.R Bodmer. Relativistic calculation of nuclear matter and the nuclear surface. *Nucl. Phys.*, A292(3):413–428, (1977).

[BBDG95] J.P. Blaizot, J.F. Berger, J. Dechargé, and M. Girod. Microscopic and macroscopic determinations of nuclear compressibility. *Nucl .Phys.*, A591(3):435–457, (1995).

[BCGT05] V. Baran, M. Colonna, V. Greco, and M. Di Toro. Reaction dynamics with exotic nuclei. *Phys. Rep.*, 410(5-6):335–466, (2005).

[BCK85] E. Baron, J. Cooperstein, and S. Kahana. Type II supernovae in $12M_{\odot}$ and $15M_{\odot}$ stars: The equation of state and general relativity. *Phys. Rev. Lett.*, 55(1):126–129, (1985).

[BF99] M. Baldo and L.S. Ferreira. Nuclear liquid-gas phase transition. *Phys. Rev. C*, 59(2):682–703, (1999).

[BGH85] M. Brack, C. Guet, and H.B. Hakansson. *Phys. Rep.*, 123:275, (1985).

[BM90] R. Brockmann and R. Machleidt. Relativistic nuclear structure. 1. Nuclear matter. *Phys. Rev. C*, 42(5):1965–1980, (1990).

[Bod91] A.R Bodmer. Relativistic mean field theory of nuclei with a vector meson self-interaction. *Nucl. Phys.*, A526(3-4):703–721, (1991).

[Bom99] I. Bombaci. *Netron Stars Structure and the Nuclear Equation of State.* International Rev. Nucl. Phys. (World Scientific. Singapore), (1999).

[BR68] S.A. Bludman and M.A. Ruderman. Possibility of the Speed of Sound Exceeding the Speed of Light in Ultradense Matter. *Phys. Rev.*, 170(5):1176–1184, (1968).

[BS66] R. Blankenbecler and R. Sugar. Linear Integral Equations for Relativistic Multichannel Scattering. *Phys. Rev.*, 142(4):1051–1059, (1966).

[BT92] R. Brockmann and H. Toki. Relativistic density dependent Hartree approach for finite nuclei. *Phys. Rev. Lett.*, 68:3408, (1992).

[Cha90] S.J. Chang. *Introduction to Quantum Field Theory.* Lect. Notes Phys. Vol.29 (World Scientific. Singapore), (1990).

[Chi77] S.A. Chin. A relativistic many-body theory of high density matter. *Ann. Phys. (N.Y)*, 108(2):301–367, (1977).

[CPn$^+$90] M. Centelles, M. Pi, X. Vi nas, F. Garcias, and M. Barranco. Self-consistent extended Thomas-Fermi calculations in nuclei. *Nucl. Phys. A.*, 510(3):397–416, (1990).

[DG90] R.M. Dreizler and E.K.U. Gross. *Density functional theory.* Springer-Verlag, Berlin, (1990).

[dJL98a] F. de Jong and H. Lenske. Asymmetric nuclear matter in the relativistic Brueckner-Hartree-Fock approach. *Phys. Rev. C*, 57(6):3099–3107, (1998).

[dJL98b] F. de Jong and H. Lenske. Relativistic Brueckner-Hartree-Fock calculations with explicit intermediate negative energy states. *Phys. Rev. C*, 58(2):890–899, (1998).

[Erk74] K. Erkelenz. Current status of the relativistic two-nucleon one boson exchange potential. *Phys. Rep.*, 13(5):191–258, (1974).

[Fah98] Claes Fahlander. Heavy ion physics in Lund. `http://wwwnsg.nuclear.lu.se/annrep9798/images/fig21.gif` , (1997-1998).

[Fie37] M. Fierz. Zur Fermionischen Theorie des β-Zerfalls. *Z. Phys*, 104:553, (1937).

[FLW95] C. Fuchs, H. Lenske, and H.H. Wolter. Density dependent hadron field theory. *Phys. Rev. C*, 52(6):3043–3060, (1995).

[FPT97] M. Farine, J.M. Pearson, and F. Tondeur. Nuclear-matter incompressibility from fits of generalized Skyrme force to breathing-mode energies. *Nucl. Phys.*, A615(2):135–161, (1997).

[FW06] C. Fuchs and H.H. Wolter. Modelization of the EOS. *Eur. Phys. J.*, A30:5, (2006).

[Gad05] Kh. Gad. Bulk properties of nuclear matter from extended Brueckner theory. *J.Phys. G:Nucl. Part. Phys.*, 32:799, (2005).

[GRT90] Y.K. Gambhir, P. Ring, and A. Thimet. Relativistic mean field theory for finite nuclei. *Ann. Phys. (N.Y)*, 198(1):132–179, (1990).

[GSI] GSI Conceptual Design Report, http://www.gsi.de/GSI-Future.

[Hau88] P.E. Haustein. *At. Data Nucl. Data Tables* **39**, 185, (1988).

[HK64] P. Hohenberg and W. Kohn. Inhomogeneous Electron Gas. *Phys. Rev.*, 136(3B):B864–B871, (1964).

[HK93] S. Haddad and M. K.Weigel. Finite nuclear systems in a relativistic extended Thomas-Fermi approach with density-dependent coupling parameters. *Phys. Rev. C*, 48(6):2740–2745, (1993).

[HKL01a] F. Hofmann, C.M. Keil, and H. Lenske. Application of the density dependent hadron field theory to neutron star matter. *Phys. Rev. C*, 64(2):025804, (2001).

[HKL01b] F. Hofmann, C.M. Keil, and H. Lenske. Density dependent hadron field theory for asymmetric nuclear matter and exotic nuclei. *Phys. Rev. C*, 64(3):034314, (2001).

[HM87] B. Ter Haar and R. Malfliet. Nucleons, mesons and deltas in nuclear matter a relativistic Dirac-Brueckner approach. *Phys. Rep.*, 149(4):207–286, (1987).

[Hol74] K. Holinde. Two-nucleon forces and nuclear matter. *Phys. Rep.*, 68(3):121–188, (1974).

[HP01] C.J. Horowitz and J. Piekarewicz. Neutron Star Structure and the Neutron Radius of 208Pb. *Phys. Rev. Lett.*, 86:5647, (2001).

[HP02] C.J. Horowitz and J. Piekarewicz. Constraining URCA cooling of neutron stars from the neutron radius of ^{208}Pb. *Phys. Rev. C*, 66(5):055803, (2002).

[HS84] C. J. Horowitz and Brian D. Serot. Two-nucleon correlations in a relativistic theory of nuclear matter. *Phys. Lett.*, B137(5-6):287–293, (1984).

[HS87] C. J. Horowitz and Brian D. Serot. The relativistic two-nucleon problem in nuclear matter. *Nucl. Phys. A*, 464(4):613–699, (1987).

[HvH58] N.M. Hugenholtz and L. van Hove. Instabilities in asymmetric nuclear matter. *Physica.*, 24:363, (1958).

[IZ80] C. Itzykson and J.-B. Zuber. *Quantum field theory*. McGraw-Hill, Singapore, (1980).

[JHM87] C.H. Johnson, D.J. Horen, and C. Mahaux. Unified description of the neutron$-^{208}$Pb mean field between -20 and +165 MeV from the dispersion relation constraint. *Phys. Rev. C*, 36(6):2252–2273, (1987).

[JM89] M. Jaminon and C. Mahaux. Effective masses in relativistic approaches to the nucleon-nucleus mean field. *Phys. Rev. C*, 40(1):354–367, (1989).

[KBB$^+$94] A. Krasznahorkay, A. Balanda, J.A. Bordewijk, S. Brandenburg, M.N. Harakeh, N. Kalantar-Nayestanaki, B.M. Nyak, J. Timr, and A. van der Woude. Excitation of the isovector GDR by inelastic α-scattering as a measure of the neutron skin of nuclei. *Nucl. Phys. A*, 567(3):521–540, (1994).

[KG] (ed.) K. Grosse. Darmstadt GSI. Scientific report 2005. GSI-2006-1.

[KHL00] C.M. Keil, F. Hofmann, and H. Lenske. Density dependent hadron field theory for hypernuclei. *Phys. Rev. C*, 61(6):064309, (2000).

[KL02] C. Keil and H. Lenske. Hypernuclear Auger effect within density dependent relativistic hadron field theory. *Phys. Rev. C*, 66(5):054307, (2002).

[KPLT85] K. Kolehmainen, M. Prakash, J.M. Lattimer, and J.R. Treiner. Surface and curvature properties of neutron-rich nuclei. *Nucl. Phys. A*, 439(3):535–572, (1985).

[Len04] H. Lenske. *Density Dependent Relativistic Field Theory.* Lect. Notes Phys. 641:147-174 (Springer, Berlin Heidelberg.), (2004).

[LF95] H. Lenske and C. Fuchs. Rearrangement in the density dependent relativistic field theory of nuclei. *Phys. Lett. B*, 345(4):355–360, (1995).

[LGB$^+$02] B. Liu, V. Greco, V. Baran, M. Colonna, and M. Di Toro. Asymmetric nuclear matter: The role of the isovector scalar channel. *Phys. Rev. C*, 65(4):045201, (2002).

[Li01] B.-A. Li. Probing the isospin-dependence of the nuclear equation of state. *Nucl. Phys. A*, 681(1-4):434–437, (2001).

[LKLB97] C.-H. Lee, T.T.S. Kuo, G.Q. Li, and G.E. Brown. Symmetry energy of nuclear matter and properties of neutron statrs in a relativistic approach. *nucl-th/9703034v1*, (1997).

[LKP97] G.A. Lalazissis, J. König, and P.Ring. New parametrization for the Lagrangian density of relativistic mean field theory. *Phys. Rev. C*, 55(1):540–543, (1997).

[LMB92] G.Q. Li, R. Machleidt, and R. Brockmann. Properties of dense nuclear and neutron matter with relativistic nucleon-nucleon interactions. *Phys. Rev. C*, 45(6):2782–2794, (1992).

[LME93] K. Langanke, J.A. Maruhn, and S.E. Koonin (Eds.). *Computational nuclear physics 2. Nuclear reactions.* Lect. Notes Comp. Phys. 2 (Springer, Berlin Heidelberg New York.), (1993).

[LMGZ04] Wenhui Long, Jie Meng, Nguyen Van Giai, and Shan-Gui Zhou. New effective interactions in relativistic mean field theory with nonlinear terms and density-dependent meson-nucleon coupling. *Phys. Rev. C*, 69:034319, (2004).

[LNVR05] G.A. Lalazissis, T. Nikšić, D. Vretenar, and P. Ring. New relativistic mean-field interaction with density-dependent meson-nucleon couplings. *Phys. Rev. C*, 71(2):024312, (2005).

[LQMN+88] M. Lopez-Quelle, S. Marcos, R. Niembro, A. Bouyssy, and N.V. Giai. Asymmetric nuclear matter in the relativistic approach. *Nucl. Phys. A*, 483(3-4):479–492, (1988).

[LRE04] G.A. Lalazissis, P. Ring, and D. Vretenar (Eds.). *Extended density functionals in nuclear structure physics.* Lect. Notes Phys. 641 (Springer, Berlin Heidelberg.), (2004).

[Mac89] R. Machleidt. *Advances in Nuclear Physics,* **19**. Plenum, N.Y., (1989).

[Mal88] R. Malfliet. Relativistic theory of nuclear matter and finite nuclei. *Prog. Part. Nucl. Phys.*, 21:207–291, (1988).

[MGW+01] Zy. Ma, N. Van Giai, A. Wandelt, D. Vretenar, and P. Ring. Isoscalar compression modes in relativistic random phase approximation. *Nucl. Phys.*, A686(1-4):173–186, (2001).

[MHE87] R. Machleidt, K. Holinde, and Ch. Elster. The Bonn meson-exchange model for the nucleonnucleon interaction. *Phys. Rep.*, 149(1):1–89, (1987).

[MV79] A.H MacDonald and S.H. Vosko. A relativistic density functional formalism. *J. Phys.*, C12:2977, (1979).

[NDVR04] T. Nikšić, G.A. Lalazissis D. Vretenar, and P. Ring. Ground-state properties of rare-earth nuclei in the relativistic Hartree-Bogoliubov model with density-dependent meson-nucleon couplings. *Phys. Rev. C*, 69(4):047301, (2004).

[Neg82] J.W. Negele. The mean-field theory of nuclear structure and dynamics. *Rev. Mod. Phys.*, 54(4):913, (1982).

[NVFR02] T. Nikšić, D. Vretenar, P. Finelli, and P. Ring. Relativistic Hartree-Bogoliubov model with density-dependent meson-nucleon couplings. *Phys. Rev. C*, 66(2):024306, (2002).

[NVR02] T. Nikšić, D. Vretenar, and P. Ring. Relativistic random-phase approximation with density-dependent meson-nucleon couplings. *Phys. Rev. C*, 66(6):064302, (2002).

[OS86] E. Osnes and D. Strottmann. Causal constraints on the nuclear equation of state. *Phys. Lett. B.*, 166:5–9, (1986).

[PnGB88] M. Pi, X. Vi nas, F. Garcias, and M. Barranco. $\hbar^4$-order variational Thomas-Fermi calculations of finite nuclei: The local case. *Phys. Lett. B.*, 215(1):5–9, (1988).

[PNVR04] N. Paar, T. Nikšić, D. Vretenar, and P. Ring. Quasiparticle random phase approximation based on the relativistic Hartree-Bogoliubov model. II. Nuclear spin and isospin excitations. *Phys. Rev. C*, 69(4):054303, (2004).

[PS95] Michael E. Peskin and D.V. Schroeder. *An Introduction to quantum field theory.* Addison-Wesley, USA, (1995).

[Raj78] A.K. Rajagopal. Inhomogeneous relativistic electron gas. *J. Phys. C.*, 11:L943, (1978).

[RC73] A.K. Rajagopal and J. Callaway. Inhomogeneous Electron Gas. *Phys. Rev. B.*, 7(5):1912–1919, (1973).

[Rei99] P.-G. Reinhard. Skyrme forces and giant resonances in exotic nuclei. *Nucl. Phys. A.*, 649(1-4):305–314, (1999).

[SDE92] C. Speicher, R.M. Dreizler, and E. Engel. Density functional approach to quantumhadrodynamics: Theoretical foundations and construction of extended thomas-fermi models. *Ann. Phys.*, 213(2):312–354, (1992).

[See95] See, e.g., C.J. Pethick, and D.G. Ravenhall and C.P. Lorenz. The inner boundary of a neutron-star crust. *Nucl. Phys. A.*, 584(4):675–703, (1995).

[Ser79a] Brian D. Serot. A relativistic nuclear field theory with π and ρ mesons. *Phys. Lett. B.*, 86(2):146–150, (1979).

[Ser79b] Brian D. Serot. Errata. *Phys. Lett. B*, 87(4):403–406, (1979).

[SG95] Arno Schindlmayr and R. W. Godby. Density-functional theory and the v-representability problem for model strongly correlated electron systems. *Phys. Rev. B*, 51(16):10427–10435, (1995).

[SH94] V.E. Starodubsky and N.M. Hintz. Extraction of neutron densities from elastic proton scattering by ^{206,207,208}Pb at 650 MeV. *Phys. Rev. C*, 49(4):2118–2135, (1994).

[Sky59] T.H.R. Skyrme. The effective nuclear potential. *Nucl. Phys.*, 9(4):615–634, (1959).

[SMK+03] J.R. Stone, J.C. Miller, R. Koncewicz, P.D. Stevenson, and M.R. Strayer. Nuclear matter and neutron-star properties calculated with the Skyrme interaction. *Phys. Rev. C*, 68(3):034324, (2003).

[SSK88] R.K. Su, H.Q. Song, and T.T.S. Kuo. Speed of sound in asymmetric nuclear matter with skyrme interactions. *Phys. Rev. C*, 37(4):1770–1773, (1988).

[SW86] B.D. Serot and J.D. Walecka. *In Advances in Nuclear physics*. Plenum, New York, (1986).

[SYB+04] D.V. Shetty, S.J. Yennello, A.S. Botvina, G.A. Souliotis, M. Jandel, E. Bell, A. Keksis, S. Soisson, B. Stein, and J. Iglio. Symmetry energy and the isospin dependent equation of state. *Phys. Rev. C*, 70(1):011601, (2004).

[SYK87] R.K. Su, S.D. Yang, and T.T.S. Kuo. Liquid-gas and superconducting phase transitions of nuclear matter calculated with real time Green's function methods and Skyrme interactions. *Phys. Rev. C*, 35(4):1539–1550, (1987).

[SYLK86] R.K. Su, S.D. Yang, G.L. Li, and T.T.S. Kuo. Critical Neutron-Proton asymmetry of hot nuclear matter. *Mod. Phys. Lett. A.*, 1(2):71–80, (1986).

[SYS07] D.V. Shetty, S.J. Yennello, and G.A. Souliotis. Density dependence of the symmetry energy and the equation of state of isospin asymmetric nuclear matter. *Phys. Rev. C*, 75(3):034602, (2007).

[Tho70] Richard H. Thompson. Three-Dimensional Bethe-Salpeter Equation Applied to the Nucleon-Nucleon Interaction. *Phys. Rev. D*, 1(1):110–117, (1970).

[TW99] S. Typel and H. H. Wolter. Relativistic mean field calculations with density-dependent meson-nucleon coupling. *Nuc. Phys. A*, 656(3-4):331–364, (1999).

[VB72] D. Vautherin and D.M. Brink. Hartree-Fock Calculations with Skyrme's Interaction. I. Spherical Nuclei. *Phys. Rev. C*, 5(3):626–647, (1972).

[VLB+97] D. Vretenar, G.A. Lalazissis, R. Behnsch, W. Pöschl, and P. Ring. Monopole giant resonances and nuclear compressibility in relativistic mean field theory. *Nucl. Phys. A.*, 621(4):853–878, (1997).

[VNR03] D. Vretenar, T. Nikšić, and P. Ring. A microscopic estimate of the nuclear matter compressibility and symmetry energy in relativistic mean-field models. *Phys. Rev. C*, 68(2):024310, (2003).

[VR87] G. Vignale and M. Rasolt. Density-functional theory in strong magnetic fields. *Phys. Rev. Lett.*, 59(20):2360–2363, (1987).

[VR88] G. Vignale and M. Rasolt. Current- and spin-density-functional theory for inhomogeneous electronic systems in strong magnetic fields. *Phys. Rev. B*, 37(18):10685–10696, (1988).

[Wal74] J.D. Walecka. A theory of highly condensed matter. *Ann. Phys. (N.Y)*, 83(2):491–529, (1974).

[Wei72] S. Weinberg. *Gravitation and Cosmology*. Wiley, New York, (1972).

[Wic50] G.C. Wick. The evaluation of the collision matrix. *Phys. Rev.*, 80(2):268–272, (1950).

[ZBL99] W. Zuo, I. Bombaci, and U. Lombardo. Asymmetric nuclear matter from an extended Brueckner-Hartree-Fock approach. *Phys. Rev. C*, 60(2):024605, (1999).

Deutsche Zusammenfassung

Die Zustandsgleichung von Kernmaterie (EOS) spielt eine wichtige Rolle bei der Untersuchung von Kerneigenschaften, Schwerionenkollisionen sowie astrophysikalischen Objekten wie Neutronensterne und Supernovae. In letzter Zeit schenkte man den Untersuchungen der Zustandsgleichung von asymmetrischer Kernmaterie besondere Beachtung aufgrund astrophysikalischer Anwendungen (Neutronensterne) [See95] und neuen Experimente, [KG] die Kerne fernab der Stabilität untersuchen. Ein anderer Schwerpunkt liegt im Bereich hoher Dichten, welcher in Kürze durch verschiedene Experimente, Z.B. das CBM in Darmstadt [GSI], untersucht werden soll.

Voraussetzungen und verschiedene theoretische Aspekte für die Formulierung einer Dichtfunktionaltheorie für nuklearen Systeme werden betrachtet. Der Existenzbeweis von Hohenberg-Kohn [HK64] wird auf Vielteilchensysteme mit starken Wechselwirkung übertragen.

Wir zeigten, dass Lorentzinvarianz der Lagrangedichte, die Kovarianz der Feldgleichungen und thermodynamische Konsistenz eine Formulierung in Form von Vertexfunktionalen erfordert, welche selbst von den Feldoperatoren abhängen. Dabei wurde die Beziehung der Vertexfunktionale zu den Dirac-Brückner-in-medium Wechselwirkungen und den zugehörigen Selbstenergien benutzt. Die Lösungen der Feldgleichungen wurden im Rahmen der relativistischen Mittel-Feld-Näherung betrachtet.

Wir untersuchten die Zustandsgleichung der Kernmaterie im Rahmen der relativistischen dichteabhängigen Hadronenfeldtheorie (DDRH). Wir haben die folgenden Eigenschaften symmetrischer und asymmetrischer Kernmaterie sowie reiner Neutronenmaterie berechnet:

- Energiedichte,
- Druck,
- Bindungsenergie,

- Symmetrie-energie
- effektive Nukleonenmasse,
- Kompressibilität und
- Schallgeschwindigkeit im Medium

und als Funktionen der Dichte und des Asymmetrieparameters untersucht.

Wir vergleichen unsere Ergebnisse mit denen des phänomenologischen dichteabhängigen Modelle. Alle Modelle erfüllen die Grundbedingungen einer realistischen Zustandsgleichung.

Weiterhin vergleichen wir unsere Ergebnisse für die Symmetrieenergie mit neuesten experimentellen Daten [SYS07]. Beide Zugänge liefern eine gute Ubereinstimmung bei niedrigen Dichten. Bei hohen Dichten liefern weitgehend die phänomenologischen Modelle jedoch eine "weichere" Abhängigkeit als unser mikroskopisches Modell. Dieser Unterschied kam durch unsere Berücksichtigung des δ-Mesons erklärt werden.

Wir hoffen, dass zukünftige Experimente klären können welche Vorhersagen zutreffen.

Acknowledgments

Learning is a life long experience for everyone. I am extremely grateful for the opportunity of being a PhD candidate. The fact that my candidacy took place in Germany has greatly enriched my life in ways I could not have foreseen. The completion of this thesis would not have been possible without the support of many people. It is my honor now to express my gratitude to you all.

First of all, I would like to express my deepest thanks to my supervisor Prof. Dr H. Lenske for being an excellent supervisor. In fact he has been more than a supervisor to me. He has been my mentor and a trusted counselor. He always had his door open for me and always found ways to encourage me.

I also would like to thank Prof. Dr. U. Mosel for providing me with invaluable opportunities to work in his friendly and supportive research group. In particular, I am grateful for the encouragement and support that were provided by all the diligent and prolific professors during my study.

Thank you to Dr. A. Larionov, PD. Dr. S. Leupold, Dr. G. Martens and Dr. N. Tsoneva for being there for me whenever I had questions.

I am very grateful to Dr. A. Gagyi-Palffy, who was so kind to spend many hours reading the manuscript thoroughly and correcting the English spelling and grammar. I greatly value the scientific discussions that she contributed to my work.

I thank Prof. Dr. G. Braunss, Prof. Dr. E. Salzborn and Prof. Dr. W. Scheid for kindly agreeing to serve on my thesis committee.

I am very thankful for the financial support that I received from the Deutsche Forschungs Gemeinschaft and the Bundesministerium für Bildung und Forschung.
Thank you Prof. Dr. Dr. W. Cassing, Prof. Dr H. Lenske and Prof. Dr. U. Mosel for making it all possible.

Thank you to Mrs. E.Jung for taking care of countless paperwork for me.

Special thanks go to my friends Dr. A. Gagyi-Palffy, T. Leitner, Dr. O. Linnyk,

Dr. L. Alvarez-Ruso, O. Buss, S. Bender, M. Destefanis, Dr. Z. Gagyi-Palffy, P. Konrad, Dr. V. Shklyar, Dr. P. Watson who made my journey of learning more enjoyable and fun. And a very special thanks goes to my dear friend Olena who is always there for me as a good friend.

I thank to Sabrina and Alexandra for their help and support especially in the beginning of my study in Germany.

Many thanks go to my middle and high school teacher Uranchimeg and childhood friends Nandia, Naraa and Jeemaa. I am very blessed to have all of you in my life. I could always count on you.

Apart from my colleagues and friends, I thank to my whole family for their unconditional love and support. Without their support, I would not have been where I am.

I especially would like to thank my mother and father for teaching me to always strive for learning.